Dipl.-Ing. Raphael Neubauer, BSc

Desulfurizing Liquid Fuels from Petroleum Feedstocks to Operate SOFC-based Auxiliary Power Units

Doctoral Thesis

In fulfilment of the requirements
for the degree
Doctor of Technical Sciences

submitted to

Graz University of Technology

Faculty of Mechanical Engineering and Economic Sciences

Supervisor
Univ.-Prof. Dipl.-Ing. Dr.techn. Christoph Hochenauer

Second Supervisor
Ao.Univ.-Prof. Dipl.-Ing. Dr. techn. Karl Gatterer

Graz, April 2018

Affidavit

I hereby declare that I am the sole author of this thesis, that I have not used any sources other those cited, and that I have made explicit reference to the sources of all material that was quoted, whether directly or indirectly. The document uploaded to the TUGraz online platform is identical to this text.

Graz, _____   _____

           Date   Signature

Abstract

In terms of environmental pollutants, sulfuric compounds are one of the major contaminants in hydrocarbon-based fuels. Furthermore, sulfur-containing fuels (e.g. jet and diesel fuels) lead to massive performance degradation when used in fuel-cell-based systems. Therefore, the ultra-deep desulfurization of hydrocarbon-based fuels is of major importance from an environmental, technological, and economical point of view. However, via the currently used hydrodesulfurization process, ultra-deep desulfurization below $10\,ppmw$ of total sulfur is both expensive and inefficient. Several alternative technologies have been investigated in recent years, among which adsorptive desulfurization has shown great potential as a cost-effective and efficient method for the desulfurization of hydrocarbon-based fuels. The simplicity of the adsorptive approach makes it particularly attractive for both stationary and mobile applications.

This thesis focuses on the use of adsorptive on-board desulfurization units to operate solid-oxide-fuel-cell-based auxiliary power units (SOFC-based APUs) with jet and diesel fuels. For the adsorptive approach, silver-based adsorbents are investigated since these types of adsorbents provide the possibility of thermal on-board regeneration in an oxidizing atmosphere. Within this work, several specific aspects of on-board desulfurization and regeneration are considered; thus, this thesis is divided into the following three parts: (i) Identification and characterization of the main adsorption mechanisms, (ii) evaluation and quantification of the desulfurization performance under realistic operating conditions, and (iii) development, characterization, and quantification of a novel and system-integrated regeneration strategy for SOFC-based APUs.

Comprehensive experimental investigations, theoretical considerations, and a wide range of different methods of analysis are used within this work. The major findings are as follows: (i) Three adsorption mechanisms are identified as the major interactions involved in the overall adsorption of sulfur heterocycles on silver impregnated aluminum oxide (Ag-Al_2O_3). The two stronger interactions use silver cations as adsorption sites, whereas the significantly weaker interaction uses acidic centers of the aluminum oxide. However, the incorporation of silver into the porous structure of aluminum oxide significantly increases the number of acidic centers. In addition, (ii) it is found that the selectivity of adsorption is strongly influenced by the type of sulfur heterocycle as well as the presence of polycyclic aromatic hydrocarbons (PAHs), where the latter decreases the adsorption kinetics of the sulfur heterocycle dibenzothiophene. Both

the adsorption selectivity and the influence of PAHs on the adsorption of sulfur heterocycle are thereby influenced by the adsorption temperature. Further, (iii) the novel regeneration approach using hot APU off-gas achieved full regeneration of the adsorption capacity of Ag-Al$_2$O$_3$ over 14 cycles of operation. The regeneration mechanisms identified shows that a higher amount of water in the regeneration gas makes it possible to reduce the regeneration temperature.

These findings provide essential insight into the process of adsorptive desulfurization via silver-based adsorbents. The adsorption mechanisms identified are therefore important for an understanding of different adsorption results under various conditions. This knowledge is essential for the design of on-board desulfurization units and for the synthesis of further optimized adsorbents. The novel and system-integrated regeneration strategy presented herein is thus of major importance for real applications since it is both very efficient and requires no bulky heat exchanger, nor any additional tanks or reagents. In addition, to the best of the author's knowledge this is the first time that full thermal regeneration has been reported for any type of adsorbent in an oxidizing atmosphere after adsorption of dibenzothiophene. All of these findings highlight the fact that adsorptive desulfurization provides the possibility to operate SOFC-based APUs with commercial hydrocarbon-based fuels, such as jet and diesel fuels.

Kurzfassung

Schwefelverbindungen in kommerziellen Kraftstoffen sind verantwortlich für schwerwiegende Umweltverschmutzungen. Darüber hinaus führen schwefelhaltige Kraftstoffe (wie zum Beispiel Kerosin und Diesel) zu massive Degradationserscheinungen bei der Verwendung in Brennstoffzellen-basierten Systemen. Aus diesem Grund ist die Tiefentschwefelung von Kohlenwasserstoff-basierten Kraftstoffen aus ökologischer, technologischer und ökonomischer Sicht von enormer Bedeutung. Allerdings ist die Tiefentschwefelung unter einen Gehalt von $10\,ppm$ Schwefel mit Hilfe der konventionellen hydrierenden Entschwefelung in Raffinerien ineffizient und kostspielig. Aus diesem Grund wird intensiv an alternativen Technologien geforscht. Im Zuge dessen wurde die adsorptive Entschwefelung als effiziente, wirtschaftliche und zukunftsträchtige Technologie identifiziert. Die Einfachheit des Verfahrens ist dabei von besonders großer Bedeutung, sowohl für stationäre, als auch mobile Anwendungen.

Der Fokus dieser Arbeit liegt auf adsorptiven on-board Entschwefelungseinheiten um Hilfsaggregate basierend auf Festoxidbrennstoffzellen (SOFC-APUs) mit Kerosin und Diesel zu betreiben. Für die adsorptive Entschwefelung wurden silberbasierte Adsorbenzien untersucht, da diese die Möglichkeit einer thermischen on-board Regeneration in oxidierender Atmosphäre ermöglichen. In dieser Arbeit wurde im speziellen auf die relevanten Aspekte einer adsorptiven on-board Entschwefelung eingegangen. Dadurch ergeben sich folgende Schwerpunkte: (i) Identifizierung und Charakterisierung der relevanten Adsorptionsmechanismen, (ii) Evaluierung und Quantifizierung der Entschwefelungsperformance unter realitätsnahen Betriebsbedingungen und (iii) Entwicklung, Charakterisierung und Quantifizierung einer neuen und systemintegrierten Regenerationsstrategie für SOFC-APUs.

Im Zuge dieser Arbeit wurden umfangreiche experimentelle Untersuchungen, theoretische Betrachtungen und eine Vielzahl an analytischen Methoden durchgeführt. Folgende Erkenntnisse sind dabei Entstanden: (i) Drei relevante Adsorptionsmechanismen wurden für die Adsorption von heterozyklischen Schwefelverbindungen an Silber imprägniertem Aluminiumoxid (Ag-Al_2O_3) identifiziert. Bei den zwei stärkeren Interaktionen fungieren Silberkationen als aktive Zentren. Die deutlich schwächere Interaktion basiert auf Säurezentren, wobei die Imprägnierung mit Silber die Anzahl der aktiven Säurezentren deutlich erhöht. Zusätzlich zeigte sich, dass (ii) die Selektivität der Adsorption signifikant vom Typ der Schwefelverbindung und der Anwesenheit von polyzyklischen aromatischen Kohlenwasserstoffen (PAHs) abhängig ist,

wobei PAHs vor allem die Adsorptionskinetik der Schwefelverbindungen Dibenzothiophen verringert. Die Selektivität der Adsorption und auch der Einfluss von PAHs wird dabei durch die Adsorptionstemperatur beeinflusst. Darüber hinaus zeigen die Ergebnisse der neuen Regenerationsstrategie basierend auf heißem APU-Abgas (iii) eine vollkommene Regeneration der Adsorptionskapazität von $Ag-Al_2O_3$ über 14 Betriebszyklen. Der identifizierte Regenerationsmechanismus zeigt dabei, dass ein höherer Wassergehalt im Regenerationsgas die Möglichkeit bietet, die nötige Regeneratiosstemperatur zu senken.

Diese Forschungsergebnisse führen zu wichtigen Erkenntnisse über die Vorgänge der adsorptiven Entschwefelung mit Hilfe von silberbasierten Adsorbenzien. Die identifizierten Adsorptionsmechanismen sind dabei von besonderer Bedeutung, um ein tiefgreifendes Verständnis des Verhaltens der Entschwefelungsperformance unter verschiedenen Umständen zu erlangen. Dies ist im Speziellen für die Auslegung von on-board Entschwefelungseinheiten, aber auch für die Optimierung der Adsorbenssynthese essentiell. Die in dieser Arbeit vorgestellte Regenerationsstrategie ist sehr effizient und damit von enormer Bedeutung für reale Anwendungen, da weder sperrige Wärmetauscher, noch zusätzliche Reagenzien und Tanks benötigt werden. Darüber hinaus ist dies, nach bestem Wissen des Autors, die erste Arbeit, die über eine vollständige thermische Regeneration in oxidierender Atmosphäre nach Adsorption von Dibenzothiophen berichtet. All diese Ergebnisse unterstreichen, dass mit Hilfe der adsorptiven Entschwefelung die Möglichkeit geschaffen wird, SOFC-APUs mit kommerziellen Kraftstoffen wie Kerosin und Diesel zu betreiben.

Acknowledgments

Most importantly, all my life and personal career would not have been possible without the unwavering support of my parents, Stefanie, Katharina, and Daniel, and their trust in my abilities. To live does not mean solely to work. Friends are irreplaceable when it comes to getting through hard times and enjoying moments of unrivaled happiness. Thank you to all of my friends for sharing such moments with me.

To my family

Contents

List of Figures

List of Tables

Acronyms

π-Ag π-complexation between sulfur heterocycle and silver cation

π-M π-complexation between sulfur heterocycle and metal cation

-COOH   carboxylic group

-OH   hydroxyl group

4,6-DMDBT   4,6-dimethyldibenzothiophene

AIR_g ambient air

APU   auxiliary power unit

$APU_{g/wet}$ hot off-gas from an auxiliary power unit with 12.4 $mol\%$ H_2O

APU_g hot off-gas from an auxiliary power unit with 4.5 $mol\%$ H_2O

BET   Brunauer-Emmett-Teller

BJH   Barrett-Joyner-Halenda

Boyd's model   film-diffusion model by Boyd [1]

BT   benzothiophene

C_xH_y total hydrocarbons

DBT   dibenzothiophene

DFT   density functional theory

EDX   energy-dispersive X-ray

EHT   extra high tension

FAME   fatty acid methyl ester

FID   flame ionization detector

GHSV   gas hourly space velocity

HDS   hydrodesulfurization

HPLC   high performance liquid chromatography

HSAB theory	hard and soft acid base theory proposed by Pearson [2]
ICP-OES	inductively coupled plasma optical emission spectroscopy
IPD	intraparticle diffusion
LHSV	liquid hourly space velocity
MIP	molecularly imprinted polymer
MOF	metal-organic framework
ODS	oxidative desulfurization
PAH	polycyclic aromatic hydrocarbon
PASH	polycyclic aromatic sulfur heterocycle
PEMFC	proton exchange membrane fuel cell
S-Ag	acid base interaction of the sulfur atom and the silver cation
S-H	acid base interaction of the sulfur atom and a general surface acid group
S-M	acid base interaction of the sulfur atom and the metal cation
SCR	selective catalytic reduction
SEM	scanning electron microscope
SOFC	solid oxide fuel cell
TCD	thermal conductivity detector
TCFR	temperature-controlled flow rate
TPD	temperature programmed desorption
XPS	X-ray photoelectron spectroscopy
XRD	X-ray diffraction

Symbols

Symbol	Description	Unit
A	General adsorption site	-
A_o	Overall aspect ration	-
Bt	A function of $F(t)$	-
B	Boyd number	s^{-1}
C	Experiment specific constant	mg/g
$C_{m,p}$	Specific molar heat capacity	$J/mol\,K$
c	Concentration	ppmw
D_i	Effective intraparticle diffusion coefficient	m^2/s
D	Diameter	m
$F(t)$	Fractional attainment of equilibrium	-
H	Height	m
k_1	Pseudo-first order rate constant	h^{-1}
k_2	Pseudo-second order rate constant	$g/mg\,h$
k_i	Intraparticle diffusion rate constant	$mg/g\,h^{1/2}$
k_{in}	General intraparticle diffusion rate constant	$mg/g\,h^n$
m	Mass	kg
M	Molecular weight	kg/mol
$\dot{Q}$	Heat flux	W
q	Adsorption capacity	mg/g
X	General adsorptive molecule	-
R^2	Correlation coefficient	-

Symbol	Description	Unit
r	Radius of the adsorbent particle	m
ρ	Density	$\mathrm{kg/m^3}$
SV	Space velocity	$\mathrm{h^{-1}}$
T	Temperature	K
ϑ	Temperature	°C
t	Time	s
V	Volume	$\mathrm{m^3}$
$\dot{V}$	Volume flux	$\mathrm{m^3/s}$
x	Mole fraction	mol/mol

Subscripts and Superscripts

ads	Adsorbent
adsorber	Adsorber
air	Ambient air
break	Breakthrough
bulk	Bulk material (adsorbent)
calc	Calculated
eq	Equilibrium
exp	Experiment
fuel	Fuel
final	Final
i	Component *i*
off-gas	Hot off-gas from an auxiliary power unit
operation	Operation
reg	Regeneration
scale up	Scale up
set	Prescribed value
S	Sulfur
t	Time

1

Introduction

This chapter is intended to provide a basic understanding of fuel-cell-based auxiliary power units (APUs) operated with liquid hydrocarbon-based fuels from petroleum feedstock, as well as to establish why the desulfurization of these fuels is essential. Fuel-cell-based APUs can be operated by different liquid hydrocarbon-based fuels, including jet and diesel fuels. For such applications, both low-temperature fuel cells (e.g. proton exchange membrane fuel cells (PEMFCs)) and high-temperature fuel cells (e.g. solid oxide fuel cells (SOFCs)) are feasible. as has been explored by different researchers [3–8].

This thesis focuses on SOFC-based APUs operated with jet or diesel fuels and having a power output of 1 - 10 kW_{el}. Such SOFC-based APUs are a promising source of on-board electricity supply for e.g. trucks, ships, and airplanes. Nonetheless, the desulfurization approach investigated in this work is a basic unit operation, and is thus also relevant for APUs based on low-temperature fuel cells. In addition, the fundamental findings regarding the desulfurization of jet and diesel fuels presented in this work are also relevant for other liquid hydrocarbon-based fuels, such as gasoline and heating oils, and are not limited to on-board applications.

1.1. Motivation

Emissions of sulfur and its derivatives are one of the primary health hazards present in the environment. These emissions are responsible for acid rain and smog, both of which have direct and indirect negative effects on the environment and human beings. As a result, environmental regulations have successively reduced the maximum allowable sulfur levels in fuels. For example, the allowable sulfur levels in diesel fuels in the EU was successively reduced from 500 ppm to 10 ppm between 1996 and 2009 [9]. At the same time, the US Environmental Protection Agency reduced the allowable sulfur levels in diesel fuels from 500 ppm to 15 ppm [9]. However, logistic fuels still contain up to 3000 ppm of sulfur [10].

In addition to the environmental issues, fuel cells are one of the main reasons that desulfurization has gained in relevance in the last decade. Fuel cell systems are not only more efficient, but also generate less emissions and less noise in comparison to conventional combustion engines [11, 12]. Hydrocarbons are still the major feedstock for worldwide H_2 production [13]. Hydrocarbon-based fuels in particular are ideal for on-board applications and decentralized H_2 and syngas production as a result of their high energy density and availability. High conversion yields for H_2 and syngas production can be achieved via catalytic reforming at moderate temperatures (600 - 800 $°C$) [14, 15]. In this step, sulfuric compounds are converted to H_2S. A lot of research has been carried out in order to improve the fuel flexibility of different types of fuel cells and to increase their tolerance of all kinds of contaminants, including H_2S. However, even 10 *ppm* of sulfur leads to degradation in most common types of fuel cells [16]. This means that fuel cells cannot be operated with commercial sulfur containing fuels, and thus, one of the most effective tools for energy conversion is unable to use one of the most common types of fuels. As a consequence, ultra-deep desulfurization of hydrocarbon-based fuels is essential in order to overcome the main drawback of fuel-cell systems' sensitivity to sulfur.

1.2. Auxiliary Power Units (APUs) Based on Fuel Cell Technology

Fuel cells are one of the most effective tools to convert chemical to electrical energy; this technology is based on the electrochemical conversion of a fuel. Different sources of hydrogen and carbon-based compounds, e.g. CO or CH_4, can be used as fuel, depending on the type of fuel cell [17]. Fuel cell technology is not only suitable for stationary approaches [18], but is also an alternative technology for mobile applications. Thus, fuel-cell-based APUs are a promising source of on-board electricity for all kinds of vehicles, ships, and aircraft [11].

The primary advantages of a fuel-cell-based APU are their higher efficiency, reduced emissions, and lower noise generation in comparison to conventional combustion engines [12, 19]. Most vehicles, ships, and airplanes use liquid hydrocarbon-based fuels to operate their main engines. Consequently, it is logical that the fuel-cell-based APU be operated using the same type of fuel that is already available on-board. To operate the fuel cell system, a liquid hydrocarbon-based fuel has to be converted into a hydrogen-rich syngas or even high purity H_2, depending on the type of fuel cell [17]. This conversion can be achieved by means of a catalytic reformer based on partial oxidation [20], steam reforming [21], or autothermal reforming [22], which is a combination of steam reforming and partial oxidation. Within this reforming step, hydrocarbons are transformed into syngas by the addition of O_2 only (partial oxidation) or O_2 and H_2O (steam reforming and autothermal reforming). More information on the relevant reaction mechanisms can be found elsewhere [16, 23]. A schematic flow sheet of an SOFC-based APU is provided in Figure 1.1. Within this basic concept, the liquid fuel is desulfurized before it is transformed into syngas in the reformer unit in order to operate the SOFC stack.

To main engine of e.g. ship, tuck, or airplane

Fuel tank

Desulfurization unit

Reformer → SOFC stack → APU off-gas

Air blower   Water

Basic concept of an SOFC-based APU system
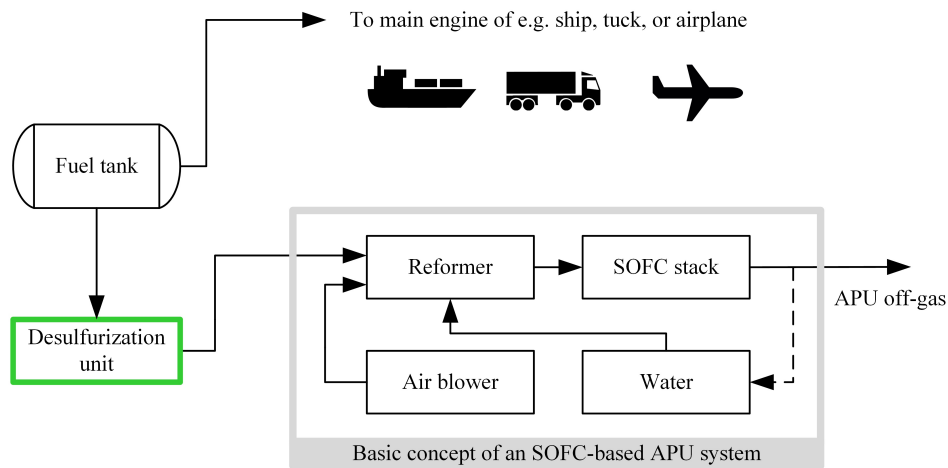
Figure 1.1.: Basic concept of an SOFC-based auxiliary power unit (APU) for ships, trucks, or airplanes.

The catalytic reforming of hydrocarbon-based fuels is part of the fuel processing step. During fuel processing, the hydrogen-rich syngas is typically produced by a Ni catalyst [16]. Further purification of the hydrogen-rich syngas depends on the type of fuel cell. For example, the advantage of high-temperature fuel cells (e.g. SOFCs), is in their tolerance to carbon monoxide in comparison to low-temperature fuel cells (e.g. PEMFC) [12]. Consequently, additional purification of the hydrogen-rich syngas is only necessary when low-temperature fuel cells are used. In the case of SOFCs, no further purification of the hydrogen-rich syngas is necessary. For this reason, this work focuses on SOFC-based APUs. Additional discussion of low-temperature fuel-cell-based APUs can be found in Section 6.5.

As mentioned above, fuel-cell-based APUs with a power output of 1 - $10\,kW_{el}$ are a very promising source of on-board electricity supply. This power range of 1 - $10\,kW_{el}$ is particularly relevant for airplanes, ships, and heavy-duty trucks [24], as indicated in Figure 1.1. The main engines of airplanes, heavy-duty trucks, and ships are usually operated with either jet or diesel fuel, which is why only jet and diesel fuels were used for the experimental investigations within this work. However, it is important to note that the fundamental findings regarding the desulfurization of jet and diesel fuels presented in this work are also relevant for other liquid hydrocarbon-based fuels from petroleum feedstock.

1.3. Sulfur Threshold Limits for SOFC-based APUs

SOFCs are high-temperature fuel cells with operating temperatures of between 600 - $1000\,^{\circ}C$ [25]. These high operating temperatures enable the catalytically activated internal reforming of hydrocarbons, generally to H_2 and CO (basically syngas) together with some CO_2 [26, 27]. Both H_2 and CO are then electrochemically oxidized to CO_2 and H_2O. This is different in the case of low-temperature fuel cells, where even small quantities (10 ppm) of CO are poisoning

[16, 26]. The ability to convert CO to CO_2 is thus a major advantage of SOFCs in comparison to low-temperature fuel cells since it dramatically simplifies the fuel processing unit (no CO clean-up). In addition, the high operation temperature of an SOFC increases its sulfur tolerance to about $1\,ppm$ of total sulfur [16, 28]. This $1\,ppm$ of total sulfur represents the threshold limit for the SOFC stack.

The advantage of on-board reforming is significantly dampened by the fact that commercial hydrocarbon-based fuels contain $10 - 5000\,ppm$ of total sulfur, depending on the class of fuel and the purpose of its use [10]; a more detailed discussion of sulfur in liquid hydrocarbon-based fuels can be found in Sections 2.1 and 2.1.1. As a result of the inconsistency with regard to the sulfur content and sulfur tolerance of commercial hydrocarbon-based fuels and SOFC stacks, respectively, on-board desulfurization is crucial in order to achieve the threshold limit of $1\,ppm$ of total sulfur for the SOFC stack. As shown in Figure 1.1, the reformer is placed upstream of the SOFC stack. Consequently, the total sulfur threshold limit of the reformer catalyst also has to be considered.

Comprehensive research has been carried out over the last decade on increasing the sulfur tolerance of the reforming catalyst [14, 29, 30]. Several researchers have reported the high sulfur tolerance of a newly developed catalyst [22, 31–33]. However, it is interesting to note that there is a tendency for the investigated time on stream in these experiments to decrease as the sulfur level in the feedstock increases [22, 32, 33]. As reported by Murata et al. [34], the activity of the reforming catalyst can decrease suddenly and dramatically after several hours of stable performance. This was observed in experiments with a $Ni/Sr-ZrO_2$ reforming catalyst, where the conversion rate suddenly dropped after $30\,h$ on stream at $3.8\,ppm$ of sulfur [34]. This is an important observation since it underline the importance of long-term experiments. At this point, it is important to emphasize that both operation temperature and steam-to-carbon ratio have a significant influence on the sulfur tolerance of the reforming catalysts [22]. It is thus recommended to keep the sulfur level in the feedstock well below $50\,ppm$ in order to prevent the long-term performance degradation of the reforming catalyst [35, 36].

A sulfur threshold limit of $50\,ppm$ for the reformer is well above the $1\,ppm$ sulfur threshold limit of the SOFC stack. Consequently, the sulfur tolerance of the SOFC stack is the limiting factor with regard to the level of desulfurization required. However, the sulfur concentration in the feed is diluted within the reformer as a result of the chemical conversion of the hydrocarbons and the addition of H_2O and O_2, as shown in Figure 1.2. The overall chemical reaction in Figure 1.2 does not represent the real conversion of fuel to syngas in a reformer unit, but is rather used to show the principle dilution mechanisms of the total sulfur concentration during reforming. The real factor of dilution is 10, as has been reported by several researchers [37, 38]. Consequently, desulfurization of the fuel to $\leq 10\,ppm$ of total sulfur is sufficient to protect both the reforming catalyst and the SOFC stack. This $10\,ppm$ of total sulfur in the liquid fuel is thus defined as the sulfur breakthrough at the outlet of the desulfurization unit within this thesis.

| Fuel | Reforming | Syngas |

$$C_8H_6S + C_8H_{18} + 5\tfrac{1}{2}O_2 + 5H_2O \longrightarrow 16CO + 16H_2 + H_2S$$

$$c_S = 16\,g\text{-}S/mol\text{-}fuel \quad \longrightarrow \quad c_S = 0.97\,g\text{-}S/mol\text{-}syngas$$

Factor of dilution = 16.5 for this principle case
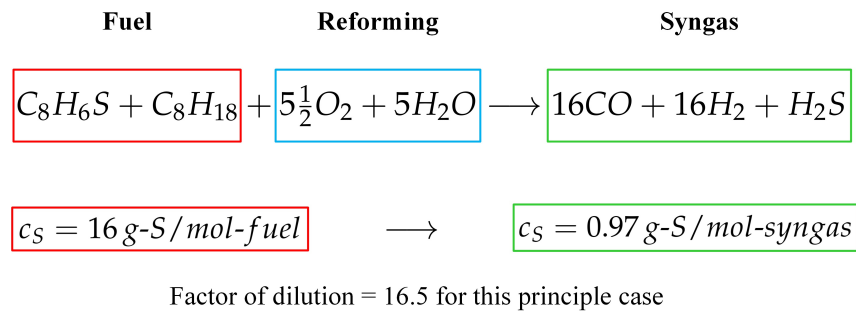
Figure 1.2.: Principle dilution mechanism of the total sulfur concentration during the reforming process.

1.4. Objectives and a Short Outline of the Thesis Structure

This thesis is based on both analytical and experimental investigations of the ultra-deep desulfurization of liquid hydrocarbon-based fuels from petroleum feedstock. As reflected by the title of this work, this thesis will focus on mobile applications, and thus, on on-board desulfurization. The on-board desulfurization unit developed in this thesis is intended to make it possible to operate SOFC-based APUs with a power range of 1 - 10 kW_{el} using commercial jet or diesel fuel. This approach would provide an efficient on-board supply of electrical energy for trucks, ships, or airplanes, even when the main engine is turned off. As a result of this aim, different aspects were considered than would be relevant to large-scale and stationary desulfurization approaches. From this point of view, the following research questions arose:

1. Which desulfurization approach fulfills the specific requirements of on-board applications?
2. What is the mechanism behind this desulfurization process?
3. How is this mechanism influenced by different types of liquid hydrocarbon-based fuels?
4. What is the service/regeneration interval of this desulfurization approach?

This thesis is basically structured according to the order of above questions. Chapter 2 provides more informations so as to develop the questions above in more detail. This includes the characterization of hydrocarbon-based fuels from petroleum feedstock and their sulfuric compounds. Chapter 2 also contains a basic discussion of the most prevalent and industrially relevant hydrodesulfurization (HDS) process and reasonable/potential alternative technologies. Within this short overview of alternative desulfurization approaches, research question 1 is answered, as adsorptive desulfurization is identified as the most promising approach for on-board desulfurization. Chapter 3 provides an overview of the experimental designs and analyses that were carried out and used within this work. More detailed descriptions and the boundary conditions of the experiments are provided where appropriate.

Chapter 4 discusses the fundamentals of adsorption mechanisms at room temperature. This chapter also includes the overall adsorption mechanism proposed for the Ag-Al$_2$O$_3$ adsorbent,

based on three individual interactions and thus provides the answer to research question 2. This answer constitutes an important finding since it provides the basic understanding necessary for further adsorbent optimizations and simulations. The proposed overall adsorption mechanism is based on findings reported in literature as well as the comprehensive theoretical considerations and experimental investigations carried out within this work. In addition, Chapter 4 also discusses the experimental investigations at equilibrium.

Chapter 5 answers research question 3 by discussing the dynamic adsorption behavior of Ag-Al$_2$O$_3$ under a wide range of reasonable conditions. This includes investigations of the adsorption kinetics, the influence of the jet and diesel fuels' composition, as well as important operating conditions. Chapter 6 focuses on reasonable on-board regeneration strategies. Within this chapter, a novel and system-integrated regeneration strategy based on hot APU off-gas is presented and studied. This discussion includes the proposed overall regeneration mechanisms under APU off-gas conditions. With this novel approach, full adsorbent regeneration was achieved over 14 cycles of regeneration without any evidence of performance degradation. This is an excellent result and underlines the importance of this work. Chapter 6 also answers research question 4, which is of great interest to real applications. In Chapter 7 of this thesis, the new findings and results were used to design a basic on-board desulfurization unit for a 5.5 kW_{el} SOFC-based APU. This chapter is intended to outline the suitability of the identified desulfurization concept for on-board desulfurization. The final, Chapter 8, summarizes the findings in this thesis and provides possible answers to the research questions in a condensed form.

2

Hydrocarbon-based Fuels and Related Desulfurization Technologies

This chapter is intended to provide more fundamental information about hydrocarbon-based fuels from petroleum feedstocks as well as their sulfuric compounds. In addition, this chapter gives a short overview of both the conventional hydrodesulfurization (HDS) process and alternative approaches, with a focus on adsorptive desulfurization. It thus provides an answer to research question 1: which desulfurization approach fulfills the specific requirements of on-board applications?.

2.1. Hydrocarbon-based Fuels from Petroleum Feedstocks

Hydrocarbon-based fuels from petroleum feedstocks can be categorized into three main refining streams: naphtha (gasoline), kerosene (jet fuel), and gas oil (diesel) [39]. Gasoline is a complex mixture of hydrocarbons with a typical boiling range of 38 - 205 °C [40]. Jet and diesel fuels are typical streams of the middle distillate fraction [38]. Jet fuel in particular is a blend of the middle distillate, with a narrower boiling range of 140 - 280 °C in comparison to diesel fuel [38, 40]. Anti-oxidants, metal deactivators, static dissipaters, corrosion inhibitors, icing inhibitors, biocides, and thermal stabilizers are commonly added to jet fuels [41]. The primary source of jet fuel blending stocks is the kerosene fraction from atmospheric crude oil distillation since stringent smoke-point specifications limit the amount of cracked feedstock that can be used [40]. This is also why jet fuel typically contains lower amounts of polycyclic aromatic hydrocarbons (PAHs) in comparison to diesel, as seen in Table 2.1.

Jet fuel denotes several commercial and military fuels, of which the most important are represented by (i) jet A, (ii) jet A-1, and (iii) JP-8. The difference between jet A and jet A-1 is the slightly lower freezing point of jet A-1 (-47 °C), which is the jet fuel used internationally for civil aviation. Jet A, on the other hand, is used primarily within the US. JP-8 is the common military jet fuel in the western part of the world, and only differs from jet A-1 in its

Table 2.1.: Typical content of monoaromatics and PAHs in jet and diesel fuel.

Fuel	Monoaromatics	PAHs
Jet fuel[a]	15 - 25 $vol.\%$	0.1 - 1.7 $vol.\%$
Diesel fuel[b]	15 - 25 $wt.\%$	4 - 10 $wt.\%$

[a] Ref. [42–44]

[b] Ref. [45, 46]

additive composition [38]. Diesel fuel has a boiling range of 180 - 400 °C, and includes several subcategories, such as automotive diesel fuel and railroad diesel fuel [40]. The main feedstocks of diesel fuel are the middle distillate and cracked stocks.

All hydrocarbon-based fuels from petroleum feedstocks contain a wide range of different non-sulfuric aromatic compounds. These compounds are monoaromatics, PAHs, and heterocyclic aromatics. Typical compounds of these groups are shown in Table 2.2.

Table 2.2.: Overview of typical non-sulfuric aromatic compounds in commercial diesel fuel.

Aromatics	Typical compounds[a]	Range of content ($wt\%$)[b]
Monoaromatics	Alkylated benzenes such as toluene	15-25
PAHs	Naphthalene, fluorene, phenanthrene	4-10
Heterocyclic aromatics (N)	Indole, quinoline, carbazole	ppm level

[a] Ref. [45, 47, 48]

[b] Ref. [45, 46]

The overview provided in Table 2.2 reflects the contents of commercial diesel fuel. Jet fuel contains similar compounds, but the range of content is different: the content of PAHs in particular is significantly lower in comparison to diesel fuel, as was shown in Table 2.1.

2.1.1. Sulfur in Hydrocarbon-based Fuels from Petroleum Feedstocks

The sulfur content of crude oil is in the range of 0.05 - 10% [49], with a world average content of about 1.25% [40]. The sulfur content and compounds in crude oil differ depending on the source of crude oil. The common types of organosulfur species are mercaptans (thiols), sulfides, disulfides, and thiophenes. After the crude oil is refined into the three main refining streams, naphtha (gasoline), kerosene (jet fuel), and gas oil (diesel), the sulfur content is reduced in a desulfurization step (typically HDS) so as to meet the fuel-specific requirements. Typical sulfur

compounds in commercial fuels include thiophene, benzothiophene (BT), dibenzothiophene (DBT), and their derivatives, such as 4,6-dimethyldibenzothiophene (4,6-DMDBT); the presence or absence of particular sulfur compounds depends on the type of fuel. An overview of the corresponding sulfur heterocycles is provided in Table 2.3.

Table 2.3.: Types of fuels and their corresponding sulfur heterocycles [50].

Type of fuel	Type of sulfur heterocycles
Gasoline	Thiophene, BT and derivatives
Jet fuel	BT, and derivatives
Diesel fuel	BT, DBT, and derivatives such as 4,6-DMDBT

After HDS, the sulfur levels of liquid fuels are in the range of 10 - 5000 ppm, depending on the type of fuel and the correlated legal requirements [10]. A more detailed description of fuel desulfurization, including the industrially relevant HDS process, is provided in the following sections.

2.1.2. Commercial Hydrodesulfurization (HDS)

Hydrodesulfurization (HDS) is the most prevalent and industrially relevant process currently used to desulfurize the common refinery streams to a particular level of total sulfur. This HDS technology consists of a catalytic process under severe conditions, including temperatures of 300 - 400 °C and an H_2 operating pressure of 20 - 100 bar [50, 51]. Typical catalysts are CoMo/γ-Al$_2$O$_3$ and NiMo/γ-Al$_2$O$_3$ [52, 53]. Within this catalytic process, the sulfur compounds undergo a direct (hydrogenolysis) or hydrogenation pathway, as shown in Figure 2.1, to form hydrocarbons and H_2S gas [39, 52]. The H_2S gas is then removed by means of amine washing, using the Claus process [52].
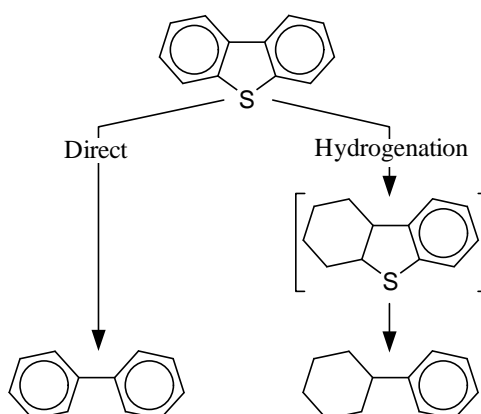
Figure 2.1.: Reaction pathways for the catalytic HDS process [53].

Within the hydrogenation pathway, prehydrogenation of one aromatic ring is followed by extraction of the sulfur atom, as shown on the right side of Figure 2.1 [53]. Knudsen, Cooper, and Topsøe [53] reported that NiMo-based catalysts have a relatively higher selectivity for

desulfurization via the hydrogenation pathway, whereas CoMo-based catalysts desulfurize primarily via the direct route. Within the direct pathway, the sulfur atom is directly extracted from the molecule, as shown on the left side of Figure 2.1. However, this direct pathway is diminished when alkyl groups are attached to the carbon atoms next to the sulfur atom [53]. As pointed out by C. Song [50, 54], the reactivity of the HDS reactions generally decreases as the size and complexity of the sulfur containing molecule increases, which is illustrated in Figure 2.2. Consequently, even more severe conditions (higher temperatures and higher H_2 operating pressure) are required to desulfurize heavier feeds containing polycyclic aromatic sulfur heterocycles (PASHs), such as BT, DBT, and their derivatives. Hence, the majority of sulfur containing compounds after HDS are the less reactive ones. This is also why the PASHs of jet fuel are typically BT and its derivatives, whereas the typical PASHs of diesel fuel are DBT and its derivatives, as shown in Figure 2.2.
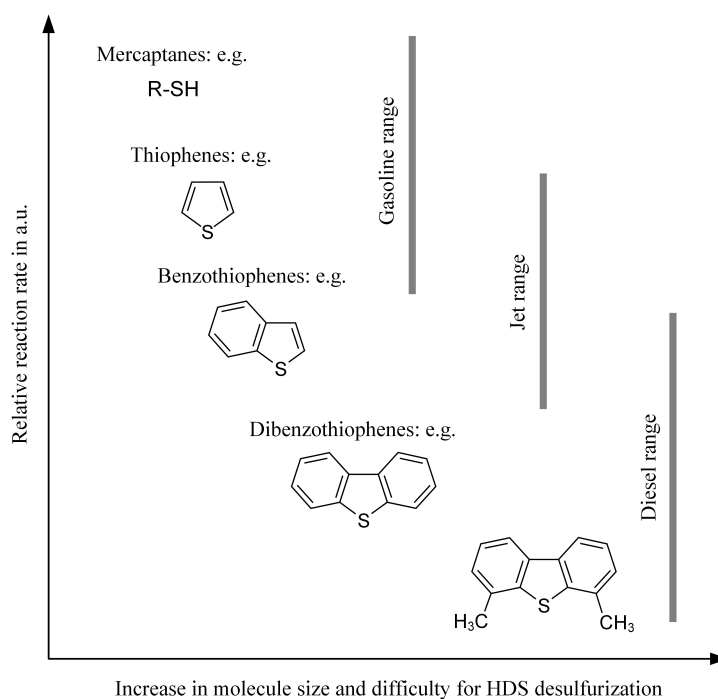
Figure 2.2.: Influence of molecular size and structure on HDS reactivity [54].

Due to increasingly stringent regulations regarding the sulfur content of fuels, the desulfurization of hydrocarbon-based fuels has become an area of great interest to researchers over the last decade. Total desulfurization by means of HDS would be possible by increasing the severity of the reaction conditions; however, this would create several problems, including increased capital and operating costs, decreased catalyst cycle length, and more hydrogen consumption [55]. Several alternative desulfurization technologies have already been investigated for their potential to overcome the inefficient conversion of the more complex PASHs under mild conditions. An overview of these different technologies is provided in the next section.

2.2. Alternative Desulfurization Technologies: A Short Review

Apart from HDS, different desulfurization technologies have been developed, rediscovered, and investigated in recent years. These technologies vary in terms of their efficiency, operating conditions, and whether they use additional reactants or not. The focus of all such alternative technologies is to overcome the drawback of HDS' poor performance when it comes to the desulfurization of PASHs. The ultra-deep desulfurization of jet and diesel fuels below 10 ppm of total sulfur is particularly challenging thanks to their high concentrations of BT, DBT, and their derivatives (cf. Table 2.3 and Figure 2.2). The following review of alternative desulfurization technologies is intended to provide an answer to research question 1: Which desulfurization approach fulfills the specific requirements of on-board applications?

2.2.1. Extraction

Desulfurization via extraction has been studied by several researchers in recent years. A wide range of different solvents have been investigated to extract organic sulfur compounds from hydrocarbon-based fuels, ranging from common polar organic solvents to ionic liquids [56]. The main advantages of extraction over HDS is the simple process design and mild (ambient) operating conditions [57, 58]. In this process, a suitable solvent, e.g. ionic liquids or an aqueous solution of hydrochloric acid or nitric acid [58, 59], is mixed with the fuel. With proper mixing, the PASHs are transferred to the solvent phase due to their higher solubility. After phase separation, the solvent is regenerated via distillation. However, the reported results show poor selectivity with this method, achieving less than 50% desulfurization in one extraction cycle. This is due to the fact that the polarity of PASHs is too close to other non-sulfuric aromatic compounds [56].

2.2.2. Oxidative Desulfurization

In order to increase the selective extraction of PASHs, oxidative desulfurization (ODS) is one of the oldest desulfurization technologies [60]. In the first step of ODS, the PASHs are oxidized to form the corresponding sulfoxides and sulfones by means of a suitable oxidant, leading to polar compounds. This first oxidation step can be activated using different catalysts, such as acetic acid, formic acid, sulfuric acid, phosphotungstic acid, or V_2O_5 [51, 61, 62]. In the second step, the sulfoxides and sulfones are separated via extraction or adsorption. This multi-stage process requires a continuous supply of an oxidant such as H_2O_2, which represents a major drawback for mobile applications.

2.2.3. Pervaporation

Pervaporation is a common separation technique for organic-organic mixtures [63] and is already used commercially for desulfurization in Grace Davison's S-brane process [64]. In the case of desulfurization, this separation technique is based on the use of a non-porous polymeric membrane that usually serves as the separating barrier [65, 66]. When the fuel feed is in contact with the membrane, the sulfuric compounds can be separated due to the higher affinity and/or quicker diffusivity in the membrane. During this separation process, the hydrocarbons and the sulfur species adsorb into the membrane with various affinities, permeate through the membrane, and can be collected as the permeate. Consequently, both the more permeable species (sulfuric compounds) in the permeate stream and the less permeable compounds (hydrocarbons) in the feed can be concentrated. In order to increase both permeability (productivity) and selectivity (separation efficiency), hybrid membranes have begun to be investigated in recent years [67]. However, at reasonable operating conditions, the selectivity of the membranes are still too low to achieve a total sulfur threshold of $\leq 10\,ppmw$ in the hydrocarbon feed [68]. This is also the major drawback of desulfurization via pervaporation for mobile applications. To overcome this drawback, Y. Wang et al. [69] proposed a two-stage desulfurization process, combining a membrane separation unit with a subsequent adsorption unit as a polishing step. However, such a combined desulfurization unit is a much more complex system than a single-step desulfurization unit, and would require additional equipment, such as a vacuum pump and condenser [65, 69]. Thus, the increased complexity of a two-stage process, along with the additional equipment necessary, and the question of the membrane's durability [68] all constitute the main reasons why pervaporation is less than attractive for on-board desulfurization units.

2.2.4. Biodesulfurization

In addition to physical methods, biodesulfurization is an alternative desulfurization approach. Two different pathways are investigated: both the destructive and non-destructive pathways. In the destructive pathway, the target molecule is biologically oxidized, wherein the molecule is destructed in multiple steps. Additional attempts have been made to isolate bacterial strains that would remove the sulfur in a non-destructive way. However, such non-destructive attempts have been futile so far. A more in-depth overview of biodesulfurization is provided in Ref. [70]. In general, reports on biodesulfurization have not successfully accomplished efficient desulfurization to sulfur levels as low as $10\,ppm$ [55]. Thus, the major challenge for biodesulfurization is to isolate or design microbial strains that are more efficient [51].

2.2.5. Adsorptive Desulfurization

Adsorptive desulfurization is one of the simplest alternative approaches, which makes it a very promising approach when used as a polishing step after HDS to produce ultra-low-sulfur fuels in a cost-effective process. This approach is based on the interaction of adsorptives from the bulk phase with the surface of the adsorbent. In the case of selective interactions, the adsorbent surface is enriched with the target compounds of adsorptives, which turn into adsorbates once adsorbed. In the case of adsorptive desulfurization, the target adsorptives are the sulfuric compounds. With this technology, two different approaches are possible: reactive and non-reactive adsorption. In the reactive pathway, the sulfur atom is split off from the adsorptive and remains on the surface of the adsorbent as an adsorbate, while the remaining hydrocarbon is recovered. Usually this approach works at high temperatures and requires a more complex system, and is thus more appropriate for stationary applications. Examples of these high temperature/reactive approaches are "TReND" and "Z-Sorb" [50]. In the non-reactive pathway, the organosulfur compound adsorbs as a whole. This simple process can be efficiently operated at temperatures as low as $20\,^{\circ}C$.

Figure 2.3 shows a possible implementation of adsorptive desulfurization in the current fuel processing system. After the refining of crude oil and the HDS step, ultra-low-sulfur fuels can be produced by an additional and stationary desulfurization step in the refinery. This would be an efficient way to provide ultra-low-sulfur fuels for commercial use in fuel-cell-based systems, for example. However, the implementation of an additional desulfurization process is also related to policy decisions in terms of whether the allowed sulfur content in fuels is reduced to $< 1\,ppm$ of total sulfur. This is particularly essential for systems driven by low-temperature fuels cells. Independent of policy decisions, mobile desulfurization units provide full flexibility. For example, adsorptive on-board desulfurization makes it possibility to use any type of commercial hydrocarbon-based fuel to operate any type of fuel-cell system.

From the discussion above, it becomes clear that adsorptive desulfurization is the most promising approach for on-board desulfurization units. Its fuel flexibility and simplicity can be seen as major advantages in comparison to other approaches. Hence, adsorptive desulfurization is the answer to research question 1: which desulfurization approach fulfills the specific requirements of on-board applications? Extensive research has been carried out and is still ongoing to improve the selectivity and adsorption capacity of organosulfur compounds. The focus of recent activities is, in particular, the development and investigation of new adsorbents. However, very few studies consider the additional requirements of fuel-cell-based APUs and small stand-alone systems with a power range of 1 - $10\,kW_{el}$. These systems require simple process design and in situ adsorbent regeneration to keep the whole system small and light. The following section provides an overview of different adsorbent formulations as well as their advantages and disadvantages in terms of the on-board desulfurization of hydrocarbon-based fuels from petroleum feedstocks.
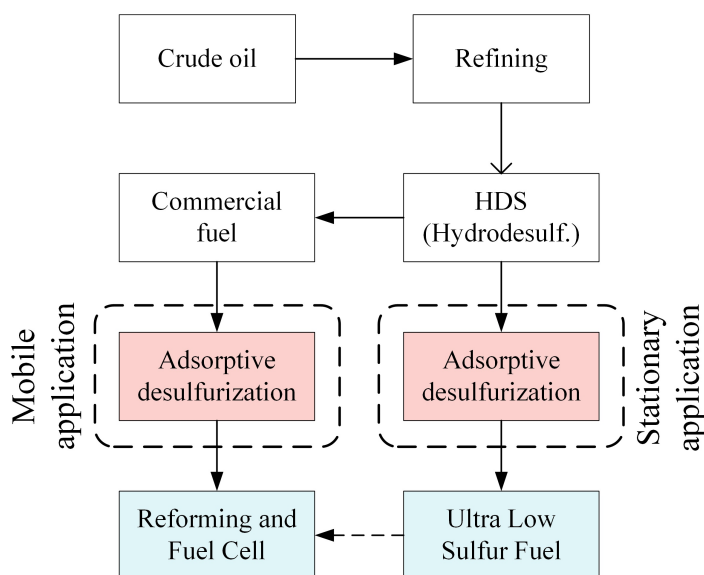
Figure 2.3.: Adsorptive desulfurization as part of the current fuel processing system.

2.2.6. Adsorptive Desulfurization: Composition and Preparation of Adsorbents

As mentioned above, extensive research has been carried out and is still ongoing in the effort to develop and prepare an efficient, highly selective, and cheap adsorbent. Improving the selectivity and adsorption capacity are still major issues that need to be resolved. This section is intended to provide a comprehensive overview of the current state of knowledge of adsorbent formulations for the adsorptive desulfurization of liquid hydrocarbon-based fuels from petroleum feedstocks. However, a complete comparative analysis of the different kinds of adsorbents is difficult because the differences in experimental conditions, fuel properties, such as sulfur compounds and concentration, as well as adsorbent formulation all have a significant influence on their overall performance [39]. An overview of the complexity of the adsorbent formulation is provided in Figure 2.4, which shows that the choice of support material, for example, influences the thermal stability and, further, the incorporation of additional functional groups, which then determine whether this adsorbent requires activation in a reducing or an oxidizing atmosphere. Thus, this section is structured according to the most influential parameters: support material, thermal stability, reaction pathway, additional functional groups, and activation, as illustrated in Figure 2.4.

The support material provides the essential porous structure, and should have a high specific surface area. Most of the adsorbents used in literature are based on zeolites, metal oxides, or activated carbon from different sources. Recently, metal-organic frameworks (MOFs) [71, 72] and molecularly imprinted polymers (MIPs) [73] have also attracted considerable attention. Carbon materials are well known as adsorbents from different adsorption processes. Activated carbon from different sources is one of the least expensive adsorbent materials among all commercial options. Desulfurization experiments with activated carbon have shown promising results for model fuels [74, 75]. However, selectivity towards organosulfur compounds is still a major
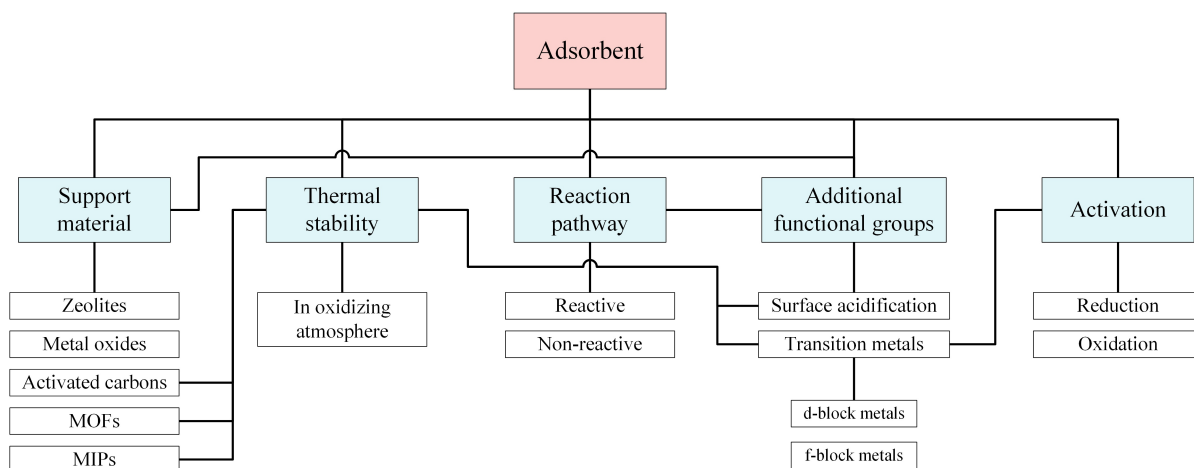
Figure 2.4.: Complexity of adsorbent formulation.

challenge, as can be seen from results using commercial fuels [45, 76]. Different modifications have been investigated that attempted to increase the functionality of carbon-based materials as a sulfur adsorbent [48, 77, 78]. In addition to activated carbons, ordered mesoporous carbon has also been investigated as an adsorbent for desulfurization [79]. The advantages of its regular mesoporous pore structure and narrow pore size distribution are dampened by its higher costs for preparation. MOFs have similar advantages compared to ordered mesoporous carbons. In recent studies, MOFs have been used as adsorbents for organosulfur compounds and shown promising results [71, 80]. A major drawback of all carbon-based adsorbents is their lack of thermal stability. High temperatures cause both surface reduction and pore collapse, thus limiting their thermal regeneration performance [74, 81–83]. Zeolites and metal oxides have a high thermal stability even in oxidizing atmospheres [84–86], and thus provide the possibility of thermal regeneration in oxidizing atmospheres. This is important because reducing gases are not available in the case of on-board applications.

As outlined in Section 2.2.5, adsorptive desulfurization can occur via two reaction pathways: the reactive pathway and the non-reactive pathway. The reactive pathway is strongly dependent on higher operating temperatures ($> 100\,^\circ C$) and the type of additional functional groups, as shown in Figure 2.4. For example, adsorption via the reactive pathway with Ni/ZnO-Al$_2$O$_3$ adsorbent showed good desulfurization performance at $350\,^\circ C$ in the presence of hydrogen [87]. Efficient desulfurization in the absence of hydrogen was also reported for Ni-based adsorbents in the temperature range of 150 to $220\,^\circ C$ [88–90]. Low-temperature adsorption is preferred for various applications, such as mobile and small stand-alone systems. Adsorption via π-complexation (non-reactive pathway), as proposed by Hernández-Maldonado and R. T. Yang [91], works at temperatures as low as $20\,^\circ C$.

As discussed above, high selectivity is still a major issue. This is why additional functional groups are incorporated into the porous structure of the support materials. These functional groups are mainly composed of transition metals. In addition, surface acidification via different

techniques had a positive effect on the overall adsorption of the basic organosulfur compounds, such as BT and DBT [92, 93]. Different transition metals are primarily incorporated by wet impregnation [41, 94, 95]. Table 2.4 provides a comprehensive overview in alphabetical order of which transition metals were studied to increase the selectivity and adsorption capacity of different types of support materials. It is important to mention, that the listed elements do not represent the actual chemical state, but rather the element involved in the adsorbent synthesis.

Table 2.4.: Overview of different transition metals that were investigated for the adsorptive desulfurization of liquid hydrocarbon-based fuels.

Transition metal	References
Ag[a]	[41, 85, 94–120]
Au[a]	[121]
Ce[b]	[35, 95, 100, 108, 116, 117, 122–132]
Co[a]	[78, 101]
Cu[a]	[41, 68, 72, 78, 82, 89, 91, 101, 104, 113, 117, 128, 132–147]
Fe[a]	[41, 113, 125, 131, 148]
La[b]	[122, 141]
Mn[a]	[41, 101]
Mo[a]	[130, 149]
Ni[a]	[35, 36, 47, 87, 89, 90, 100, 101, 113, 117, 124, 126, 129, 130, 136, 139, 141, 150–161]
Pd[a]	[137, 143]
Pt[a]	[162, 163]
Ti[a]	[94, 102, 123, 127, 164]
Zn[a]	[72, 87, 113, 117, 125, 139, 141]

[a] d-block metal in the periodic table

[b] f-block metal in the periodic table

For example, Danmaliki and Saleh [131] reported that loading the activated carbon with Ce via thermal co-precipitation significantly improved adsorption performance in comparison to blank activated carbon. Ion exchange of an ultrastable zeolite Y (a synthetic faujasite) with La significantly increased the adsorption capacity for thiophene and BT [141] from modeled fuel. Other experiments with ion-exchanged zeolites showed very good adsorption capacities for both modeled and real transportation fuels [165, 166]; in particular, the ion exchange of d-block metals, such as Cu and Ag, led to the increased adsorption capacity of organosulfur compounds [113, 128]. Many other metals from the d and f-block of the periodic table were incorporated into the porous structure of different types of support materials, as can be seen in Table 2.4. The detailed experimental conditions, observed selectivities, and adsorption capacities can be found in the corresponding references. Alongside d-block metals, metal halides can also form

π-complexation, as was reported by Y. Wang, R. T. Yang, and Heinzel [137]. For example, the high adsorption capacity of a palladium-halide-based adsorbent was demonstrated for jet fuel [137] and gasoline [163] at room temperature.

Almost all adsorbents have to be dried at around $100\,^{\circ}C$ after additional functional groups are incorporated, in order to remove solvents from the synthesis process. Depending on the precursor of the transition metal and the synthesis method, further thermal treatment may be required for most of the adsorbents to transform the additional functional groups into their active forms. The activation step is carried out between 190 and $550\,^{\circ}C$ in either a reducing or an oxidizing atmosphere [94, 96, 102, 128, 154]. This adsorbent characteristic is referred to as "Activation" in Figure 2.4 and is related to the chemical state of the adsorbent. Hence, adsorbents can be classified according to their active state in (i) reduced and (ii) oxidized adsorbents. For example, Cu-based adsorbents need to be reduced in order to obtain Cu(I) oxide as the active phase [91]. The active Cu(I) oxide is obtained through the thermally induced reduction of Cu(II) in a H_2 or He atmosphere at temperatures between 190 and $231\,^{\circ}C$ [91, 128]. A similar reduction has to be done, for example, when Ni is used as the active compound [36, 154, 167]. Silver is one of the transition metals that forms additional functional groups, which are transformed into the active phase by means of calcination in oxidizing atmospheres [94, 97]. Besides Ag, Ce, Fe, and Mn were also investigated in their oxidized forms, but were found to achieve lower adsorption capacities in comparison to Ag [41, 100]. In addition, S. Nair and Tatarchuk [101] showed that Ag performed significantly better as the active compound than Ni and Cu when these metals were incorporated into porous SiO_2 and subsequent calcined in ambient air.

The adsorbent characteristic of "Activation" is of only minor importance as long as the desulfurization unit is part of a large plant, in which reducing gases such as N_2 or H_2 are easily available. However, this work focuses on mobile desulfurization units for e.g. trucks, ships, or airplanes, which do not typically carry any of those reducing gases. Consequently, adsorbents which are active in their reduced forms do not allow of on-board regeneration since these adsorbents would require subsequent activation via reduction. As described above, Ag exhibited the best desulfurization performance of all transition metals when the adsorbent was transformed into the oxidized form via calcination. Thus, this work focuses on Ag-based adsorbents since these provide the possibility of on-board regeneration. The importance of adsorbent regeneration for on-board desulfurization units is elaborated upon in the following section.

2.2.7. Adsorbent Regeneration

The sulfur adsorption capacity at breakthrough for different adsorbents is reported to be in the range of 0.22 to 12.6 *mg-S/g-ads* for real fuels [168], and is thus significantly lower

in comparison to other adsorption processes. For example, a SO_2 adsorption capacity of more than $1000\,mg/g$ is reported in Ref. [169]. This is why adsorbent regeneration in the context of adsorptive desulfurization has been increasingly discussed within the scientific community in recent years. Effective adsorbent regeneration is of major importance for on-board desulfurization units in particular since constantly replacing the adsorbent is both inefficient and significantly increases operating costs.

There are two main types of regeneration strategies: (i) solvent-based and (ii) thermal regeneration. Solvent-based regeneration refers to the ability of different solvents to elute the adsorbed compound. This solvent-based approach has been explored in many studies, in which different polar solvents were used. Common solvents are benzene [137, 166], toluene [170, 171], diethyl ether [103, 112], and acetonitrile [149, 164]. After adsorbent regeneration, the solvent itself needs to be regenerated; thus, an additional operation step is required. For this reason, solvent-based regeneration strategies are not suitable for on-board applications, as they would require an additional solvent regeneration unit and large tanks to store both the fresh and used solvent.

Thermal regeneration, on the other hand, is based on the thermal decomposition of adsorbed organosulfur compounds, which are then desorbed from the surface. This approach is especially interesting for fuel-cell-based APUs with a power output of 1 - $10\,kW_{el}$ and stand-alone systems where no solvents are available. Thermal regeneration can be performed in different gas atmospheres, which can have a significant influence on regeneration performance [98]. Typical gas atmospheres are N_2 [72, 172], He [35, 82], H_2[90, 162], or ambient air [74, 101]. The choice of the gas atmosphere depends in particular on the chemical state of the active phase of the adsorbent, and whether it needs reduction or not. As outlined in Section 2.2.6, reducing gases are not available for the on-board desulfurization units that are integrated into fuel-cell-based APUs in trucks, ships, or airplanes. Consequently, only thermal regeneration in an oxidizing atmosphere (e.g. ambient air) is suitable for on-board applications. A more detailed description of the thermal stability and chemical state of the active phase of adsorbents is provided in Section 2.2.6.

Thermal regeneration in an oxidizing atmosphere is still a major issue in the field of adsorptive desulfurization. The problem is based on two properties of this process: (i) selectivity during adsorption and (ii) the thermal stability of the adsorbent during regeneration. Higher adsorption selectivity would increase the adsorption capacity, which is often combined with a stronger adsorbate-adsorbent interaction. For regeneration, the strong adsorbate-adsorbent interaction needs to be broken down, and thus requires a high energy input. Consequently, full regeneration risks thermally destructing the adsorbent. This is why the overall adsorption and desorption mechanisms need to be thoroughly investigated to gain deeper insight into the chemical surface reactions. Within this work, every effort was made to provide a greater understanding of the overall adsorption and desorption mechanisms of silver-based adsorbents. Additionally, this work investigates and presents a novel regeneration strategy, which

shows very promising results and fulfills all of the requirements for full integration into a 1 - $10\,kW_{el}$ SOFC-based APU for trucks, ships, or airplanes operated with jet or diesel fuels. These regeneration experiments are intended to provide an answer to research question 4: what is the service/regeneration interval of this desulfurization approach?

Chapter 3 provides detailed descriptions of the experimental investigations as well as all relevant boundary conditions, such as adsorbents synthesis, fuel properties, and investigated regeneration gases. This information is important in order to understand the results that will subsequently be presented and discussed. In addition, all methods of analysis used within this work are defined in Chapter 3.

3

Adsorbent Synthesis and Related Experiments

This chapter provides relevant information on all of the experimental investigations carried out within this work. This includes adsorbents synthesis, characterization of the investigated fuels and other reagents, as well as detailed descriptions of all experiments. These experiments are necessary in order to answer the research questions on page 5 of this work. All of the experiments were carried out several times in order to ensure high reproducibility. In addition, all sample preparations and methods of analysis are described at the end of this chapter.

3.1. Adsorbent Preparation and Physical Properties[1]

Two different types of metal oxides were investigated as support materials: γ-Al$_2$O$_3$ and anatase TiO$_2$. All samples were obtained from commercial suppliers. The five different γ-Al$_2$O$_3$ supports are consecutively numbered as Al$_2$O$_3$/1 - Al$_2$O$_3$/5, as listed in Table 3.1. The two different TiO$_2$ supports are designated as TiO$_2$/1 and TiO$_2$/2. The Brunauer-Emmett-Teller (BET) surface of the TiO$_2$ supports was in the range of 40.7 - 124.0 m^2/g, and thus significantly lower in comparison to the γ-Al$_2$O$_3$ supports with a BET surface of 163.8 - 268.8 m^2/g. The material properties of all supports are provided in Table 3.1, including the BET surface, Barrett-Joyner-Halenda (BJH) pore volume, and mean pore diameter.

All support materials were used as received (no crushing) and dried at 110 $^\circ C$ for 6 h under atmospheric conditions before further modifications were made. The blank γ-Al$_2$O$_3$ and anatase TiO$_2$ supports used in the equilibrium saturation experiments (see Section 3.3.1) were both calcined at 450 $^\circ C$ for 2 h before every experiment.

---

[1] Parts of this section were published in *Energy & Fuels* under the title "Adsorptive Desulfurization: Fast On-Board Regeneration and the Influence of Fatty Acid Methyl Ester on Desulfurization and in Situ Regeneration Performance of a Silver-Based Adsorbent" [96].

Table 3.1.: Properties of various γ-Al$_2$O$_3$ and anatase TiO$_2$-based support materials used within this work. Additional information, such as product name and vendor, is provided in the appendix in Table A.1

Designation	Support	Shape	BET surface (m^2/g)	BJH pore volume (cm^3/g)	BJH mean pore diameter (nm)
Al$_2$O$_3$/1	γ-Al$_2$O$_3$	1.5 mm spheres	163.8	0.47	11.4
Al$_2$O$_3$/2	γ-Al$_2$O$_3$	1.6 mm pellets	184.7	0.58	12.5
Al$_2$O$_3$/3	γ-Al$_2$O$_3$	1.6 mm extrudates	268.0	0.88	8.5
Al$_2$O$_3$/4	γ-Al$_2$O$_3$	1.4 mm pellets	254.6	1.11	10.8
Al$_2$O$_3$/5	γ-Al$_2$O$_3$ [a]	2 mm pellets	214.0	1.04	11.7
TiO$_2$/1	anatase TiO$_2$	1.6 mm pellets	40.7	0.32	37.8
TiO$_2$/2	anatase TiO$_2$	1.6 mm extrudates	124.0	0.57	32.5

[a] 4.5% CaO, 1% MgO, 0.5% SiO$_2$

An aqueous solution of AgNO$_3$ was used as a silver precursor to incorporate additional functional groups into the porous structure of all the support materials listed in Table 3.1. Silver was used as the active compound because it requires no activation in a reducing atmosphere, and can thus be regenerated in an oxidative atmosphere without additional activation, as discussed in Section 2.2.6. This is a major advantage for on-board desulfurization units in particular, where no reducing atmospheres are available. The aqueous solution of AgNO$_3$ was prepared by dissolving solid AgNO$_3$ of 99% purity (Alfa Aesar) in deionized water in a spray bottle made of amber glass. The elemental silver content was 12 wt.% at time of impregnation, and the volume of the solution was equal to 100% of the pore volume of the corresponding support material. For example, 1.8901 g of AgNO$_3$ was dissolved in 4.70 ml of deionized water in order to impregnate 10 g of Al$_2$O$_3$/1. For the impregnation, the dried support was sprayed with the aqueous AgNO$_3$ solution while the support particles were being thoroughly mixed. After infiltration in a sealed glass vessel for 14 h, the adsorbent was dried and calcined at 110 and 450 $°C$ in atmospheric conditions for 6 and 2 h, respectively.

3.2. Fuels and Sulfur Compounds

In this work, several different fuels were used to investigate the influence of fuel composition on the adsorption behavior of different types of PASHs. For this investigation, three different types of PASHs were used, including BT (Alfa Aesar, 98% purity), DBT (Alfa Aesar, 98% purity), and 4,6-DMDBT (Alfa Aesar, 97% purity). These three types of PASHs are representative sulfur heterocycles for commercial hydrocarbon-based fuels from petroleum feedstocks. BT is a typical compound in lighter refining streams, such as naphtha (gasoline) and kerosene (jet fuel), whereas DBT is related to gas oil (diesel) [50]. The 4,6-DMDBT compound is known to be one of the most challenging types of PASHs in terms of adsorptive desulfurization [37] and

is a sulfuric compound typical of diesel fuel with a higher degree of HDS [94]. As discussed in Section 2.1.2, BT, DBT, and 4,6-DMDBT in particular have a low conversion rate during HDS, and thus tend to be the major PASHs found in commercial fuels. For example, Ref. [173] reported that DBT was the major PASH in a high-sulfur diesel fuel with $2284\,ppm$ of total sulfur, whereas, in a diesel fuel with $433\,ppm$ of total sulfur, the concentration of DBT was only the second highest. Ref. [94] reported a high concentration of DBT in a diesel fuel with $452\,ppmw$ of total sulfur. Schade and J. T. Andersson [174] reported that DBT was still the major PASH in a diesel fuel containing $76\,ppmw$ of total sulfur. Schade and J. T. Andersson [174] also found that, even in a low-sulfur diesel $12\,wt.\%$ of $13\,ppmw$ of total sulfur was represented by DBT. S. A. Hussain and Tatarchuk [94] analyzed an ultra-low-sulfur diesel (high degree of HDS) with $7.5\,ppmw$ of total sulfur that contained only 4,6-DMDBT and other substitutes of DBT. The fuels analyzed above show that BT, DBT, and 4,6-DMDBT are representative PASHs, which is why they where used within this study.

The three different types of PASHs were dissolved in two different commercial fuels with an initial total sulfur concentration of $< 5\,ppmw$. This approach makes it possible to investigate both the individual and competitive adsorption behavior of BT, DBT, and 4,6-DMDBT in a more precise manner. The commercial fuels jet A-1 (Air BP) and diesel fuel (BP) were used because they are typical fuels for fuel-cell-based APUs in trucks, ships, and airplanes. The detailed aromatic compositions of both commercial jet A-1 and diesel fuels can be seen in Table 3.2, which shows that the total concentrations of aromatics are similar for both jet A-1 and diesel fuel. However, the diesel fuel contains significantly higher amounts of PAHs in comparison to the jet A-1. This is in agreement with literature (cf. Table 2.1), which found that jet fuel contains significantly lower amounts of PAHs than diesel fuel, due to its narrower boiling range and stringent smoke-point specifications; a more detailed discussion can be found in Section 2.1.

Table 3.2.: Content of monoaromatics and PAHs in jet A-1 and diesel fuel used within this work.

Fuel	Fuel density	Monoaromatics	PAHs	Total content of aromatics
Jet A-1	$785\,kg/m^3$	$15.8\,vol.\%$[a]	$0.25\,vol.\%$[a]	$16.05\,vol.\%$[a]
Diesel	$826\,kg/m^3$	$14.0\,wt.\%$[b]	$1.9\,wt.\%$[b]	$15.9\,wt.\%$[b]

[a] Analyzed according to ASTM D 6379

[b] Analyzed according to EN 12916

In order to investigate the role of monoaromatics and PAHs, a model fuel was prepared by dissolving the relevant sulfur heterocycles in n-octane (Alfa Aesar, 98% purity). The influence of fatty acid methyl ester (FAME) (also referred to as biodiesel) on desulfurization performance was also investigated by dissolving the relevant sulfur heterocycles in a commercially available diesel fuel (BP) with $6.63\,wt.\%$ FAME. This diesel fuel has a total aromatic content of $14.8\,wt.\%$ according to its data sheet; the fuel density is $828\,kg/m^3$ and the initial total sulfur concentration is $< 7\,ppmw$.

All of the fuels used within this work are listed in Table 3.3. Each fuel is designated according to a fixed scheme as follows: "Type of fuel"/"dissolved type of PASH"_"total sulfur concentration in $ppmw$". For example, the fuel based on jet A-1 with added DBT and a total sulfur concentration of 900 $ppmw$ is designated as "jet/DBT_900" while the fuel based on diesel with added BT and a total sulfur concentration of 300 $ppmw$ is designated as "diesel/BT_300". An overview of all of the fuels investigated is provided in Table 3.3, where detailed descriptions of the types of PASHsadded and the final total sulfur concentrations can be found.

Table 3.3.: Overview of fuel properties and total sulfur concentrations of all fuels used within this thesis.

Designation	Fuel	Added sulfur compound(s)	Total sulfur concentration ($ppmw$) [f]
octane/BT_900	n-octane [a]	BT	900
octane/DBT_900	n-octane [a]	DBT	900
jet/BT_900	Jet A-1 [b]	BT	900
jet/DBT_900	Jet A-1 [b]	DBT	900
jet/4,6-DMDBT_900	Jet A-1 [b]	4,6-DMDBT	900
jet/MIX-3_900	Jet A-1 [b]	BT, DBT, 4,6-DMDBT[e]	900
diesel/BT_300	Diesel [c]	BT	300
diesel/BT_900	Diesel [c]	BT	900
diesel/DBT_900	Diesel [c]	DBT	900
diesel/F/BT_300	Diesel with FAME [d]	BT	300
diesel/F/BT_900	Diesel with FAME [d]	BT	900

[a] Vendor: Alfa Aesar; initial total sulfur concentration: 0 $ppmw$

[b] Vendor: Air BP; initial total sulfur concentration: $< 1\,ppmw$

[c] Vendor: BP; initial total sulfur concentration: $< 5\,ppmw$

[d] Vendor: BP; initial total sulfur concentration: $< 7\,ppmw$ and with $6.63\,wt.\%$ FAME

[e] Equimolar amount of each PASH

[f] $\pm 5\%$

This large variety of fuels was used in different desulfurization experiments. By dissolving only one type of PASH in different commercial fuels, it was possible to investigate the influence of fuel composition on the overall adsorption behavior. In addition, varying the type of PASH allows to scrutinizing proposed adsorption mechanisms in a comprehensive manner. Each of these investigations with different types of fuels are essential in order to provide answers to research questions 2 and 3: what is the mechanism behind this desulfurization process, and how is this mechanism influenced by different types of liquid hydrocarbon-based fuels?

3.3. Desulfurization Experiments

For the desulfurization experiments, both static and dynamic breakthrough tests were carried out in order to investigate adsorption performance and adsorption kinetics under a wide range of conditions. Hence, all of these desulfurization experiments are essential in order find answers to research questions 2 and 3: what is the mechanism behind this desulfurization process, and how is the mechanism influenced by different types of liquid hydrocarbon-based fuels?.

3.3.1. Equilibrium Saturation Experiments

Static equilibrium saturation experiments were carried out at atmospheric pressure and three different temperatures: -10, 20, and $60\,°C$. These temperatures were investigated because they represent the relevant temperature range for an on-board desulfurization unit integrated into a fuel-cell-based APU in e.g. trucks, ships, or airplanes. For each experiment, $1\,g$ of adsorbent was mixed with $10\,mL$ of fuel in a cylindrical flask, which was then placed in a thermostat to control the adsorption temperature. The sulfur concentration of the equilibrated fuel was analyzed after $48\,h$ to determine the equilibrium saturation capacity, according to the following formula:

$$q_{eq} = \frac{V_{fuel}\rho_{fuel}(c_{S,0} - c_{S,1})}{m_{ads} \times 10^6} \tag{3.1}$$

where q_{eq} (mg/g) is the equilibrium saturation capacity, V_{fuel} (mL) is the fuel volume, ρ_{fuel} (kg/m^3) is the density of the fuel, m_{ads} (g) is the initial mass of the adsorbent, and $c_{S,0}$ and $c_{S,1}$ $(ppmw)$ are the total sulfur concentrations at the beginning and end of the experiment, respectively.

3.3.2. Kinetic Experiments

Kinetic experiments were performed by mixing $20\,mL$ of fuel with $2\,g$ of the adsorbent in a flat cylindrical vessel with an inner diameter of $90\,mm$. In this experimental setup, the $2\,g$ of adsorbent formed a single layer on the bottom of the vessel. This experimental setup is designed so as to imitate a single layer of adsorbent in a real adsorber, as shown schematically in Figure 3.1 and thus makes it possible to gain deeper insight into fundamental adsorption behaviors. It is important to note that the boundary conditions of these kinetic experiments are different than those of the dynamic breakthrough experiment described in the following sections. In the kinetic experiments, there was no filling og the adsorber; hence, the time scale of

the fundamental adsorption behaviors observed differs from that of the dynamic breakthrough experiment.
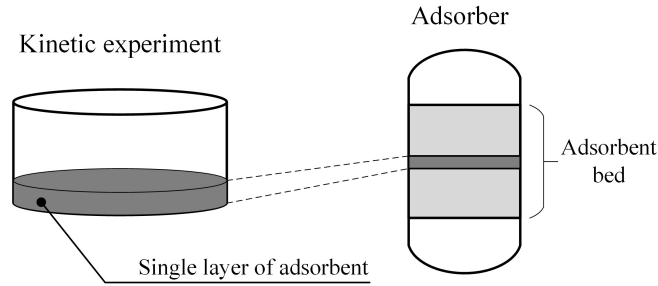
Figure 3.1.: Setup of kinetic experiment.

The kinetic experiments were performed over a period of $48\,h$ without agitation. Six samples were taken during the $48\,h$ (at 0, 0.55, 2.55, 4.72, 31, and $48\,h$) to determine the concentration changed of individual PASHs in the bulk phase. The amount of fuel and adsorbent was increased by a factor of 2 in comparison to the equilibrium saturation experiments in order to minimize the influence of sampling. The total sulfur concentration of each sample was analyzed to calculate the corresponding sulfur adsorption capacity, according to Equation 3.2:

$$q_{t+1} = q_t + \left\{ \sum \frac{V_{fuel}\rho_{fuel}}{m_{ads} \times 10^6}(c_{S,t} - c_{S,t+1}) \right\} \tag{3.2}$$

where q_t (mg/g) is the amount of total sulfur adsorbed at time t (s) and $c_{S,t}$ $(ppmw)$ is the total sulfur concentration at time t.

3.3.3. Dynamic Breakthrough Experiments

All of the dynamic breakthrough experiments were carried out at $20\,°C$ and atmospheric pressure in an individually designed test rig using $14\,g$ of adsorbent. The flow sheet of the experimental setup is illustrated in Figure 3.2, which shows the set-up of both the dynamic breakthrough experiments and the regeneration experiments (see Section 3.4).

The gray dashed lines in Figure 3.2 indicate the desulfurization experiment. In these experiments, the adsorbent was loaded into the vertical stainless-steel adsorber supported on both sides by stainless-steel sieves with a mesh size of several micrometers. The fuel was pumped vertically upward through the adsorber at a constant flow rate during the whole experiment using a peristaltic pump (Ismatec Reglo Digital). The effluent fuel was periodically sampled and analyzed to determine the total sulfur concentration of each sample.

The breakthrough curves illustrated in this work were obtained by plotting the transient sulfur concentration versus the time-dependent cumulative volume of treated fuel normalized
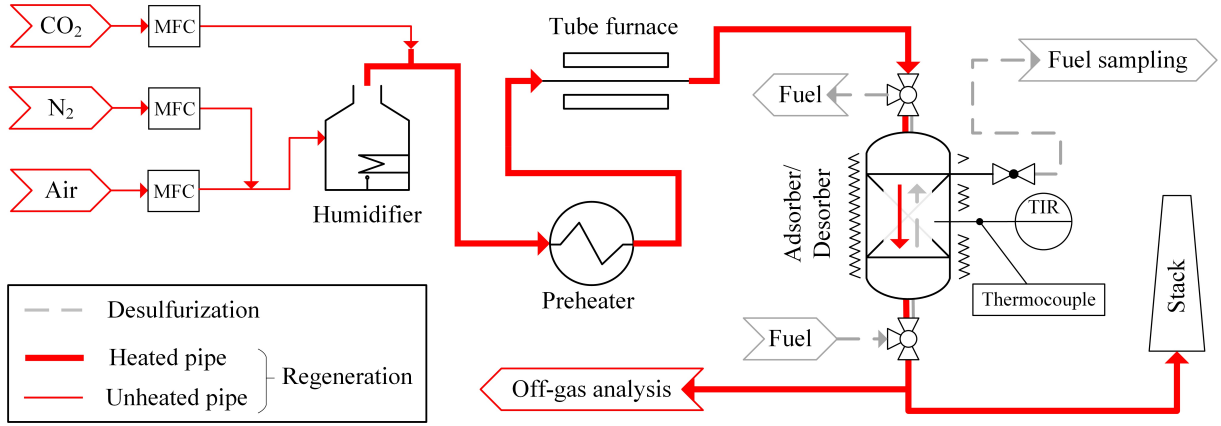
Figure 3.2.: Flow sheet diagram of the laboratory-scale desulfurization unit with thermal in situ regeneration [98].

by the mass of adsorbent ($c_S(t)$ versus $V_{fuel}(t)/m_{ads}$). All sulfur breakthrough capacities q_{break} were calculated according to Equation 3.3 where $V_{fuel,break}/m_{ads}$ is determined from the corresponding breakthrough curve at $c_{S,break} = 10\,ppmw$ via linear interpolation. The value of $c_{S,break} = 10\,ppmw$ represents the threshold limit of total sulfur for an SOFC-based APU, as described in Section 1.3, and was thus defined as sulfur breakthrough.

$$q_{break} = \frac{V_{fuel,break}}{m_{ads}}\frac{\rho_{fuel}c_{S,0}}{10^6} \tag{3.3}$$

Equation 3.3 represents the $10\,ppmw$ sulfur breakthrough capacity q_{break} in (mg/g), where $V_{fuel,break}$ (ml) is the volume of treated fuel at breakthrough, ρ_{fuel} (kg/m^3) is the fuel density of the treated fuel, $c_{S,0}$ ($ppmw$) is the initial total sulfur concentration of the treated fuel, and m_{ads} (g) is the mass of adsorbent used for the breakthrough experiment.

3.4. Regeneration Experiments

All regeneration experiments were performed in situ and subsequent to the dynamic breakthrough experiments on the same test rig, shown schematically in Figure 3.2. After each desulfurization experiment, the experimental set-up was switched into regeneration mode, as shown by the red lines in Figure 3.2. The remaining fuel inside the adsorber was gravimetrically discharged before the adsorber was flushed with regeneration gas. Three different gas mixtures were used for regeneration; these are given in Table 3.4. The first gas mixture is ambient air (referred to as ambient air (AIR_g)) with a constant moisture content of $0.1\,mol\%$. The second gas mixture is similar in its composition to the hot off-gas of an SOFC-operated APU, and thus referred to as APU_g. The moisture content of APU_g is $4.5\,mol\%$. This gas composition is based on an operation mode in which sulfur-free diesel is used as a fuel to operate the SOFC-based APU. The third gas mixture is based on APU_g with 3 times the H_2O content, and

is thus referred to as $APU_{g/wet}$. The detailed gas composition of all three gas mixtures can be seen in Table 3.4.

Table 3.4.: Detailed gas composition of the three different regeneration gases: AIR_g, APU_g, and $APU_{g/wet}$.

	Molar fraction of gas mixtures		
	AIR_g (*mol/mol*)	APU_g (*mol/mol*)	$APU_{g/wet}$ (*mol/mol*)
N_2	0.790	0.763	0.700
O_2	0.209	0.168	0.154
CO_2	0	0.024	0.022
H_2O	0.001	0.045	0.124

The regeneration gas mixture was preheated in two stages before it was fed to the adsorber at a flow rate of 2 - 5 L/min at standard conditions. The flow rate of each individual gas was controlled by mass flow controllers (MFC: Vögtlin, red-y, accuracy of $\pm 1\%$). The gas temperature was increased from $20\,°C$ to a final temperature T_{final} in a stepwise manner, according to the prescribed temperature profile. Different final temperatures were investigated, including 450, 500, and $525\,°C$. All temperatures were measured with type K thermocouples of tolerance class 1. The heating rate during the regeneration experiments was in the range of 3.5 - 8.8 K/min. At the same time, the adsorber walls were heated to the same temperature ($\pm 20\,K$) to provide an almost homogeneous temperature distribution within the adsorber. During the regeneration experiments, the concentration of total hydrocarbons (C_xH_y) in the off-gas was measured with a flame ionization detector (FID). The O_2 and CO_2 concentrations in the off-gas were recorded with a continuous gas analyzer from ABB for cross-checking. In all experiments, the adsorber was cooled down by flushing with AIR_g at a flow rate of 5 L/min at standard conditions.

3.5. Analysis of Fuel

The total sulfur concentration of liquid fuel samples was analyzed by means of inductively coupled plasma optical emission spectroscopy (ICP-OES) using an Arcos SOP from Spectro. Prior to the ICP-OES, each sample was digested with nitric acid in a microwave assisted autoclave system (Multiwave 3000, Anton Paar).

In addition to the total sulfur analysis, a sensitive and selective method was used based on gas chromatographic separation with tandem mass spectrometric detection to analyze individual sulfuric compounds. A Shimadzu TQ 8040 triple quadrupole system equipped with a Shimadzu AOC autosampler was used for the quantification of BT, DBT, and 4,6-DMDBT in the multiple reaction mode. Separation was carried out on a non-polar column (Phenomenex ZB-5 MSi, $30\,m * 0.25\,mm$ inner diameter and $0.25\,\mu m$ film thickness). The carrier gas was helium (purity 5.0) with a linear velocity of $40\,cm/s$, operated in the constant flow mode. The temperature

program started at $50\,°C$ ($1\,min$) and was increased to $250\,°C$ with a temperature ramp of $10\,°C/min$. After the run, the temperature was raised to $310\,°C$ for $2\,min$. Aliquots of $1\,\mu L$ were injected in the split mode at a split ratio of $1:50$. The Injector temperature was set to $240\,°C$, the interface temperature was $280\,°C$, and the ion source temperature was $200\,°C$. For the quantification, external calibration was used with three calibration levels of 0.1, 1, and $10\,mg/L$. All of the calibrated compounds showed excellent linearity with a regression of > 0.999.

The composition of aromatic compounds in jet A-1 and diesel fuel was determined via high performance liquid chromatography (HPLC) analysis according to ASTM D 6379 and EN 12916, respectively.

In the EU, commercial diesel fuel can be blended with up to $7\,vol.\%$ of FAME, which is also referred to as biodiesel. The FAME content in the diesel fuel used within this work was determined by mid-infrared spectrometry, according to EN 14078:2009.

3.6. Analysis of Gases

During the regeneration experiments, the C_xH_y concentration in the off-gas was measured with a FID FID2010T-NMHC from TESTA. The suction nozzle of the FID was placed at the outlet of the adsorber and the gas was transferred to the FID through a heated pipe. The length of the heated pipe was about $1.5\,m$ which, led to a small time shift in the C_xH_y concentration profile. This small time shift was taken into account during the analysis and interpretation of the data.

The O_2 and CO_2 concentrations in the off-gas were recorded by an AO2000 continuous gas analyzer from ABB, equipped with the Uras 26 and Caldos 17 modules. Again, due to the length of the suction pipe, the O_2 and CO_2 concentration profiles have a small time shift, which was taken into account during the analysis and interpretation of the data.

3.7. Material Analysis

3.7.1. XRD Analysis

X-ray diffraction (XRD) measurements were carried out using a Bruker D8 ADVANCE powder X-ray diffractometer with Cu Kα radiation (radiation wavelength = $0.154\,nm$) operated at $40\,kV$ and $40\,mA$. The XRD analysis was carried out at $20\,°C$ with a step size and scanning speed of $0.02°$ and $10\,s/step$.

3.7.2. SEM/EDX Spectroscopy

The adsorbent microstructure was examined using a Zeiss Ultra 55 field emission scanning electron microscope (SEM). All samples were coated with Cr to ensure proper conductivity. For the SEM analysis, an acceleration voltage of $7.0\,kV$ was used, which is also referred to as extra high tension (EHT) ($EHT = 7.0\,kV$). Energy-dispersive X-ray (EDX) spectroscopy was used for the chemical characterization of the adsorbent samples.

3.7.3. N$_2$ Physisorption Analysis

The physical properties, such as the BET surface and pore volume of the adsorbent, were characterized by means of N$_2$ physisorption using a TriStar II 3020 from Micromeritics. All samples were out-gassed at $120\,°C$ for $2\,h$ prior to N$_2$ physisorption in order to remove moisture. The N$_2$ adsorption/desorption isotherm was conducted at $-195.8\,°C$.

3.7.4. Temperature Programmed Desorption of Ammonia - NH$_3$-TPD

The surface acidity of the adsorbents was determined by means of the temperature programmed desorption (TPD) of ammonia using a TPDRO 1100 from Thermo Scientific; $0.2\,g$ of adsorbent was used for this analysis. The samples were purged with high purity helium ($11\,mL/min$) by increasing the temperature to $450\,°C$ at $10\,K/min$. The sample was kept at $450\,°C$ for $10\,min$, and then cooled down to $120\,°C$ under the same helium flow. The purged samples were then saturated with NH$_3$ at $120\,°C$ for $30\,min$. Subsequent flushing with helium ($11\,mL/min$) was conducted at $90\,°C$ for $15\,min$, and the samples were then cooled down to $35\,°C$ to remove the physisorbed NH$_3$. The analysis was then carried out by increasing the temperature to $650\,°C$ at $10\,K/min$. The illustrated TPD profiles were recorded using a thermal conductivity detector (TCD).

3.7.5. Elemental Analysis of the Adsorbent

The total silver content of the final adsorbent was analyzed using ICP-OES. For each sample, $35\,mg$ of ground adsorbent was digested with $7\,mL$ of nitric acid and $0.2\,mL$ of hydrofluoric acid in the microwave assisted autoclave system. A similar procedure was used to determine the elemental sulfur content of the adsorbent. Prior to the ICP-OES analysis, each sample ($100\,mg$) was digested with nitric acid in a microwave-assisted autoclave system. The carbon content in the adsorbent was analyzed by means of an element analyzer (Leco RC612), using $200\,mg$ for each sample.

4

Selective Adsorption and Related Mechanisms

This chapter provides an introduction to the basics of adsorptive desulfurization and discusses the fundamental related adsorption mechanisms. Within this work, effort was made to gain deeper insight into all of the adsorption mechanisms of silver-based adsorbents. The proposed adsorption mechanisms presented in this work are based on theoretical considerations and comprehensive experimental investigations, and provide an answer to research question 2: what is the mechanism behind this desulfurization process?

4.1. Adsorption Mechanisms at Room Temperature[1]

Adsorptive desulfurization under ambient conditions offers a promising alternative technology to produce "sulfur free" fuels ($< 1\,ppmw$) in an effective and cost-efficient manner. Different types of support materials have been doped with different elements (e.g. Ni, Zn, Fe, Ce, Ag, Cu; cf. Table 2.4) using various preparation techniques in order to synthesize selective adsorbents and increase their overall sulfur adsorption capacity. However, the understanding of the relevant adsorption mechanisms at room temperature is still incomplete. Speaking of multi-cyclic adsorption, the adsorbate-adsorbent interaction has to be below a certain value of bond energy to enable desorption and regeneration of the spent adsorbent. An overview of the different types of bindings and their typical range of bond energy is provided in Figure 4.1. For each type of multi-cyclic adsorption, King [175] proposes a bond energy of below $60\,kJ/mol$ for easy adsorbent regeneration. The lower limit of bond energy is determined by the selectivity of the adsorption sites. Too little bond energy and selectivity can lead to the occupation of adsorption sites by other non-sulfuric compounds with similar molecular structures. This is a real challenge since hydrocarbon-based fuels contain high amounts of several non-sulfuric

---

[1]Parts of this section were published in the *Chemical Engineering Journal* under the title "Acid base interaction and its influence on the adsorption kinetics and selectivity order of aromatic sulfur heterocycles adsorbing on Ag-Al2O3" [97].

aromatic compounds, as discussed in Section 2.1. The restriction of the bond energy to 8 - $60\,kJ/mol$ still includes several bond types, such as the Van der Waals interaction, acid-base interactions, and pi bonds, as shown by the likely range for reversible chemical complexing in Figure 4.1.
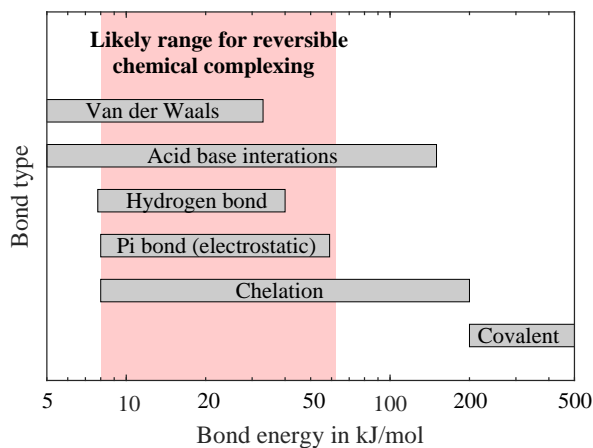
Figure 4.1.: Different types of bindings and their range of bond energy [175].

Adsorption based on chemical complexation bonds can have a high capacity and selectivity for diluted solutions in comparison to weaker Van der Waals forces, as suggested by King [175]. Yet, chemical complexation bonds are weak enough to be broken by simply increasing the temperature. This approach was investigated by Yang and co-workers [91, 166, 176], who proposed π-complexation between d-block metals and PASHs as selective adsorption mechanisms. The π-complexation is based on two PASH interactions with metal cations: the metal cations form the usual σ-bonds with their s-orbitals. In addition, the d-orbitals of the metal cations can back-donate electron density to the antibonding π-orbital (π*) of the thiophenic ring [91]. This adsorption mechanism is referred to as a π-M interaction, in which M represents a d-block metal. A π-M interaction is stronger with a thiophenic ring in comparison to a benzene ring [155], and thus allows the selective adsorption of PASHs. However, the experimental investigations carried out within this work indicate that at least one additional adsorption mechanism has to be involved in the overall adsorption of PASHs on silver-based adsorbents such as Ag-Al$_2$O$_3$. For the sake of clarity, these results will be presented later in this work (Section 4.1.3 et seq.). Nonetheless, these experimental investigations combined with comprehensive theoretical considerations form the basis of the adsorption mechanisms proposed below, which were also published in Ref. [97].

The role and importance of acidic centers on solid surfaces are well known from a wide range of industrially relevant heterogeneous reactions. Acid centers on solid surfaces can be categorized into two types: Lewis and Brønsted. Lewis acid sites are electron acceptors, which are coordinatively unsaturated centers, whereas Brønsted sites are proton donors. PASHs, such as BT and DBT, have two lone-pairs of electrons on the sulfur atom [177]; accordingly, PASHs are Lewis bases. This basic characteristic of PASHs enables to form additional chemical

complexation via acid-base interactions. One possible acid-base interaction is based on metallic cations such as Ag^+ (a Lewis acid) which interacts with BT (a Lewis base) to form a stable adduct [110]. In this chemical complexation, the metal cation interacts with the sulfur atom of BT, where the lone pairs of electrons are located; this adsorption mechanism is referred to as S-M interaction. This type of interaction was also reported for cerium (Ce) doped TiO_2 [127] and Ce-exchanged zeolite [135], which showed good selectivity towards BT in the presence of naphthalene.

Several non-metallic acid sites are known from catalytic processes. These non-metallic acid sites, including different types of hydroxyl groups (-OHs) and carboxylic groups (-COOHs), represent additional adsorption sites for acid-base interactions besides metal cations [92, 178]. The interaction of a basic PASH with a non-metallic acid site is referred to as an S-H interaction, where H represents a general non-metallic acid site. The acidic strength of acid sites strongly depends on the nature of their constituents, composition, preparation, and pre-treatments of the solid material [179, 180]. Previous research has dealt with the correlation between the preparation method and the strength and concentration of acid sites [92].

The adsorptive desulfurization of liquid fuels at room temperature is a complex process that includes the competitive adsorption of PASHs via different adsorption mechanisms and of different strengths. From comprehensive investigations carried out within this work the following adsorption mechanisms are proposed for silver-based adsorbent: the three types of π-M, S-M, and S-H interactions are shown for a silver incorporated aluminum oxide (Ag-Al_2O_3) in Figure 4.2 where the metal cation M is represented by silver (Ag).

(a) π-complexation between sulfur heterocycle and silver cation (π-Ag)

(b) acid base interaction of the sulfur atom and the silver cation (S-Ag)

(c) acid base interaction of the sulfur atom and a general surface acid group (S-H)
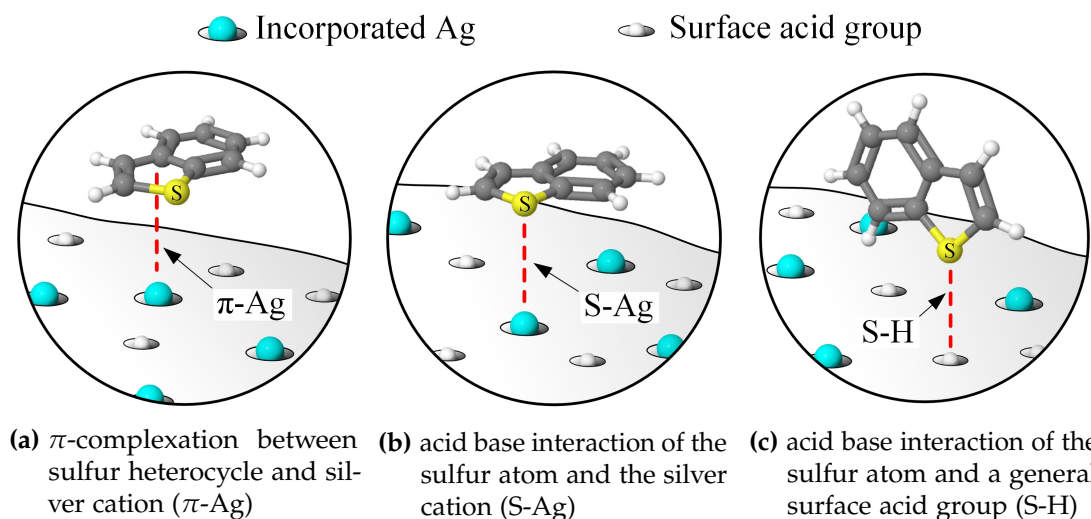
Figure 4.2.: Relevant adsorption mechanisms for sulfur heterocycles adsorbing on the Ag-Al_2O_3 adsorbent at room temperature [97].

The π-Ag interaction is based on the findings of Hernández-Maldonado and R. T. Yang [91], where the thiophenic ring interacts with the Ag^+ cation as shown in Figure 4.2a. In addition, the S-Ag interaction is based on an acid-base interaction in which the sulfur atom interacts directly

with the Ag^+ cation, as shown in Figure 4.2b. The S-H interaction is an additional acid-base interaction, in which the sulfur atom of the sulfur heterocycle interacts with a non-metallic acidic group, as shown in Figure 4.2c. These three types of π-M, S-M, and S-H interactions are important adsorption mechanisms for silver-based adsorbents at room temperatures, and thus provide the answer to research question 2: what is the mechanism behind this desulfurization process? A more detailed discussion of the active silver phase and further characterization of the S-Ag and S-H interaction can be found in Section 4.1.3.

4.1.1. The Role of Support Material[2]

Different types of porous metal oxides have been investigated in recent years as researchers study the influence of different support materials on overall desulfurization performance [94, 95, 101]. The influence of the support material is two-fold: (i) it makes it possible to incorporate active materials (e.g. Ni, Cu, Ag) into the porous structure of the support material, and (ii) it provides additional active adsorption sites for PASHs adsorption. Both effects are influenced not only by the type of material used, but also by the preparation method and precursors used to synthesize the porous metal oxides [181].

Within this work, commercially available metal oxides were screened in order to identify a highly active support material. Figure 4.3 shows the equilibrium saturation capacity for jet/DBT_900 fuel (cf. Table 3.3) determined according to Equation 3.1 for all types of support materials investigated (cf. Table 3.1). The BET surface of the corresponding support material is also given in Figure 4.3.
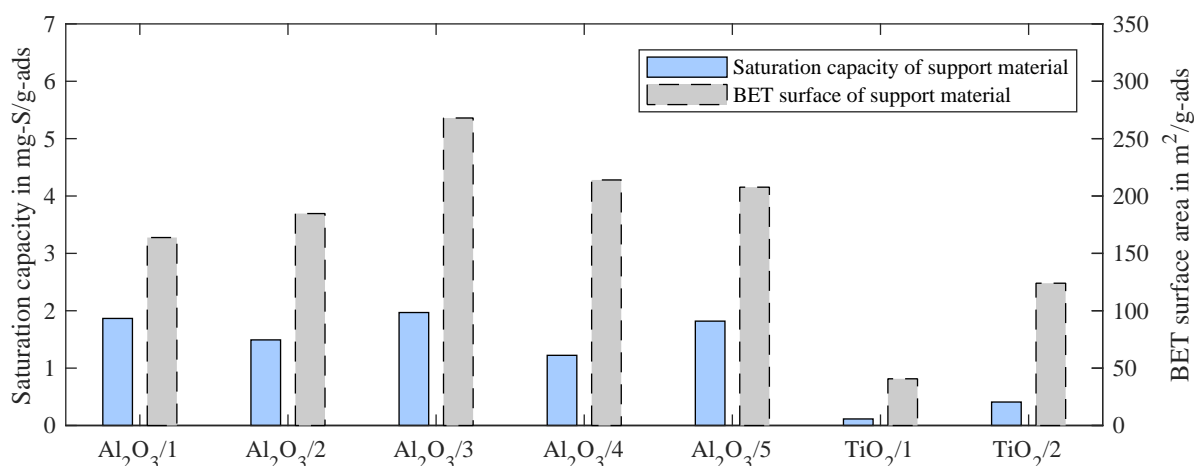
Figure 4.3.: Equilibrium saturation capacity and BET surface of various support materials (adsorbent: Al_2O_3, TiO_2; fuel: jet/DBT_900; adsorption temperature: $20\,°C$).

The adsorption of PASHs on blank support materials, such as Al_2O_3 and TiO_2, is based on the S-H interaction, as discussed in Section 4.1. The common thermally activated supports SiO_2 and TiO_2 usually have lower surface acidity in comparison to γ-Al_2O_3 [102, 182]. This is in agreement with the results presented in Figure 4.3 where support materials based on γ-Al_2O_3 showed higher equilibrium saturation capacities in comparison to support materials based on anatase TiO_2. In the case of γ-Al_2O_3 supports, the lowest equilibrium saturation capacity of 1.22 mg-S/g-ads was observed for support material $Al_2O_3/4$. By contrast, the equilibrium saturation capacities of $TiO_2/1$ and $TiO_2/2$ were observed to be 0.11 and 0.41 mg-S/g-ads, respectively, which are both significantly lower in comparison to all equilibrium saturation capacities observed for γ-Al_2O_3 supports.

Apart from their acidity, anatase TiO_2 supports also have a lower BET surface in comparison to the γ-Al_2O_3 supports, which is one of the major drawbacks of TiO_2-based adsorbents and catalysts [183]. However, from these results it can be concluded that the adsorption capacities of Al_2O_3, SiO_2, and TiO_2 are not influenced by the BET surface, but rather by the surface specific density of active acidic sites. For example, $Al_2O_3/1$ has a BET surface of 163.8 m^2/g, which is well below the BET surface of 268.0 m^2/g in the case of $Al_2O_3/3$. However, the equilibrium saturation capacity of $Al_2O_3/3$ was observed to be 1.97 mg-S/g-ads and thus only marginally higher in comparison to $Al_2O_3/1$, with 1.87 mg-S/g-ads. This result indicates that $Al_2O_3/1$ has a higher surface specific density of active acidic sites in comparison to $Al_2O_3/3$. This is not only important for adsorption, but also for the incorporation of silver into the porous structure of support materials as will be discussed in the following section.

4.1.2. The Role of Silver[3]

Silver is one of the few metals which is active in its oxidized form [96, 97]. This is a major advantage for mobile and stand-alone systems because Ag-based adsorbents can be regenerated in oxidizing atmospheres without subsequent activation in H_2 or N_2. Consequently, Ag was used as the active metal to impregnate the different support materials based on γ-Al_2O_3 and anatase TiO_2 listed in Table 3.1. The procedure of the adsorbent synthesis is described in detailed in Section 3.1.

The effect of Ag impregnation was investigated by means of equilibrium saturation experiments using jet/DBT_900 as fuel. Figure 4.4 shows the equilibrium saturation capacity q_{eq} according to Equation 3.1 for all blank and Ag impregnated supports listed in Table 3.1. Additionally, the surface specific equilibrium saturation capacity (mg-S/m^2-ads) of Ag impregnated supports is shown in Figure 4.4; this is calculated by dividing the equilibrium saturation capacity (mg-S/g-ads) by the corresponding BET surface (m^2-ads/g-ads).

---

[3]Parts of this section were published in the *Chemical Engineering Journal* under the title "Acid base interaction and its influence on the adsorption kinetics and selectivity order of aromatic sulfur heterocycles adsorbing on Ag-Al2O3" [97].
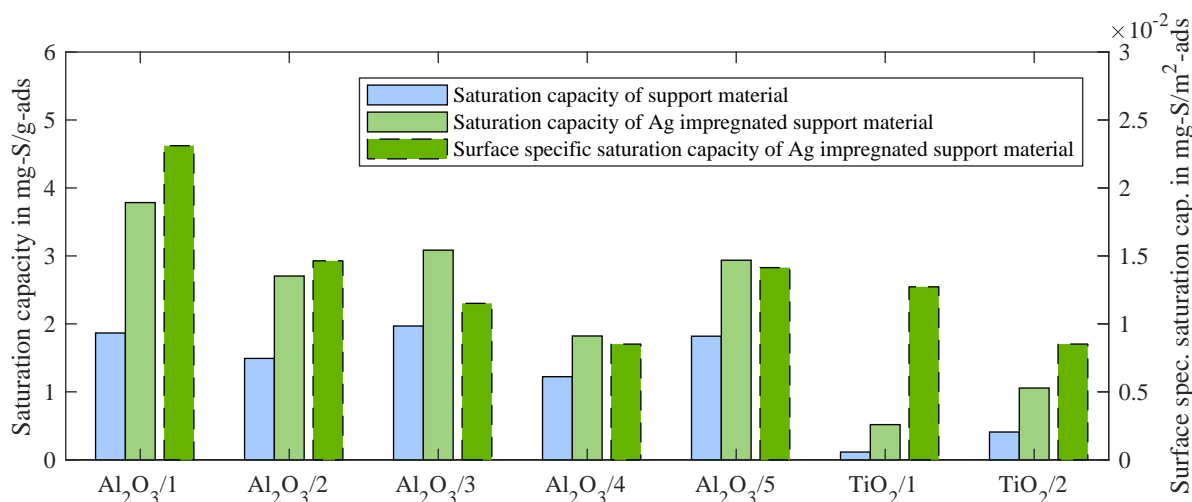
Figure 4.4.: Influence of Ag incorporation on saturation capacity (adsorbent: Al_2O_3, Ag-Al_2O_3, TiO_2, Ag-TiO_2; fuel: jet/DBT_900; adsorption temperature: $20\,°C$).

Incorporating active Ag into the porous structure significantly increased the equilibrium saturation capacity of all of the support materials. For example, the equilibrium saturation capacity of $Al_2O_3/5$ increased significantly from 1.82 to 2.94 $mg\text{-}S/g\text{-}ads$ when $Al_2O_3/5$ was impregnated with Ag. It can be seen in Figure 4.4, the effect of Ag incorporation has a stronger impact on the equilibrium saturation capacity in the case of anatase TiO_2 supports ($TiO_2/1$ and $TiO_2/2$). The equilibrium saturation capacities of both blank $TiO_2/1$ and $TiO_2/2$ more than doubled after Ag impregnation, reaching 0.52 and 1.06 $mg\text{-}S/g\text{-}ads$, respectively. However, their equilibrium saturation capacity is still low in comparison to the Ag impregnated γ-Al_2O_3 adsorbents. In particular, the equilibrium saturation capacity of support $Al_2O_3/1$ increased significantly from 1.86 to 3.76 $mg\text{-}S/g\text{-}ads$ after Ag incorporation.

As discussed in the previous section, the BET surface should be also considered in comparing different support materials. Thus, the surface specific saturation capacities for Ag-incorporated adsorbents can also be seen in Figure 4.4, which represents their equilibrium saturation capacity in relation to the surface area ($mg\text{-}S/m^2\text{-}ads$). The results show that TiO_2-based adsorbents have a high density of active adsorption sites after Ag impregnation. For example, the silver impregnated support $TiO_2/1$ has a surface specific saturation capacity of $1.27 \times 10^{-2}\,mg\text{-}S/m^2\text{-}ads$ which is well above the surface specific saturation capacity of the Ag-impregnated support $Al_2O_3/4$, achieving $0.85 \times 10^{-2}\,mg\text{-}S/m^2\text{-}ads$. However, the low specific surface area of the $TiO_2/1$ support ($40.7\,m^2/g$ as can be seen in Figure 4.3) leads to a very low mass-based equilibrium saturation capacity of only 0.52 $mg\text{-}S/g\text{-}ads$ only. The highest mass and surface specific saturation capacities were observed for Ag-impregnated $Al_2O_3/1$, at 3.76 $mg\text{-}S/g\text{-}ads$ and $2.30 \times 10^{-2}\,mg\text{-}S/m^2\text{-}ads$, respectively. This is interesting because support $Al_2O_3/1$ has the lowest BET surface of all the investigated γ-Al_2O_3 supports. Consequently, $Al_2O_3/1$ was chosen as the most suitable support to prepare the Ag-Al_2O_3 adsorbent by means of the synthesis procedure described in Section 3.1. These results further highlight that neither adsorption

capacity nor the potential to incorporate additional adsorption sites are limited by the specific surface area, but rather by its chemical composition.

Additional effort was made to gain deeper insight into the processes that take place while the adsorbent is being synthesized. For this reason, a break through experiment was carried out using the blank $Al_2O_3/1$ support. In this experiment, $0.6\,g$ of dried $Al_2O_3/1$ support was loaded into a micro adsorber made of polytetrafluorethylene (PTFE). A stock solution with $2.99 \pm 0.09\,wt.\%$ Ag was prepared by dissolving $AgNO_3$ in deionized water. This aqueous $AgNO_3$ solution was pumped into the micro adsorber at a volume flow rate of $0.025\,mL/min$ at standard conditions. At the bottom of the micro adsorber, the effluent solution was collected over the time and analyzed by ICP-OES to determine its elemental silver content.

Figure 4.5 shows the breakthrough curve of elemental silver from the experiment described above. The Ag content of the first sample (at $t = 19\,min$) of the effluent aqueous $AgNO_3$ solution was $0.97\,wt.\%$ which is well below the initial Ag content of $2.99\,wt.\%$. With time, the Ag content in the effluent solution increased to a final value of $2.58\,wt.\%$ after $72\,min$. This breakthrough curve clearly shows that not only does the aqueous $AgNO_3$ solution fill the pores of the support, but also that the silver phase of the dissolved $AgNO_3$ adsorbs on the surface of the $Al_2O_3/1$ support. This is an important finding since it indicates the homogeneous distribution of the Ag phase within the porous structure of the support during infiltration. This homogeneous distribution of the Ag phase was confirmed by a SEM analysis, which is presented and discussed in Section 4.1.3 (cf. Figure 4.8).
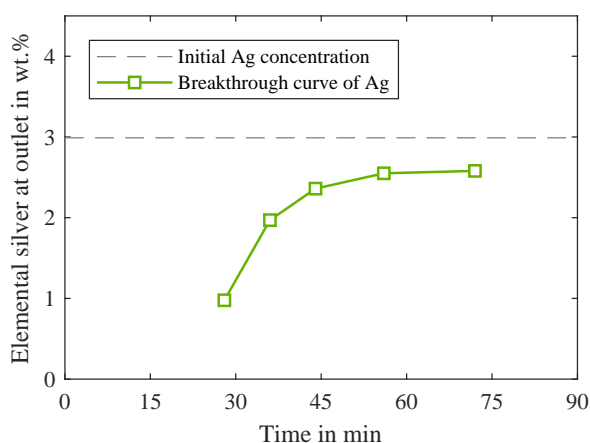
Figure 4.5.: Breakthrough curve of elemental silver obtained by pumping an aqueous $AgNO_3$ solution through an adsorber filled with $Al_2O_3/1$ (adsorbent: $Al_2O_3/1$; liquid: aqueous $AgNO_3$ solution; adsorption temperature: $20\,°C$).

L. Yang et al. [107] proposed inhomogeneous distribution of the silver phase during wet impregnation of mesoporous silica with an aqueous solution of $AgNO_3$. They suggest that during solvent volatilization, the solution concentration increases in the inner part of the pores, leading to a gradient distribution on the support surface [107]. This phenomenon was reported for a mesoporous SiO_2, but does not apply to porous γ-Al_2O_3 supports, including $Al_2O_3/1$.

As clearly indicated by the Ag breakthrough curve in Figure 4.5, the active adsorption of the silver phase during infiltration prevents a gradient distribution during solvent volatilization in the case of $Al_2O_3/1$. Thus, it is concluded that acid sites are involved in the adsorption of the silver phase during infiltration. Consequently, active adsorption of the silver phase during infiltration is limited in the case of SiO_2 supports since SiO_2 has a significantly lower surface acidity in comparison to γ-Al_2O_3 supports [102, 182].

The physical properties of the adsorbent, such as BET surface and pore volume, were determined by N_2 physisorption so as to further analyze the effect of incorporating Ag into the porous structure of the support material. Table 4.1 shows the physical properties of blank $Al_2O_3/1$ and Ag-Al_2O_3 based on $Al_2O_3/1$ support material.

Table 4.1.: Physical properties of blank and silver incorporated $Al_2O_3/1$ adsorbents.

Adsorbent	BET surface (m^2/g)	BJH pore volume (cm^3/g)	BJH mean pore diameter (nm)
$Al_2O_3/1$	163.8	0.47	9.3
Ag-Al_2O_3[a]	141.1	0.42	9.5

[a] Based on the $Al_2O_3/1$ support material

The BET surface was reduced from 163.8 to 141.1 m^2/g by incorporating silver into the porous structure of the $Al_2O_3/1$ support. The BJH pore volume decreases only slightly from 0.47 to 0.42 cm^3/g in the case of Ag-Al_2O_3 whereas the BJH mean pore diameter increased slightly. The pore size distribution of blank $Al_2O_3/1$ and Ag-Al_2O_3 based on the $Al_2O_3/1$ support material is shown in Figure 4.6.
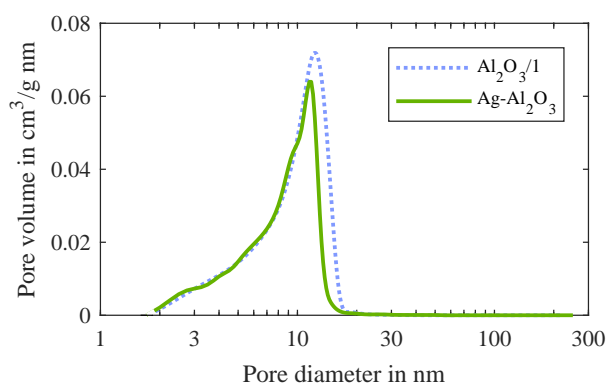
Figure 4.6.: Pore size distribution of blank $Al_2O_3/1$ and after silver incorporation (Ag-Al_2O_3) [97].

All results show that the silver phase was successfully and homogeneously dispersed on the surface of the pore channels of the support material (cf. also SEM image in Figure 4.8c) with pore size distribution in the range of $1.9 - 50\,nm$ (cf. Figure 4.6). All of the experiments subsequently reported and discussed within this thesis were carried out with the Ag-Al_2O_3 adsorbent based on the support $Al_2O_3/1$.

4.1.3. The Active Silver Phase and the HSAB Theory[4]

As described in Section 4.1, the active Ag adsorption site for both π-Ag and S-Ag interaction is the Ag^+ cation [109, 184]; metallic Ag particles are not able to adsorb sulfur heterocycles [109]. The active Ag phase is formed during the thermal treatment of the Ag impregnated support. Figure 4.7 shows the XRD pattern of the $Ag-Al_2O_3$ adsorbent. In addition to γ-Al_2O_3 (ICSD database; PDF: 10-425), Ag_2CO_3 was also detected by XRD analysis [185]. This Ag_2CO_3 represents the active Ag phase, as reported in Ref. [109]. The XRD pattern also shows the peaks for metallic silver [186]. This metallic silver is related to metallic Ag particles on the surface of the $Ag-Al_2O_3$ adsorbent particle, which were also detected by SEM analysis, as shown in Figure 4.8a.
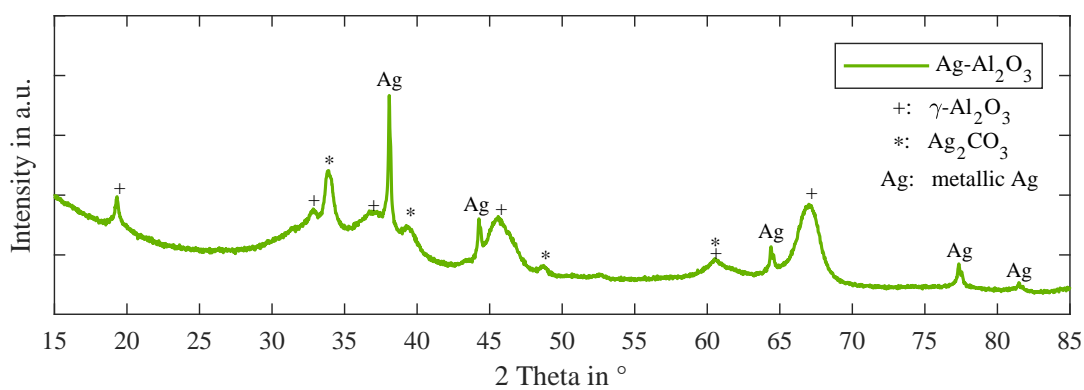
Figure 4.7.: XRD pattern of $Ag-Al_2O_3$ [99].

The metallic Ag particles detected are in the range of 1 - 2 μm, as shown in Figure 4.8a, and are not distributed homogeneously on the surface of the $Ag-Al_2O_3$ adsorbent. This inhomogeneity results from the preparation method (cf. Section 3.1), during which excess $AgNO_3$ solution remains on the particle surface and forms these small Ag particles [96]. The formation of metallic Ag particles on the surface demonstrates that the process of synthesizing the adsorbent has the potential to be significantly improved, and further indicates a potential opportunity to reduce the Ag content of the adsorbent without decreasing the number of active Ag adsorption sites. This correlates with results reported by S. A. Hussain and Tatarchuk [94], where the impregnation of Ag/TiO_2 with 12 and 8 $wt.\%$ Ag showed similar desulfurization performance.

Figure 4.8b shows the EDX pattern from the center of the fractured surface of the $Ag-Al_2O_3$ adsorbent. In addition to the support's O_2 and Al elements, the EDX pattern clearly shows the presence of Ag and C, which are related to Ag_2CO_3, representing the active silver phase. The corresponding SEM image from the center of the fractured surface is shown in Figure 4.8c and

---

[4]Parts of this section were published in the *Chemical Engineering Journal* and *Energy & Fuels* under the titles "Acid base interaction and its influence on the adsorption kinetics and selectivity order of aromatic sulfur heterocycles adsorbing on Ag-Al2O3" [97] and "Thermal in Situ and System-Integrated Regeneration Strategy for Adsorptive On-Board Desulfurization Units" [98].

(a) Metallic Ag particles on the surface of Ag-Al₂O₃

(b) EDX of the fractured surface of Ag-Al₂O₃

(c) Nano dispersed Ag₂CO₃ within the porous structure of Ag-Al₂O₃
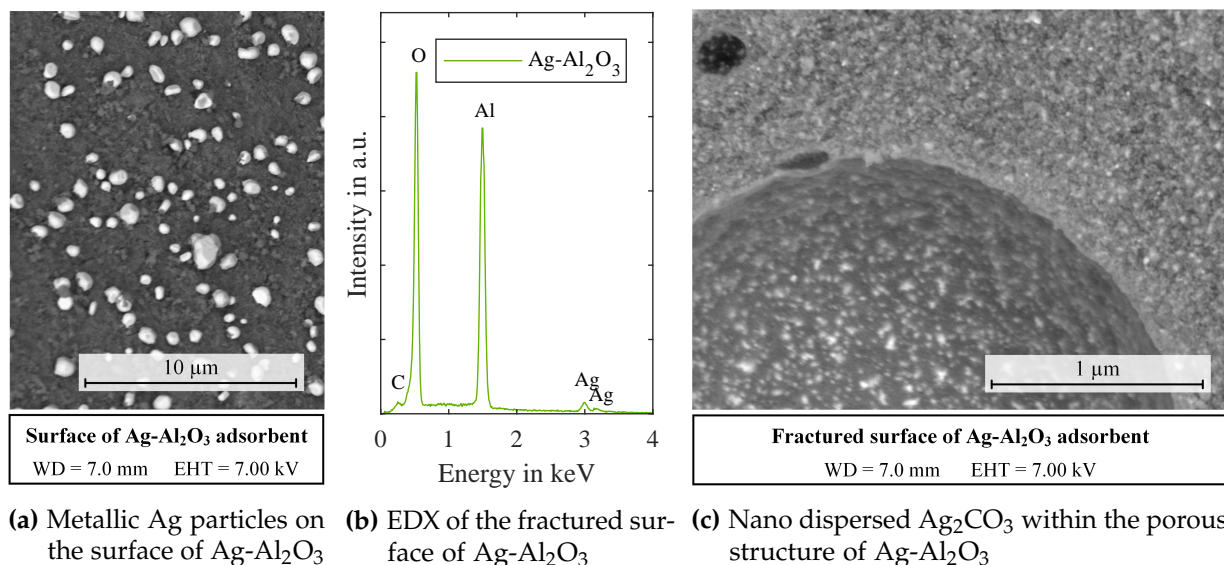
Figure 4.8.: Material analysis of Ag-Al₂O₃: (a) SEM image of the surface of Ag-Al₂O₃, (b) SEM image of the fractured surface of Ag-Al₂O₃, and EDX pattern of Ag-Al₂O₃.

shows the homogeneous distribution of the active Ag phase particles (bright dots) in the range of $40\,nm$ within the porous structure of the adsorbent. Both SEM and EDX analysis showed no radial Ag gradient on the fractured surface of the Ag-Al₂O₃ adsorbent, and thus confirm that the active Ag phase is homogeneously distributed within the porous structure of the Al₂O₃/1 support (cf. discussion of Figures 4.5 and 4.6).

The interactions with the active silver phase can be further characterized as follows: according to the hard and soft acid base theory proposed by Pearson [2] (HSAB theory), stable interactions are formed favorably between acids and bases of a similar hardness. The Ag^+ cation of the active Ag phase is a soft acid according to the HSAB theory [113]. Both BT and DBT are Lewis bases, in which the S atom of the thiophenic ring has two lone pairs of electrons; one σ lone-pair and one π lone-pair of electrons [177]. This electron configuration enables thiophenic compounds to act as either hard or soft bases [177]. According to the HSAB theory, the S-Ag mechanism can be described as soft-soft interactions where the Ag^+ cation acts as a soft acid and interacts with the sulfur heterocycle as a soft base (π lone-pair of electrons). Within this S-Ag interaction, the S atom donates its π lone-pair of electrons to the Ag^+ cation [135].

In contrast to the S-Ag mechanism, the S-H mechanism can be described as a hard-hard interaction. Consequently, the σ lone-pair of electrons (hard base) of the sulfur heterocycle interacts favorably with a hard acid site of the adsorbent. Additional analyses were carried out to gain deeper insight into the surface acid composition of the Ag-Al₂O₃ adsorbent. TPD of probe molecules is a common method to analyze the surface acidity of catalysts and adsorbents [152]. In this work, the hard base NH₃ [187] was used as a probe molecule to investigate the overall surface acidity of the blank Al₂O₃/1 support and the related Ag-Al₂O₃ adsorbent. The corresponding NH₃-TPD profiles are shown in Figure 4.9.
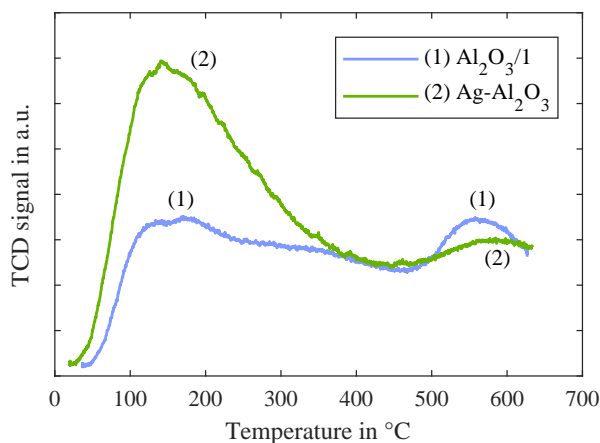
Figure 4.9.: NH_3-TPD profiles of (1) blank $Al_2O_3/1$ and (2) Ag-Al_2O_3 [97].

Both NH_3-TPD profiles show two considerable peaks: the first in the range of 100 to 200 °C and the second in the range of 500 to 600 °C. These two peaks indicate weak and strong acid sites on both the blank $Al_2O_3/1$ support and the Ag-Al_2O_3 adsorbent[188]. The NH_3-TPD analysis showed a loss in strong acid sites for Ag-Al_2O_3 in comparison to the blank $Al_2O_3/1$ support. This loss in strong acid sites indicates that the incorporation of Ag replaced some of the strong acid sites, as was also observed in Ref. [102]. In contrast, the Ag impregnation significantly increased the number of weak acid sites in comparison to the blank $Al_2O_3/1$ support. This phenomenon is in agreement with results reported by S. A. Hussain and Tatarchuk [102], who related the increased acidity to additional -OH groups formed during preparation. These -OH groups provide a H^+ cation, which is a hard acid [187]. The higher amount of weak but hard acid sites (-OH groups) in the case of Ag-Al_2O_3 confirms the importance of the S-H interaction, which can also be described by the HSAB theory.

4.2. Adsorption Selectivity

Adsorption selectivity is a complex phenomenon based on the interaction of the active adsorption site, the adsorbate, and potential adsorptives. Consequently, the adsorption selectivity of Ag-Al_2O_3 depends on the fuel composition and the types of PASHs present in the fuel. In addition, the physical conditions, including the adsorption temperature, have a strong impact on the selectivity of adsorption. Thus, it is important to investigate and quantify the influence of these parameters on the desulfurization performance of an Ag-Al_2O_3-based desulfurization unit under relevant conditions for fuel-cell-based APUs. To investigate the adsorption selectivity of Ag-Al_2O_3, several fuels with and without non-sulfuric aromatic compounds were used. More details on the experimental set-up and fuels used are provided in Section 3.3. The results of the comprehensive investigations reported in this section are intended to provide an answer to research question 3: how is the mechanism influenced by different types of liquid hydrocarbon-based fuels?

4.2.1. Influence by the Type of PASH[5]

A more fundamental investigation of the relevant adsorption mechanisms is necessary in order to understand the adsorption selectivity of different types of PASHs. For this reason, equilibrium saturation experiments were carried out under the same conditions, but with different types of PASHs. This approach made it possible to investigate the adsorption behavior of individual PASHs more specifically. For these experiments, BT, DBT, and 4,6-DMDBT were used as representatives of the most common types of PASHs in gasoline, jet fuel, and diesel fuel, as discussed in Section 2.1.1. In addition, jet/MIX-3_300 was used as a fuel containing BT, DBT, and 4,6-DMDBT (cf. Table 3.3) in order to study the influence of competitive adsorption on adsorption selectivity. The results of these equilibrium saturation experiments are shown in Figure 4.10. The results clearly show a selectivity order of BT > DBT > 4,6-DMDBT for individual adsorption on Ag-Al$_2$O$_3$. The equilibrium saturation capacities observed for BT, DBT, and 4,6-DMDBT are 4.6, 3.76, and 2.45 mg-S/g-ads, respectively.
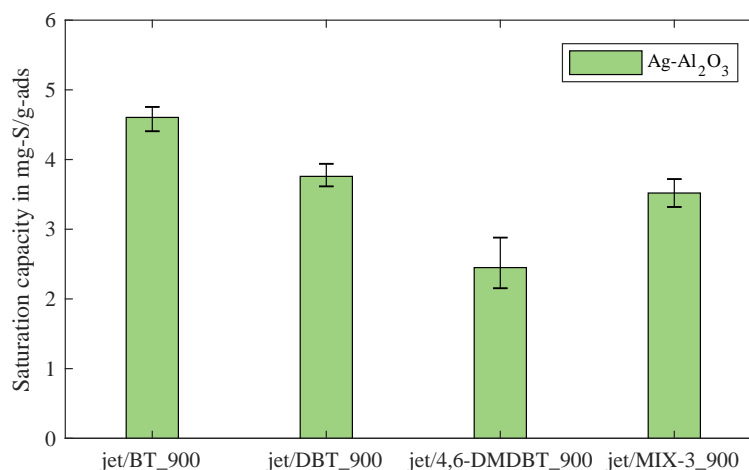
Figure 4.10.: Individual and competitive equilibrium saturation capacity of Ag-Al$_2$O$_3$ for different types of PASHs (adsorbent: Ag-Al$_2$O$_3$; fuel: jet/BT_900, jet/DBT_900, jet/4,6-DMDBT_900, jet/MIX-3_900; adsorption temperature: 20 $^\circ C$).

Several researchers have reported different individual selectivity orders for Ag-SiO$_2$ and Ag-TiO$_2$ than that of Ag-Al$_2$O$_3$. For Ag-SiO$_2$ and Ag-TiO$_2$, DBT was the most adsorbed sulfur heterocycle, leading to an individual selectivity order of DBT > BT [41, 103, 107]. These experiments were performed with a model fuel using a single PASH dissolved in n-octane or decane. Within this work, additional saturation experiments were carried out using n-octane as a model fuel (octane/BT_900 and octane/DBT_900, cf. Table 3.3). These experiments were carried out in order to exclude the possibility that aromatic compounds and fuel additives in real jet A-1 change the selectivity order for Ag-Al$_2$O$_3$. The results in Figure 4.11a show that the selectivity order of Ag-Al$_2$O$_3$ is BT > DBT in both n-octane and jet A-1. Consequently, the

---

[5]Parts of this section were published in the *Chemical Engineering Journal* under the titles "Acid base interaction and its influence on the adsorption kinetics and selectivity order of aromatic sulfur heterocycles adsorbing on Ag-Al2O3" [97].

different selectivity order of Ag-Al$_2$O$_3$ in comparison to Ag-SiO$_2$ and Ag-TiO$_2$ must originate from the contribution of the support material to the adsorption mechanism itself. This insight is of great importance since it was the basis of this investigation of additional adsorption mechanisms (as presented in Section 4.1 and further discussed in Section 4.1.3) and makes it possible to understand the change in the selectivity order of Ag-Al$_2$O$_3$ in comparison to Ag-SiO$_2$ and Ag-TiO$_2$.

The drying and calcination of Ag impregnated metal oxides lead to the formation of Ag$^+$ cations on the surface of the adsorbent [184]. These Ag$^+$ cations allow sulfur heterocycles to be adsorbed via π-Ag as well as S-Ag interaction (cf. Section 4.1). Both π-Ag and S-Ag interactions are based on the Ag$^+$ cation, and thus do not involve the support material itself, but rather the active Ag phase. However, surface acidic groups from the support material are involved in the adsorption of basic compounds like thiophenic molecules via the S-H interaction, as described in Section 4.1. A. H. M. S. Hussain et al. [110] performed density functional theory (DFT) calculations for the adsorption of sulfur heterocycles on a Ag-TiO$_2$ complex. The results of these DFT calculations are summarized in Table 4.2 and are extended with selectivity order determined by Gao et al. [177].

Table 4.2.: Adsorption mechanisms of Ag-based adsorbents and the related adsorption energies for BT and DBT.

Type of binding	Adsorption energy of BT (kJ/mol)[a]	Adsorption energy of DBT (kJ/mol)[a]	Relative strength of adsorption
π-Ag	-117.9	-126.2	DBT > BT[a]
S-Ag	-104.7	-117.3	DBT > BT[a]
S-H	-54.4	-	BT > DBT[b]

[a] Ref. [110]

[b] Ref. [177]

The π-Ag interaction has the highest adsorption energy of all three types of bindings, according to Table 4.2. Within this π-Ag interaction, DBT has a higher adsorption energy than BT. Consequently, the selectivity of the π-Ag interaction is DBT > BT. The same is true for the S-Ag interaction, which differs only in terms of the slightly lower adsorption energies, but has the same selectivity order of DBT > BT. The S-H interaction has a significantly lower adsorption energy in comparison to the strong π-Ag and S-Ag interactions. Within this S-H mechanism, the σ lone-pair of electrons of the S atom interacts with one of the support material's acid sites. As shown by Shiraishi et al. [189], BT has a higher electron density on the σ lone-pair orbital than DBT. This leads to a selectivity order of BT > DBT in the case of the S-H interaction [177].

Competitive saturation experiments were carried out with jet/MIX-3_900 to scrutinize the theoretical consideration of the main adsorption mechanism. In these experiments, an adsorption capacity of 3.52 mg-S/g-ads was observed for Ag-Al$_2$O$_3$ (cf. Figure 4.10). This equilibrium

saturation capacity is between the individual equilibrium saturation capacities of DBT and 4,6-DMDBT. The species composition of the equilibrated jet/MIX-3_900 fuel was analyzed to gain deeper insight into the competitive adsorption. Figure 4.11b shows the initial and final concentrations of BT, DBT, and 4,6-DMDBT in the bulk phase of jet/MIX-3_900 during static saturation experiments with Ag-Al$_2$O$_3$. Analysis of the bulk phase showed that the total sulfur concentration of BT dropped from 285 to 49 $ppmw$, whereas the total sulfur concentrations of DBT and 4,6-DMDBT decreased by only 151 and 65 $ppmw$, respectively, after reaching the equilibrium state. Hence, these results show that BT was the most adsorbed PASH. The overall competitive selectivity order for jet/MIX-3_900 is thus the same as was observed in the saturation experiments carried out with individual sulfur compounds (cf. Figure 4.10).

(a) Influence of fuel additives and aromatic compounds

(b) Competitive selectivity
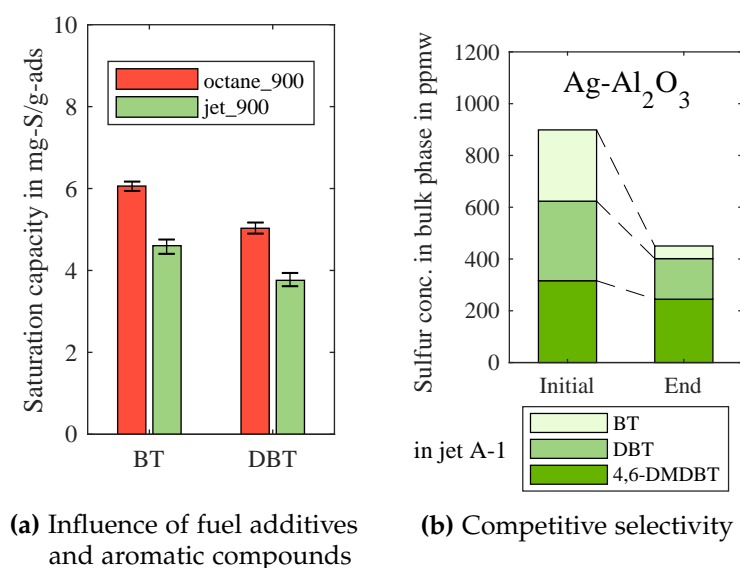
Figure 4.11.: Individual and competitive adsorption on Ag-Al$_2$O$_3$: (a) equilibrium saturation capacity of Ag-Al$_2$O$_3$ and (b) composition of the bulk phase (jet/MIX-3_900) at the beginning and at equilibrium [97] (adsorbent: Ag-Al$_2$O$_3$; fuel: octane/BT_900, octane/DBT_900, jet/BT_900, jet/DBT_900, jet/MIX-3_900; adsorption temperature: 20 °C).

In comparison to individual adsorption, in the competitive adsorption investigations both the adsorption capacities of DBT and 4,6-DMDBT were substituted by BT. The enhanced adsorption of BT in the case of individual adsorption (cf. Figure 4.10) indicates that the S-H interaction plays a major role in reaching the final selectivity order of BT > DBT > 4,6-DMDBT. Furthermore, the selectivity order of the S-H interaction (BT > DBT) from Table 4.2 corresponds to the results observed in the competitive adsorption experiment shown in Figure 4.11b. The different selectivity order reported for Ag-SiO$_2$ and Ag-TiO$_2$ in Ref. [41, 103, 107] seems to be caused by the acidic properties of the supports, and thus emphasizes the impact of the S-H interaction. As discussed in Section 4.1.3, the Ag-Al$_2$O$_3$ adsorbent has a high number of weak acid sites, which are involved in the S-H adsorption mechanism. According to literature, the common thermal activated supports SiO$_2$ and TiO$_2$ have lower surface acidities in comparison to the γ-Al$_2$O$_3$ support [102, 182]. This correlates with the selectivity order observed, as described above.
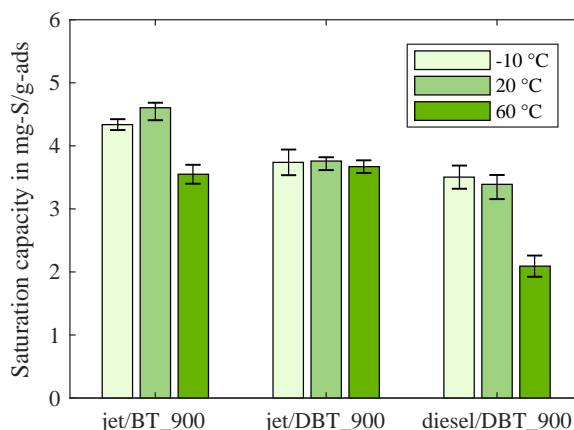
Figure 4.12.: Equilibrium saturation capacities for different types of fuels at adsorption temperatures of -10, 20, and $60\,^{\circ}C$ (adsorbent: Al_2O_3, Ag-Al_2O_3; fuel: jet/BT_900, jet/DBT_900, diesel/DBT_900; adsorption temperature: -10, 20, $60\,^{\circ}C$) [99].

The weak S-H interaction (specific selectivity order of BT $>$ DBT) is responsible for the overall adsorption selectivity order of BT $>$ DBT at $20\,^{\circ}C$. The influence of the adsorption temperature on the adsorption capacity is shown in Figure 4.12 for -10, 20, and $60\,^{\circ}C$. This range of -10 - $60\,^{\circ}C$ covers the reasonable operating temperatures of fuel-cell-based APUs for trucks, ships, and airplanes. At -10 and $20\,^{\circ}C$, the equilibrium saturation capacity of BT is in the range of $4.5\,mg$-S/g-ads whereas only $3.7\,mg$-S/g-ads was observed for DBT. This effect is caused by the weakness of the S-H interaction, which only plays a role at temperatures $< 60\,^{\circ}C$. At temperatures of $\geq 60\,^{\circ}C$, however, the S-H interaction is too weak to contribute to the overall adsorption. Consequently, the equilibrium saturation capacity of BT drops to the same level as that of DBT ($3.6\,mg$-S/g-ads). In the case of jet A-1 fuel, both the stronger π-Ag and S-Ag interactions showed no decline in the selectivity of adsorption for the whole temperature range of -10 - $60\,^{\circ}C$. However, in the case of diesel fuel, the average equilibrium saturation capacity was observed to be $3.5\,mg$-S/g-ads at $-10\,^{\circ}C$, then decreased slightly to $3.4\,mg$-S/g-ads at $20\,^{\circ}C$, and finally dropped to $2.1\,mg$-S/g-ads at $60\,^{\circ}C$. These are important findings, since they characterize the three adsorption mechanisms identified (π-Ag, S-Ag, and S-H interaction) in a comprehensive manner. This characterization of the important adsorption mechanisms is essential in order to be able to model and predict the adsorption behavior of Ag-Al_2O_3 for different types of PASHs under relevant operation conditions for mobile desulfurization units. The influence of fuel type on adsorption selectivity is discussed in the next section.

4.2.2. Influence by the Type of Fuel[6]

Different types of fuels, such as jet or diesel fuel, contain different types of PASHs (cf. Table 2.3). In addition to the type of PASH, non-sulfuric aromatic compounds, fuel additives, and nitrogen-containing compounds have a significant influence on the adsorption capacity. PAHs have similar molecular structures to PASHs, and thus compete, in particular, for adsorption on the surface of the adsorbent [45, 148, 190]. The concentrations of monoaromatics and PAHs in the jet A-1 and diesel fuel used within this work are given in Table 3.2. Both types of fuels contain similar amounts of monoaromatics. However, the PAHs concentration in the diesel fuel is significantly higher in comparison to jet A-1, which has also been reported in literature (cf. Table 2.1).

Equilibrium saturation experiments were carried out with modeled (n-octane) and real fuels (jet A-1 and diesel) to quantify the effect of aromatic compounds and fuel additives on the desulfurization performance of Ag-Al_2O_3; the results of these equilibrium saturation experiments are shown in Figure 4.13. The competing effects of the aromatics and fuel additives can be clearly seen in Figure 4.13, which shows a decrease in the equilibrium saturation capacity of the real fuels (jet A-1 and diesel) in comparison to the model fuel, n-octane. This effect is independent of the type of PASH.
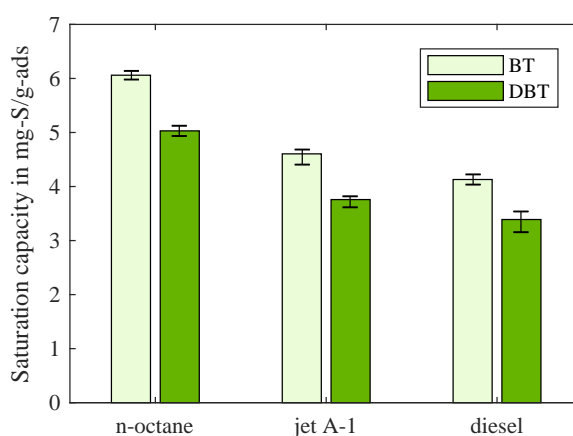
Figure 4.13.: Equilibrium saturation capacity of BT and DBT, and the influence of the type of fuel (adsorbent: Ag-Al_2O_3; fuel: octane/BT_900, octane/DBT_900, jet/BT_900, jet/DBT_900, diesel/BT_900, diesel/DBT_900; adsorption temperature: 20 °C) [99].

As shown in Figure 4.13, the average equilibrium saturation capacity of BT in n-octane was 6.0 *mg-S/g-ads* and thus 1.0 *mg-S/g-ads* higher in comparison to DBT in n-octane. This difference is related to the weak S-H interaction, which makes a major contribution to the overall adsorption mechanism of BT, but only a minor one in the case of DBT, as discussed above. The reduced equilibrium saturation capacity of DBT was also observed for both the jet A-1 and

---

[6]Parts of this section were published in *Journal of Power Sources* and *Energy & Fuels* under the titles "Adsorptive on-board desulfurization over multiple cycles for fuel-cell-based auxiliary power units operated by different types of fuels" [99] and "Adsorptive Desulfurization: Fast On-Board Regeneration and the Influence of Fatty Acid Methyl Ester on Desulfurization and in Situ Regeneration Performance of a Silver-Based Adsorbent" [96].

diesel fuels; for all fuels, the equilibrium saturation capacity of DBT was 0.75 - 1.0 $mg\text{-}S/g\text{-}ads$ lower in comparison to BT. These results indicate that the selectivity of the S-H interaction does not lose its selectivity in the presence of aromatics. However, the selectivity of the π-Ag and S-Ag interactions seems to slightly decrease in the presence of aromatic compounds. This becomes clear by comparing the average equilibrium saturation capacities of BT and DBT in the case of n-octane (no aromatics) with those of the two real fuels (high aromatic content, cf. Table 3.2). The average equilibrium saturation capacity of DBT dropped from 5.0 in the case of n-octane to 3.7 $mg\text{-}S/g\text{-}ads$ when DBT was adsorbed out of jet A-1. In the case of DBT in diesel, the average equilibrium saturation capacity was 3.4 $mg\text{-}S/g\text{-}ads$ and thus at the same level as DBT in jet A-1. Similar results were observed for BT, where the presence of aromatics reduced the average equilibrium saturation capacity from 6.0 $mg\text{-}S/g\text{-}ads$ in n-octane to 4.6 and 4.1 $mg\text{-}S/g\text{-}ads$ in jet/BT and diesel/BT, respectively. Consequently, the equilibrium saturation capacity of Ag-Al$_2$O$_3$ for both BT and DBT is reduced by 1.3 - 1.9 $mg\text{-}S/g\text{-}ads$ in the presence of aromatics and fuel additives.

As discussed above, the declines in the equilibrium saturation capacities in the case of jet A-1 and diesel fuel are related to the presence of fuel additives, and aromatics, in particular [41, 45]. These compounds compete for adsorption, and thus reduce the amount of PASHs adsorbed on Ag-Al$_2$O$_3$. At an adsorption temperature of 20 $^\circ C$, this competitive effect is slightly higher in the case of diesel in comparison to jet fuel, as shown by the results presented in Figure 4.13. In this study, both jet A-1 and diesel fuel have similar contents of total aromatics, which are 16.05 $vol.\%$ and 15.9 $wt.\%$, respectively. However, the PAHs concentration in diesel is 1.9 $wt.\%$, and thus significantly higher in comparison to jet fuel, with a PAHs concentration of 0.25 $vol.\%$ (cf. Table 3.2).

The influence of the higher PAHs concentration in diesel fuel can be clearly seen by comparing the results presented in Figure 4.12. In both fuels, jet/DBT_900 and diesel/DBT_900, DBT is the target compound of adsorption with the same concentration of 900 $ppmw$ of total sulfur. The average equilibrium saturation capacity of DBT in jet A-1 fuel is 3.7 $mg\text{-}S/g\text{-}ads$ for the whole temperature range of -10 - 60 $^\circ C$. In the case of diesel, the average equilibrium saturation capacity of DBT is 3.5 $mg\text{-}S/g\text{-}ads$ at $-10\,^\circ C$ and decreases to 3.4, and finally 2.1 $mg\text{-}S/g\text{-}ads$ at 20 and 60 $^\circ C$, respectively. Similar results were also reported in Ref. [45, 156], where the adsorption capacity of diesel fuel had already significantly decreased at room temperature. In the case of the Ag-Al$_2$O$_3$ adsorbent, this effect becomes relevant at an adsorption temperature of $\geq$ 60 $^\circ C$, where the π-Ag and S-Ag interactions significantly lose their selectivity towards DBT in the presence of PAHs. Consequently, the adsorption temperature of mobile desulfurization units should be kept below 60 $^\circ C$ so as to best exploit the excellent desulfurization performance of Ag-Al$_2$O$_3$ for all types of fuels.

In the case of automotive diesel, FAME, which is also referred to as biodiesel, is blended into diesel fuels in order to replace fossil fuels with renewable ones. The admixture of FAME to

regular automotive diesel is regulated in the US and the EU, which allow up to 5 and 7 $vol.$% of FAME, respectively [157, 191]. The effect of FAME on the adsorption capacity was investigated by means of equilibrium saturation experiments, as described in Section 3.3.1. Figure 4.14a shows the equilibrium saturation capacity of the two fuels, diesel/BT_900 and diesel/F/BT_900, which contain 0.0 and 6.63 $wt.$% of FAME, respectively (cf. Table 3.3).
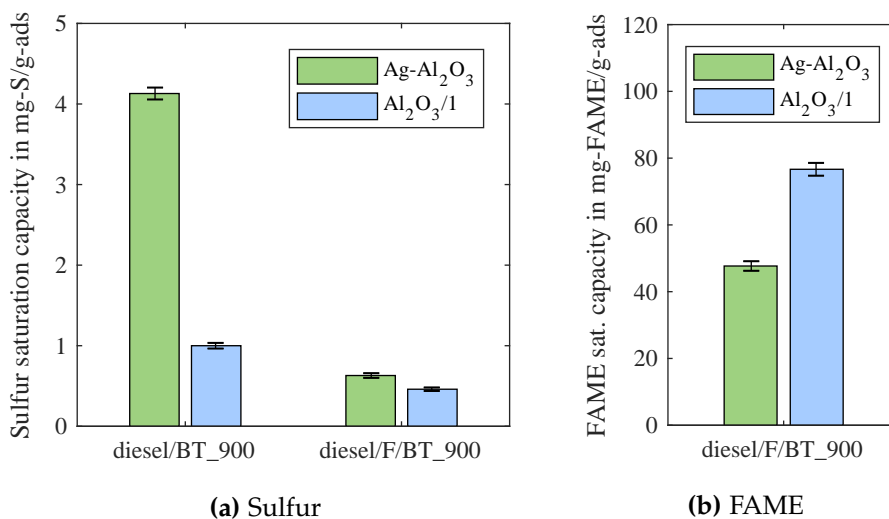
(a) Sulfur   **(b)** FAME

Figure 4.14.: Influence of Ag incorporation on the Saturation capacity of $Al_2O_3/1$ for (a) sulfur and (b) FAME (adsorbent: $Al_2O_3/1$, Ag-Al_2O_3; fuel: diesel/BT_900, diesel/F/BT_900; adsorption temperature: 20 $°C$) [96].

As discussed above, the incorporation of active silver into the porous structure of $Al_2O_3/1$ significantly increased its equilibrium saturation capacity. In the case of diesel/BT_900, the incorporation of silver increased the equilibrium saturation capacity from 1.0 to 4.1 mg-S/g-ads. The equilibrium saturation capacity of Ag-Al_2O_3 dropped significantly, to 0.63 mg-S/g-ads, when the same experiments were carried out with the FAME-containing diesel, diesel/F/BT_900. Additional saturation experiments were carried out with the blank support material $Al_2O_3/1$ in order to quantify the promoting effect of silver in the presence of FAME. The corresponding results are depicted in Figure 4.14a, which shows that FAME nearly deactivates the promoting effect of silver. These results indicate that the active adsorption sites for BT are blocked by FAME-molecules, which thereby inhibit the adsorption of BT on the adsorbent surface. Similar results were reported by Pieterse et al. [157], where FAME had a great influence on the sulfur adsorption performance of an activated Ni-based adsorbent.

The same saturation experiments were repeated by mixing 2.5 g of adsorbent with 5 mL of diesel/F/BT_900. In these experiments, the FAME concentration in the bulk phase was analyzed to determine the saturation capacity of FAME for the blank $Al_2O_3/1$ and the corresponding Ag-impregnated Ag-Al_2O_3. These results are presented in Figure 4.14b and show a FAME-saturation capacity of 76.7 mg/g-ads in the case of blank $Al_2O_3/1$. This FAME-saturation capacity was significantly reduced to 47.7 mg/g-ads when the blank $Al_2O_3/1$ was impregnated with Ag to synthesize Ag-Al_2O_3. These results confirm that FAME adsorbs within the porous

structure of the adsorbents. By incorporating Ag into the porous structure of Al$_2$O$_3$/1, the adsorption of FAME was significantly reduced. However, at the same time, the sulfur adsorption capacity only slightly increased.

From these results, it can be concluded that the incorporation of silver deactivates more FAME adsorptions sites than are formed, and thus, that incorporating silver increases the selectivity towards PASH in comparison to FAME adsorption. These results also demonstrate the sensitivity of the desulfurization performance of Ag-Al$_2$O$_3$ in terms of fuel substitutes based on FAME. Nonetheless, this finding is more of scientific interest than it is relevant for real applications since the admixing of FAME is only regulated in the US and EU for ultra-low-sulfur diesel ($\leq 10\,ppmw$ of total sulfur) only. Nevertheless, these results once more highlight that adsorption selectivity is strongly influenced by fuel additives and substitutes, and thus outline the importance of experiments with real, sulfur-rich fuels.

4.3. Summary of Adsorption Mechanisms Related to Ag-Al$_2$O$_3$

Adsorptive desulfurization is a very promising approach for the ultra-deep desulfurization of hydrocarbon-based fuels. For the selective adsorption of sulfuric compounds, the adsorptive-adsorbent interaction strength has to be above a certain value. However, in the context of regeneration, adsorptive strength should not exceed a certain value in order to enable full regeneration of the adsorbent. Chemical complexation bonds can have a high capacity and selectivity for diluted solutions, and are thus an ideal adsorption mechanism. Furthermore, acid-base interactions provide a wide range of possible adsorption mechanisms that allow both selective adsorption and easily break down during regeneration.

Several support materials have been investigated in literature with regard to their own adsorption capabilities, and the possibility of incorporating active adsorption sites into their micro-structures. Previous research has included activated carbons, MOFs, zeolites, and metal oxides. For mobile and stand-alone desulfurization units, only thermal regeneration in an oxidative atmosphere is reasonable, as discussed in Section 2.2.7. Consequently, activated carbons are not suitable for mobile or stand-alone systems since they are not stable at higher temperatures in oxidative atmospheres. Metal oxides are thermally and chemically stable, and are thus ideal supports for adsorbent synthesis. In addition, metal oxides provide different types of acidic centers, which are potential sulfur adsorption sites, and which are also important for the incorporation of active d-block metals. Of all the d-block metals, silver is one of the few that is active in its oxidized form, and can thus be regenerated in an oxidative atmosphere without subsequent reduction.

Silver-incorporated aluminum oxide (Ag-Al$_2$O$_3$) is active in its oxidized form and provides the possibility of π-complexation between sulfur heterocycles and the active silver phase.

Moreover, direct sulfur-metal interactions and the possibility of acid-base interactions with sulfur heterocycles underline the suitability of Ag-Al$_2$O$_3$ as a potential adsorbent for mobile and stand-alone desulfurization units. The adsorption mechanisms proposed in this chapter are able to explain the different adsorption behaviors of Ag-Al$_2$O$_3$ observed in the experimental investigations. The major findings of these investigations are, in particular, the characterization of the adsorption selectivity under various conditions and the contribution of the three individual adsorption mechanisms to the overall adsorption behavior of Ag-Al$_2$O$_3$. Hence, the adsorption mechanisms proposed in Section 4.1 were validated comprehensively, and furthermore provide an answer to research question 2: what is the mechanism behind this desulfurization process? In addition, research question 3 - how is the mechanism influenced by different types of liquid hydrocarbon-based fuels? - is also partly answered within this chapter by investigating the influence of different fuel compositions on the desulfurization performance of Ag-Al$_2$O$_3$ at equilibrium. The adsorption kinetics and breakthrough performance of Ag-Al$_2$O$_3$ are discussed in Chapter 5. The results presented so far emphasize the fact that Ag-Al$_2$O$_3$ is an excellent adsorbent for use in on-board desulfurization units for fuel-cell-based APUs operated with jet or diesel fuel, and thus also the importance of further investigations in this research area.

5

Dynamic Adsorption and Related Kinetics

Within this chapter, the adsorption kinetics and the dynamic adsorption performance of Ag-Al$_2$O$_3$ are investigated and discussed. Different experiments were carried out in order to determine the contribution of the three identified adsorption mechanisms to the overall dynamic adsorption behavior of PASHs. For this study, different kinetic models were used to analyze the experimental data. In addition, every effort was made to quantify the dynamic influence of different types of liquid hydrocarbon-based fuels on the three identified adsorption mechanisms in order to provide an answer to research question 3: how is this mechanism influenced by different types of liquid hydrocarbon-based fuels?

5.1. Introduction and Relevant Models to Analyze the Kinetic Data

The general adsorption process can be described by the reaction equation expressed in Equation 5.1, where the adsorptive X adsorbs on the adsorbent A; the opposite reaction is defined as desorption [192].

$$X + A \longleftrightarrow XA \tag{5.1}$$

The equilibrium of the adsorption reaction in Equation 5.1 can be described by different isotherm equations. Both the Freundlich and Langmuir isotherm equations are typically used to describe the adsorption of sulfur heterocycles on different adsorbents [129, 154]. In these equations, equilibrium adsorption capacity is a function of the adsorptive concentration. According to this correlation, an increased concentration of sulfur heterocycles in the bulk phase

leads to higher adsorption capacities [193]. This is especially important for weak adsorptive-adsorbent interactions with low adsorption energies, such as the S-H interaction (cf. Table 4.2). In the case of the stronger π-Ag and S-Ag interactions, even low adsorptive concentrations lead to high adsorption capacities [175].

The adsorption of adsorptives from the bulk phase is a complex process, including film or external diffusion, pore diffusion, surface diffusion, and adsorption on the adsorbent. The adsorption kinetics describes the rate of adsorption of the adsorptive onto the surface of the adsorbent. Consequently, the adsorption kinetics is defined as the reaction rate of Equation 5.1, which describes the transient behavior of adsorption until the macroscopic state of equilibrium is reached.

5.1.1. Adsorption Kinetic Models[1]

Several theoretical models can be used to express the adsorption mechanisms of solute onto sorbent. Within these models, the pseudo-first and the pseudo-second order equations are two of the most popular [194]. The pseudo-first order equation by Lagergren [195] is based on an empirical rate equation and is used to describe sorption kinetics in systems, that are not far from equilibrium [194], or for the initial period of the first reaction step [196]. The pseudo-first order equation is provided in the appendix as Equation A.1 (see page 113). For the whole adsorption process and systems including the adsorption of aromatic compounds, the pseudo-second order model applies [196]. This pseudo-second order model is based on a highly efficient empirical equation [197, 198] that is able to represent systems in which intraparticle diffusion or the adsorption reaction itself is the rate limiting step. Within this work, the kinetic experiments consider the whole adsorption process of PASHs, which are aromatic compounds. Consequently, the highly efficient pseudo-second order model was used to analyze the data from the kinetic experiments. The frequently used pseudo-second order model proposed Ho and McKay [199] is described by Equation 5.2,

$$\frac{dq_t}{dt} = k_2(q_{eq} - q_t)^2 \tag{5.2}$$

where q_t (mg/g) is the adsorption capacity at time t (h), q_{eq} (mg/g) is the adsorption capacity at equilibrium, and k_2 ($g/mg\,h$) is the pseudo-second order rate constant. Integration of Equation 5.2 with the boundary condition of $q_{t,(t=0)} = 0$ and rearrangement of the equation results in the non-linearized form of the pseudo-second order model, as shown in Equation 5.3.

This non-linearized form can be transformed to a linearized form of the pseudo-second order model, as seen in Equation 5.4.

$$q_t = \frac{k_2 q_{eq}{}^2 t}{1 + k_2 q_{eq} t} \tag{5.3}$$

$$\frac{t}{q_t} = \frac{1}{q_{eq}} t + \frac{1}{k_2 q_{eq}{}^2} \tag{5.4}$$

Analysis of the kinetic data monitored is usually based on Equation 5.4 by plotting t/q_t versus t, which should show a linear relationship. This procedure makes it possible to determine the q_{eq} and k_2 parameters directly from the slope and the intercept of the linearized plot, respectively.

5.1.2. Diffusion Models[2]

Two different diffusion models were used to analyze the experimental data. The film-diffusion model by Boyd [1] can be used to evaluate whether or not diffusion is limited by film-diffusion or other steps within the adsorption process [200]. The intraparticle diffusion (IPD) model by Weber and Morris was proposed to evaluate whether only the IPD alone or two or more steps influence the overall adsorption process [193].

The film-diffusion model by Boyd [1] is a single-resistance model, which assumes that the main resistance of diffusion is in the boundary layer that surrounds the adsorbent particle. This model describes the transient behavior of the fractional attainment of equilibrium $F(t)$ according to Equation 5.5, where q_t (mg/g) is the adsorption capacity at time t (s) and q_{eq} (mg/g) is the adsorption capacity at equilibrium; the variable B represents the Boyd number which is defined by the Equation 5.6. This model is based on the assumption of a spherical adsorbent particle with a radius r, and D_i (m^2/s) represents the effective intraparticle diffusion coefficient.

$$F(t) = \frac{q_t}{q_{eq}} = 1 - \left(\frac{6}{\pi^2}\right) \sum_{n=1}^{\infty} \left(\frac{1}{n^2}\right) exp(-n^2 B t) \tag{5.5}$$

$$B = \frac{\pi^2 D_i}{r^2} \tag{5.6}$$

---

[2]Parts of this section were published in the *Chemical Engineering Journal* under the title "Acid base interaction and its influence on the adsorption kinetics and selectivity order of aromatic sulfur heterocycles adsorbing on Ag-Al2O3" [97].

By applying the Fourier transformation and then integrating Equation 5.5, Reichenberg [202] obtained the following approximations for $F(t) \leq 0.85$ and $F(t) > 0.85$, shown in Equations 5.7 and 5.8, respectively. In order to obtain the values for Bt, the fractional attainment of the equilibrium $F(t)$ is calculated by q_t/q_{eq}. This value of $F(t)$ is then used to determine Bt according to Equations 5.7 and 5.8. A plot of Bt versus t can thereby lead to a multi-linear plot, indicating that film-diffusion is only the rate controlling step in the initial time period [200].

$$F(t) \leq 0.85: \quad Bt = \left(\sqrt{\pi} - \sqrt{\pi - \frac{\pi^2 F(t)}{3}} \right)^2 \tag{5.7}$$

$$F(t) > 0.85: \quad Bt = -\ln \frac{\pi^2}{6} - \ln(1 - F(t)) \tag{5.8}$$

The IPD model proposed by Weber and Morris [201] is also a single-resistance model based on a general representation of the kinetics according to Equation 5.9, where the intercept is related to the mass transfer across the boundary layer [203]. Within Equation 5.9, q_t (mg/g) is the adsorption capacity at time t (s), k_{in} ($mg/g\,h^n$) is the general intraparticle diffusion rate constant, and C is an experiment specific constant:

$$q_t = k_i t^n + C \tag{5.9}$$

The IPD model proposed by Weber and Morris [201] is based on Equation 5.9, expecting the value of the exponent to be $n = 0.5$ (for Fickian diffusion and plate geometry) [203], as seen in Equation 5.10, where k_i ($mg/g\,h^{1/2}$) is the intraparticle diffusion rate constant:

$$q_t = k_i t^{1/2} + C \tag{5.10}$$

This IPD model is based on the assumption that the external mass transfer resistance (film-diffusion) is not significant or only significant for a very short time period at the beginning of diffusion [200]. The different mechanisms of mass transfer involved in the overall process can be seen in the different slopes in the linear plot of q_t versus $t^{1/2}$, obtained by piecewise linear regression. These different slopes in the linear plot can further be related to different steps occurring during adsorption [204]. The following section contains a more detailed discussion of the different steps.

5.2. Adsorption Kinetics and the Contribution of Different Adsorption Mechanisms[3]

The following section presents and discusses the results obtained from different kinetic experiments for Ag-Al$_2$O$_3$. All of these experiments were carried out as described in Section 3.3.2. Within these kinetic experiments, the concentration of BT or DBT in the bulk phase was analyzed over time. Both of the time-dependent bulk concentrations from the individual kinetic experiments with BT and DBT are illustrated in Figure 5.1. The bulk concentration of total sulfur significantly decreased within the first $60\,min$ in both the BT and DBT experiments. However, the bulk concentration of DBT decreased faster than that of BT, indicating a faster adsorption kinetics of DBT. It is interesting to note that the final bulk concentration in the BT experiment was $308.6\,ppmw$ of total sulfur, and thus significantly below the final bulk concentration of the DBT experiment, which was only $490.5\,ppmw$ of total sulfur. These results indicate that the adsorption kinetics of DBT is faster than that of BT, but that more BT adsorbs at a slower rate.
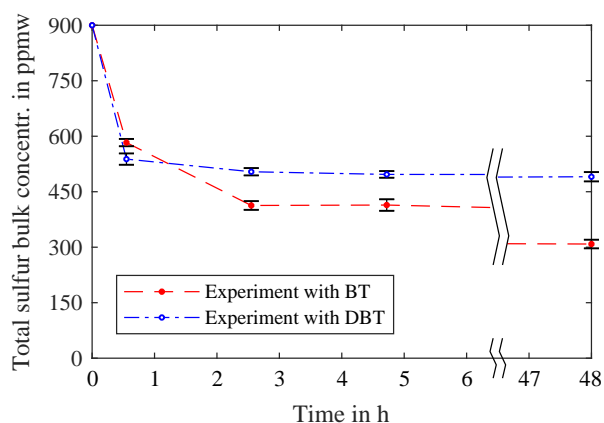
Figure 5.1.: Total sulfur concentration in the bulk phase obtained from individual kinetic experiments with jet/BT_900 and jet/DBT_900 using Ag-Al$_2$O$_3$ as adsorbent (adsorbent: Ag-Al$_2$O$_3$; fuel: jet/BT_900, jet/DBT_900; adsorption temperature: $20\,^\circ C$) [97].

The results of the kinetic experiments were analyzed using the pseudo-second order model. Linearized and non-linearized fits according to Equations 5.4 and 5.3 are presented in Figure 5.2a and 5.2b, respectively. The plot of t/q_t versus t shows a linear relationship, and thus indicates that the adsorption of BT and DBT both obey pseudo-second order kinetics. Figure 5.2c shows the magnified area a) from Figure 5.2b, where it is evident that the selectivity order is separated into two areas. In the first area, q_t is in the order of DBT > BT until $t = 1.3\,h$. In the second area, q_t changes to BT > DBT, including the final equilibrium adsorption capacity q_{eq} at $48\,h$. This final selectivity order of BT > DBT at $t = 48\,h$ was also observed in the equilibrium saturation experiments presented and discussed in Section 4.2.1.

---

[3]Parts of this section were published in the *Chemical Engineering Journal* under the title "Acid base interaction and its influence on the adsorption kinetics and selectivity order of aromatic sulfur heterocycles adsorbing on Ag-Al2O3" [97].

(a) Linearized fit with $R^2 \geq 0.9997$ for both types of PASHs

(b) Non-linearized fit with $R^2 \geq 0.9907$ for both types of PASHs

(c) Magnified area a) of the non-linearized fit
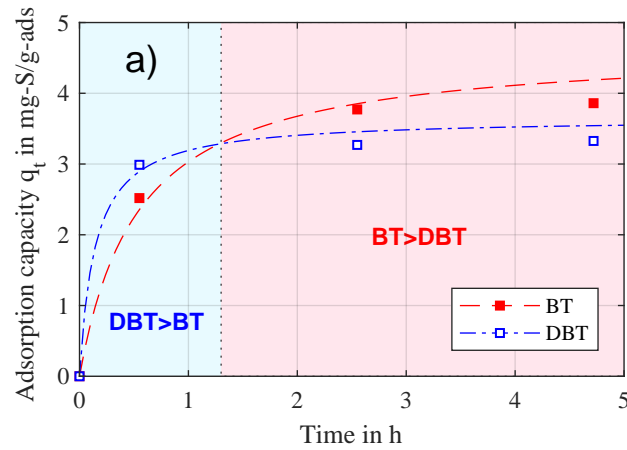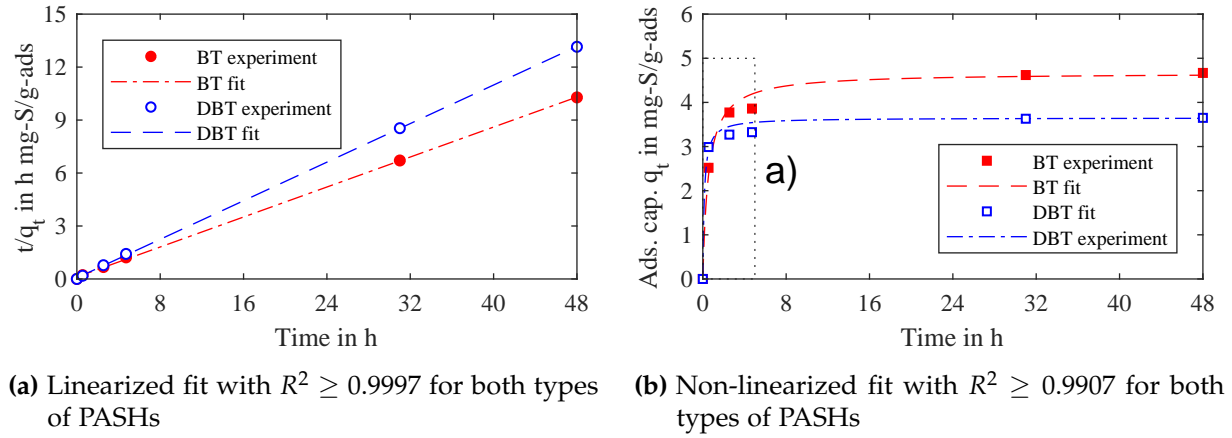
Figure 5.2.: Analysis of kinetic data by the pseudo-second order model: (a) linearized fit according to Equation 5.4, (b) non-linearized fit according to Equation 5.3, and (c) magnified area a) of panel (b) (adsorbent: Ag-Al$_2$O$_3$; fuel: jet/BT_900, jet/DBT_900; adsorption temperature: 20 °C) [97].

Table 5.1 provides the model parameters and the corresponding correlation coefficient R^2 of BT and DBT for the linearized pseudo-second order model, according to Equation 5.4. The results show that the calculated adsorption capacity at equilibrium $q_{eq,calc}$ differs only slightly from the value obtained from the experiments at $t = 48\,h$, while the correlation coefficient R^2 is ≥ 0.9997 for both types of PASHs.

Table 5.1.: Pseudo-second order model parameters for the adsorption of BT and DBT on Ag-Al$_2$O$_3$ from jet A-1 fuel.

	$q_{eq,exp}$ (mg-S/g-ads)	$q_{eq,calc}$ (mg-S/g-ads)	k_2 (g/mg h)	R^2
jet/BT_900	4.67	4.71	0.40	0.9997
jet/DBT_900	3.65	3.66	1.22	0.9999

These results show that the adsorption of BT and DBT both obey pseudo-second order kinetics, and thus, that the overall adsorption rate is limited by intraparticle diffusion or the adsorption reaction itself [197]. Additionally, the kinetic data were analyzed by the pseudo-first order equation by Lagergren [195] in order to verify the findings of Plazinski, Rudzinski, and

Plazinska [194] and Ho and McKay [196], who state that the pseudo-first order equation is not suitable for the present case (cf. Section 5.1.1). The results and relevant equations of the pseudo-first order model are found in Appendix A.2, and confirm that the pseudo-first order model is not suitable for the present case. These results reinforce the interpretations of the pseudo-first and pseudo-second order models' characteristics as proposed by Plazinski, Rudzinski, and Plazinska [194] and Ho and McKay [196].

The kinetic data were further analyzed using Boyd's film-diffusion model [1] as well as the intraparticle diffusion (IPD) model proposed by Weber and Morris [201]. These two models were used to gain deeper insight into the adsorption kinetics of BT and DBT. Figure 5.3 shows the plot of Bt (according to the discontinuous function given by Equations 5.7 and 5.8) versus t for the kinetic data obtained from the kinetic experiments with BT and DBT.
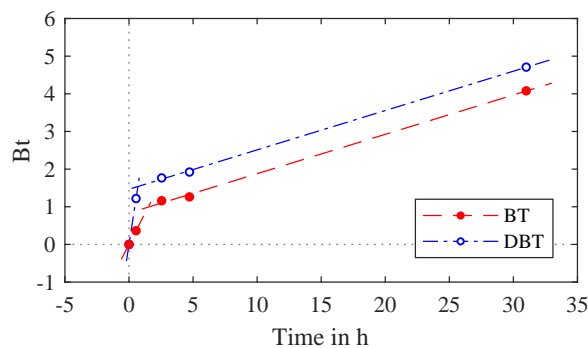
Figure 5.3.: Boyd's plot of the two individual kinetic experiments with BT and DBT as representative types of PASHs (adsorbent: Ag-Al$_2$O$_3$; fuel: jet/BT_900, jet/DBT_900; adsorption temperature: 20 °C) [97].

According to Boyd's model, the plot of Bt versus t (also referred to as Boyd's plot) is a linear plot and passes through the origin when the IPD controls the rate of mass transfer. If the plot is non-linear or linear but does not pass through the origin, it can be concluded that mass transfer is controlled by either film-diffusion or a chemical reaction [200]. In Figure 5.3, the curves of BT and DBT are clearly non-linear curves, which thus indicates that film-diffusion is the rate-controlling step at the beginning of adsorption for both types of PASHs. The results of the kinetic experiments shown in Figure 5.1 indicate that initial adsorption occurs via the stronger π-Ag and S-Ag interactions, where the overall adsorption rate is limited by film-diffusion according to the Boyd's plot (Figure 5.3). The non-linearity of both curves in Figure 5.3 further indicates that IPD eventually takes control of the overall adsorption rate in the second period. This transition from film-diffusion to the IPD stage is based on a significant reduction in the adsorptive concentration in the bulk phase.

The IPD model by Weber and Morris [201] was used to further examine the overall adsorption of PASHs. The plot of q_t according to Equation 5.10 versus $t^{1/2}$ can lead to multi-linearity, indicating that two or more steps occur [204]. This plot of q_t versus $t^{1/2}$ (also referred to as a Weber Morris plot) is presented in Figure 5.4 and shows three-stage behavior for both BT and

DBT adsorption. These three stages are indicated by (1), (2), and (3), where the beginning and end of each stage is indicated by a letter (A, B, C, D) on the top of Figure 5.4.
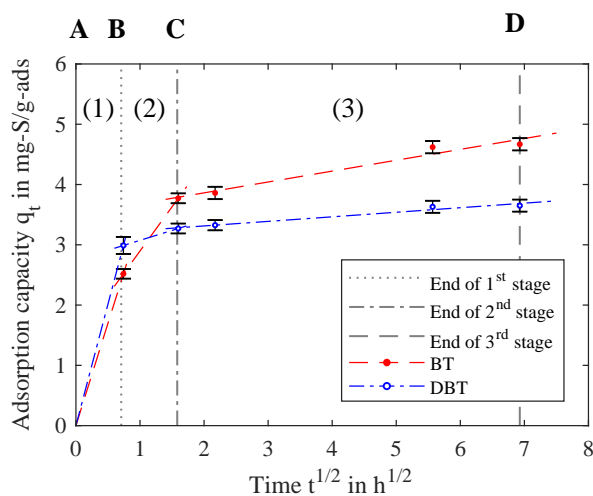
Figure 5.4.: Weber Morris plot of the two individual kinetic experiments with BT and DBT as representative types of PASHs (adsorbent: Ag-Al$_2$O$_3$; fuel: jet/BT_900, jet/DBT_900; adsorption temperature: 20 °C) [97].

The first sharp line in the Weber Morris plot represents external surface adsorption and instantaneous adsorption. In this first stage (1) of the Weber Morris plot, both DBT and BT adsorb via the stronger π-Ag and S-Ag interactions, in which film-diffusion is the rate-limiting step, according to the Boyd's plot. The second step is the gradual adsorption stage (2), where IPD dominates. In this second stage (2), the S-H interaction with the selectivity order of BT > DBT becomes more relevant due to the fact that much higher amounts of BT (from 2.52 - 3.78 mg-S/g-ads) adsorb in comparison to DBT (from 2.99 - 3.27 mg-S/g-ads); see Figure 5.4. Adsorption via S-H interaction is influenced by the concentration of adsorptives in the pores. The increase in the adsorptive concentration in the pores is controlled by the IPD, thereby reducing the adsorption kinetics in the second stage. The third step is the final equilibrium step. This third stage can be caused by two phenomena: (a) an extremely low concentration of adsorptive in the solution, or (b) an excess of micro pores [193, 204]. In this study, the third stage (3) is related to the diffusion and adsorption of adsorptive into the micro pores. This is determined by the fact that the equilibrium total sulfur concentration was above 300 $ppmw$ after 48 h (cf. Figure 5.1). The same kinetic behavior was reported for the adsorption of DBT on activated Al$_2$O$_3$ from n-octane by Srivastav and Srivastava [193].

Scheme 5.1 illustrates the gradual adsorption of BT/DBT on Ag-Al$_2$O$_3$ according to the three stages identified in the Weber Morris plot (Figure 5.4). The first stage (1) is the time between A-B, the second stage (2) is the time between B-C, and the third stage (3) is the time between C-D. The white circles in Scheme 5.1 represent dissolved BT/DBT molecules, and thus adsorptives, whereas the gray and black circles represent adsorbed BT/DBT molecules, and thus adsorbates. The bulk concentrations of BT/DBT shown in Scheme 5.1 correspond to the data from the kinetic experiments shown in Figure 5.1. Within the first stage (A-B),

the high bulk concentration of BT/DBT leads to a high diffusion rate of adsorptive into the pores. Once BT/DBT collides with the pore wall, it adsorbs on the surface, most likely via the strong π-Ag or S-Ag interaction. In this stage (1), the adsorption rate of BT/DBT is limited by film-diffusion. The pore size distribution of the Ag-Al$_2$O$_3$ adsorbent is in the range of 1.9 - 50 nm, with a mean pore diameter of 9.5 nm (cf. Table 4.1 and Figure 4.6). The size of both BT and DBT molecules is below 1 nm [141]. Consequently, the adsorption rate is not influenced by the pore size distribution of Ag-Al$_2$O$_3$ within stage (1).
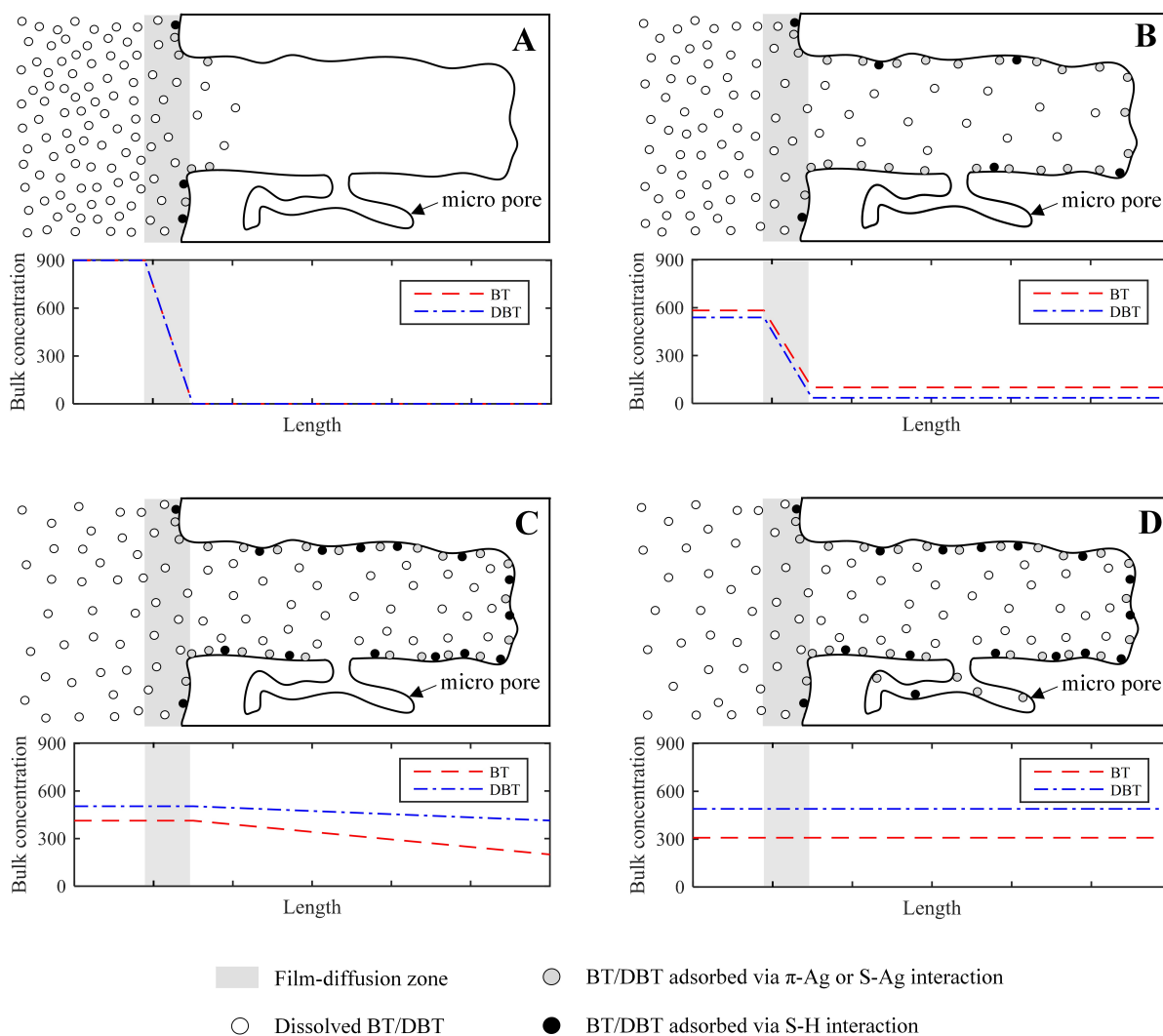
Scheme 5.1: Gradual adsorption of BT/DBT on Ag-Al$_2$O$_3$ according to the three identified stages: First stage A-B, second stage B-C, and third stage C-D [97].

The faster adsorption of DBT in the first stage is related to the higher binding energy of the π-Ag and S-Ag interaction in comparison to BT. This higher binding energy leads to a higher probability of adsorption, thereby maintaining a low adsorptive concentration in the pores. The lower DBT concentration in the pores results in an increased diffusion rate, and thus leads to the overall faster adsorption rate of DBT in comparison to BT. The transition from the first stage to the second is caused by the decreasing adsorptive concentration in the bulk phase. In the second stage (B-C), the adsorptive concentration increases within the pores, as illustrated in

Scheme 5.1. Consequently, the diffusion rate is reduced by a decreasing concentration gradient, and finally limited by IPD. The S-H interaction is strongly influenced by the concentration of adsorptives in the pores, and thus becomes more relevant in the second stage. Both the slower diffusion rate and weaker interaction (via S-H interaction) are responsible for the slower adsorption rate in the second stage in comparison to the first. For DBT, the adsorption rate is even lower, which is caused by the weaker S-H interaction and lower concentration gradient in comparison to BT. In the third stage (C-D), most of the adsorption takes place in micro-pores, where the adsorption rate is limited by diffusion and adsorption into micro-pores. As determined from the Weber Morris plot shown in Figure 5.4, the contributions to the overall adsorption capacity are 11 and 18% for DBT and BT in the third stage, respectively. In this stage, the molecule sizes of BT and DBT are relevant factors, where the smaller critical diameter for BT ($0.6\,nm$) leads to a 7% higher overall adsorption capacity in comparison to DBT, which has a critical diameter of $0.8\,nm$ [205].

These findings are important for the scientific community because they make it possible to correlate different adsorption behaviors with the relevant adsorption interactions. These correlations are essential in order to describe and further predict the overall adsorption behaviors of PASHs adsorbing on Ag-Al$_2$O$_3$. In addition, these results validate the adsorption mechanisms that were identified and discussed in Section 4.1, and are thus fundamental to this work's ability to answer research questions 2 and 3: what is the mechanism behind this desulfurization process, and how is the mechanism influenced by different types of liquid hydrocarbon-based fuels?

5.3. Breakthrough Performance

The ultra-deep desulfurization of fuels is essential in order to protect catalysts and electrodes in the reformer and the fuel cell from sulfur poisoning. As a consequence, breakthrough performance is the parameter used to quantify desulfurization performance for real applications. As discussed in Section 5.2, the adsorption kinetics describes the rate of adsorption and is thus the link between equilibrium and breakthrough performance.

The sulfur threshold limit of fuel cells is $\leq 1\,ppm$ of total sulfur [16, 206]. Upstream of the fuel cell stack, the total sulfur concentration is diluted in the reformer [38] by a factor of 10. Consequently, a total sulfur concentration of $10\,ppmw$ at the outlet of the desulfurization unit is the maximum total sulfur concentration, which fulfills the required sulfur concentration of $\leq 1\,ppm$ at the inlet of an SOFC stack. Therefore, $10\,ppmw$ of total sulfur were defined as breakthrough. The sulfur threshold limits in an SOFC-based APU and dilution during reforming are discussed in more detail in Section 1.3. The breakthrough curves illustrated in this work were obtained by plotting the transient sulfur concentration versus the cumulative volume of treated fuel normalized by the mass of adsorbent. All of the breakthrough capacities

reported herein were calculated from the related breakthrough curve at the $10\,ppmw$ sulfur threshold limit, and are given as mg sulfur per g of adsorbent (mg-S/g-ads).

5.3.1. Influence of the Type of PASH[4]

Breakthrough experiments with different types of PASHs were carried out to investigate the influence of the type of PASH on breakthrough performance. This was necessary because the adsorption mechanisms and related strengths differ for each type of PASH, as discussed in Section 4.1. The kinetic experiments described in Section 5.2 were carried out in order to better understand the contribution of the three identified adsorption mechanisms to the adsorption kinetics. These investigations were carried out as batch experiments, which have different boundary conditions (no filling of the adsorber), and thus a different time scale than break-through experiments (cf. discussion of Figure 3.1). For this reason, additional breakthrough experiments were carried out to quantify the dynamic desulfurization performance at a time scale relevant to real on-board desulfurization units. However, the findings from the kinetic experiments are essential to an understanding of the following results.

Figure 5.5 shows the breakthrough curves of Ag-Al$_2$O$_3$ for the three different types of PASHs BT, DBT, and 4,6-DMDBT in jet A-1 at an liquid hourly space velocity (LHSV) of $0.85\,h^{-1}$. The breakthroughs of BT, DBT, and 4,6-DMDBT were detected at 2.26, 3.20, and $1.25\,ml$/g, respectively. The corresponding breakthrough capacities are calculated according to Equation 3.3 and are 1.63, 2.21, and $0.90\,mg$-S/g-ads for BT, DBT, and 4,6-DMDBT, respectively. By comparing the breakthrough capacities with the corresponding equilibrium saturation capacities from Figure 4.10, the following can be observed. In the case of BT and 4,6-DMDBT, the breakthrough capacity (1.63 and $0.90\,mg$-S/g-ads) was around 35% of the corresponding saturation capacity (4.60 and $2.45\,mg$-S/g-ads). This differs from the case of DBT, where the breakthrough capacity ($2.21\,mg$-S/g-ads) was about 60% of the corresponding saturation capacity ($3.76\,mg$-S/g-ads). This is interesting because all three breakthrough experiments with BT, DBT, and 4,6-DMDBT were carried out at the same LHSV of $0.85\,h^{-1}$. These results show that the individual break-through capacities decrease in the following order: DBT > BT > 4,6-DMDBT. This selectivity order differs from that observed in the individual saturation experiments, which was observed to be BT > DBT > 4,6-DMDBT, as shown in Figure 4.10. Hence, these results indicate that DBT has a faster adsorption kinetics than BT, which correlates with the findings of the investigation of adsorption kinetics presented and discussed in Section 5.2.

As identified by the kinetic analysis in Section 5.2, the overall adsorption is described by three stages, as schematically illustrated in Scheme 5.1. Within the first stage, the high PASH concentration leads to a high diffusion rate of adsorptives into the pores of the adsorbent. Once

---

[4]Parts of this section were published in the *Chemical Engineering Journal* under the title "Acid base interaction and its influence on the adsorption kinetics and selectivity order of aromatic sulfur heterocycles adsorbing on Ag-Al2O3" [97].
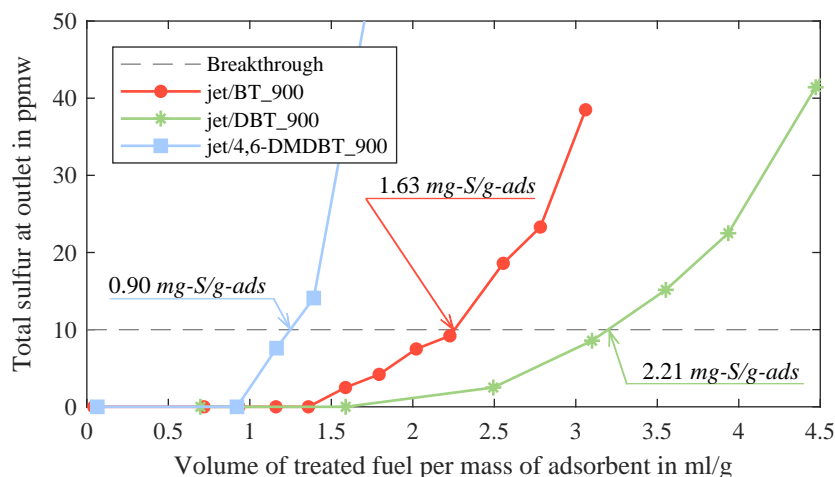
Figure 5.5.: Breakthrough curves of different types of PASHs dissolved in jet A-1 fuel at the same LHSV of $0.85\,h^{-1}$ (adsorbent: Ag-Al$_2$O$_3$; fuel: jet/BT_900, jet/DBT_900, jet/4,6-DMDBT_900; adsorption temperature: $20\,°C$; LHSV: $0.85\,h^{-1}$).

the PASH molecule hits the adsorbent wall, it most likely adsorbs via one of the two strong π-Ag or S-Ag interactions. The diffusion coefficients of both BT and DBT are similar [207], and thus are only a function of the PASH concentration and the temperature. Consequently, the faster adsorption rate of DBT in the first stage is related to the higher binding energy of the π-Ag and S-Ag interactions in comparison to BT. This higher binding energy leads to a higher probability of adsorption, thereby keeping the concentration of adsorptives in the pores low. The lower concentration of DBT in the pores results in an increased diffusion rate, and thus leads to the overall faster adsorption rate of DBT in comparison to BT.

In the second stage shown in Scheme 5.1, the concentration of adsorptives within the pores increases, leading to a reduced diffusion rate, which is finally limited by IPD as described in Section 5.2. With an increasing concentration of PASHs within the pores of the adsorbent, the weak S-H interaction becomes more relevant. However, this weak S-H interaction only plays a crucial role for BT, and thus, the BT adsorption capacity becomes significantly stronger and exceeds DBT's adsorption capacity at the end of the second stage, as seen in Figure 5.4. In the third and final stage of the adsorption kinetics, most of the adsorption takes place in micro-pores. This stage is negligible in terms of breakthrough performance at an LHSV of $0.85\,h^{-1}$ and will thus not be discussed further in this section (see Section 5.2 for more discussion).

From the above, it becomes clear that the contribution of the S-H interaction in the second stage is the key to an understanding of the different selectivity orders at breakthrough (DBT > BT) and at equilibrium saturation (BT > DBT). As mentioned above, the change from DBT > BT to BT > DBT takes place within the second stage. This is also shown in Figure 5.2c for the kinetic experiments, where the time of change was determined to be $t = 1.3\,h$. Consequently, the selectivity order of DBT > BT for individual breakthrough experiments at an LHSV of $0.85\,h^{-1}$ can be related to $t < 1.3\,h$ of the kinetic time scale. At this point, it is important to reiterate

that the time scales of the kinetic and breakthrough experiments are not the same as a result of their different boundary conditions (cf. discussion regarding Figure 3.1). These results show that the influence of the type of PASH on breakthrough performance differs from its influence at equilibrium saturation capacity because of the different adsorption mechanisms involved in the overall adsorption process. The selectivity order at breakthrough is also strongly influenced by the LHSV, and thus underlines the importance of this operating parameter for the design of adsorptive desulfurization units. A more detailed discussion of the influence of the LHSV on the desulfurization performance is found in Section 5.3.3.

Besides individual breakthrough experiments, breakthrough experiments with the fuel jet/MIX-3_900 were also carried out to study the influence of the competitive adsorption of BT, DBT, and 4,6-DMDBT on the breakthrough performance of Ag-Al$_2$O$_3$. Figure 5.6 shows the breakthrough curve for the Ag-Al$_2$O$_3$ desulfurizing jet/MIX-3_900 at an LHSV of $0.85\,h^{-1}$. The composition of sulfur compounds in the effluent fuel is marked by contrasting colors. The competitive breakthrough capacity was $1.04\,mg\text{-}S/g\text{-}ads$ and thus only $0.14\,mg\text{-}S/g\text{-}ads$ above the individual breakthrough capacity of 4,6-DMDBT. The main sulfur heterocycle in the effluent fuel was 4,6-DMDBT, in addition to a significant lower concentration of DBT; no BT was detected at breakthrough. The observed selectivity order of BT > DBT > 4,6-DMDBT for competitive adsorption differs from that observed in the individual breakthrough experiments (DBT > BT > 4,6-DMDBT).
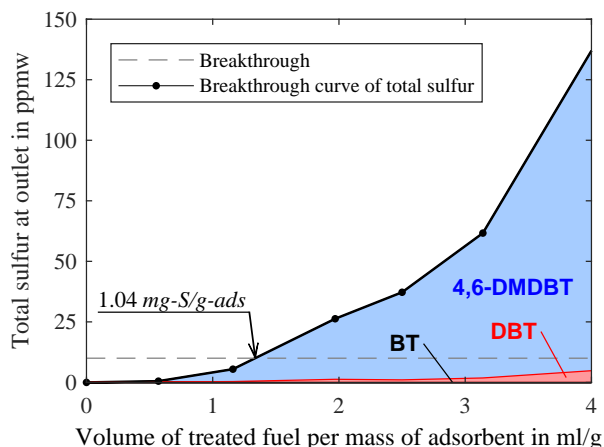
Figure 5.6.: Breakthrough curve of jet/MIX-3_900 showing the detailed PASH composition of the effluent fuel (adsorbent: Ag-Al$_2$O$_3$; fuel: jet/MIX-3_900; adsorption temperature: $20\,^{\circ}C$; LHSV: $0.85\,h^{-1}$) [97].

The relative adsorption strengths of BT and DBT could be the key to understanding the different selectivity orders of competitive and individual adsorption. As discussed above, the π-Ag and S-Ag interactions in the first stage, together with the S-H interaction in the second stage, contribute to the breakthrough performance of individual PASHs at an LHSV of $0.85\,h^{-1}$. Consequently, the same interactions are relevant for the competitive breakthrough performance since the LHSV was kept at $0.85\,h^{-1}$ for both the individual and competitive breakthrough experiments. Therefore, both BT and DBT adsorb on Ag-Al$_2$O$_3$ at the same time via π-Ag and S-Ag interaction in the case of competitive adsorption. According to Table 4.2, the relative

adsorption energies for the π-Ag and S-Ag interactions are in the order of DBT > BT. However, the substitution of adsorbed BT with DBT might be negligible within the short time period of the first two stages since the relative strengths of adsorption are very close to each other (cf. Table 4.2); hence, with an increased time scale substitution may occur.

The switch in the selectivity order to BT > DBT in the case of competitive adsorption seems to be caused by the contribution of the weak acid-base interaction, S-H. All of the results presented so far have shown that the selectivity order of the S-H interaction is BT > DBT. Hence, the additional S-H adsorption sites for BT seem to lead to a final competitive selectivity order of BT > DBT > 4,6-DMDBT in the competitive breakthrough experiments. These results are confirmed by S. A. Hussain and Tatarchuk [94], who used Ag/TiO_2-Al_2O_3 as their adsorbent, prepared by incorporating titanium before silver into a blank γ-Al_2O_3 support. They observed the same selectivity order of BT > DBT > 4,6-DMDBT for real fuels containing various sulfur heterocycles.

5.3.2. Influence of the Type of Fuel[5]

Desulfurization performance strongly depends on the type of fuel, as discussed in Section 4.2.2 with regard to equilibrium saturation. The influence of the type of fuel is related to its constituents, including non-sulfuric aromatic compounds, fuel additives, nitrogen-containing compounds, and different types of PAHs. These PAHs have similar molecular structures to the sulfur heterocycles, and thus compete, in particular, for adsorption on the surface of the adsorbent [45, 148, 190]. For this reason, it is crucial to understand and quantify the influence of PAHs on the breakthrough performance of Ag-Al_2O_3 in order to design a fuel-flexible on-board desulfurization unit for SOFC-based APUs.

Breakthrough experiments were carried out to investigate the influence of the type of fuel on the overall breakthrough performance. This includes not only selectivity at equilibrium, but also the time-dependent selectivity at breakthrough, which is a function of the diffusion and substitution mechanisms of different compounds. DBT was used as the representative PASH and was dissolved in jet A-1 and diesel fuel. Figure 5.7 shows the breakthrough curves for jet/DBT_900 and diesel/DBT_900 at the same LHSV of $0.85\,h^{-1}$. The corresponding breakthrough capacities in mg-S/g-ads were calculated according to Equation 3.3.

As shown in Figure 5.7, the breakthrough capacity for jet/DBT_900 was observed to be 2.2 mg-S/g-ads. This breakthrough capacity dropped to 1.0 mg-S/g-ads when DBT was adsorbed out of diesel fuel (diesel/DBT_900). Similar results were reported by Xiao et al. [45], using activated carbon as their adsorbent. Ma, Sprague, and C. Song [156] also reported good desulfurization
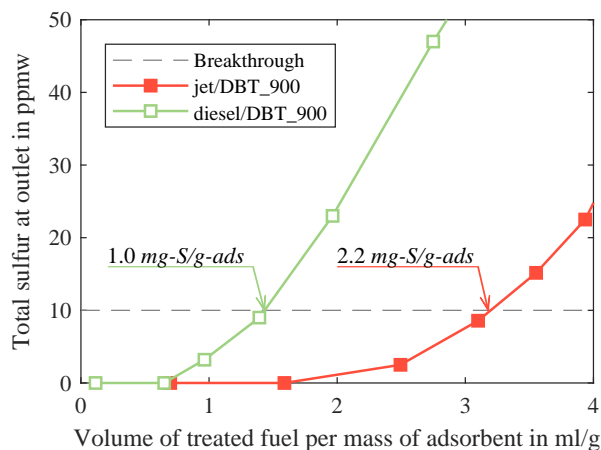
Figure 5.7.: Breakthrough curve of jet/DBT_900 and diesel/DBT_900 at the same LHSVs (adsorbent: Ag-Al$_2$O$_3$; fuel: jet/BT_900, diesel/DBT_900; adsorption temperature: $20\,°C$; LHSV: $0.85\,h^{-1}$) [99].

performance using a Ni-based adsorbent for gasoline and jet fuel, but not diesel fuel. In both Ref. [45, 156], this effect is related to the adsorption mechanism having insufficient selectivity towards PASHs in the presence of PAHs.

These findings differ from the present work because the equilibrium saturation capacities of Ag-Al$_2$O$_3$ for both jet/DBT_900 and diesel/DBT_900 are 3.7 and 3.4 mg-S/g-ads, and thus at the same level at $20\,°C$ (cf. Figure 4.12). However, the lower breakthrough capacity of diesel/DBT_900 in comparison to jet/DBT_900, shown in Figure 5.7, is related to its slower adsorption kinetics rather than insufficient selectivity. The results indicate that the slower adsorption kinetics is caused by the significantly higher concentrations of PAHs in diesel fuel (1.9 wt.%) in comparison to jet fuel (0.25 vol.%, cf. Table 3.2). The concentration of PAHs in diesel/DBT_900 is thus more than 21 times that of DBT (900 $ppmw$ of total sulfur). Consequently, the probability of PAHs adsorption is much higher than DBT in the case of diesel/DBT_900. The subsequent substitution of the adsorbed PAHs with DBT is only a matter of time, and eventually forced by a slightly higher selectivity towards DBT. This substitution with DBT leads to the same equilibrium saturation capacity after $48\,h$ for both types of fuels (cf. Figure 4.12) when the adsorption temperature is below $60\,°C$.

Beside PAHs, FAME also influences the desulfurization performance of Ag-Al$_2$O$_3$, as discussed in Section 4.2.2 for the equilibrium saturation capacity. The influence of FAME on breakthrough capacity was investigated by performing the same breakthrough experiment with diesel/BT_300 (FAME-free) and diesel/F/BT_300 (6.63 wt.% FAME). The results of these experiments are presented in Figure 5.8a. In the case of diesel/F/BT_300, a breakthrough capacity of 0.17 mg-S/g-ads was observed. This breakthrough capacity is around 77% of the correlated saturation capacity of 0.22 mg-S/g-ads. The breakthrough capacity for diesel/BT_300 was 1.04 mg-S/g-ads. These results show that a FAME content of 6.63 wt.% reduced the breakthrough capacity by over 83% compared to the breakthrough capacity of diesel/BT_300. This indicates that FAME molecules block the active adsorption sites of Ag-Al$_2$O$_3$. This inhibiting effect was also

observed by Pieterse et al. [157] using an activated Ni-based adsorbent. They also suggest hat the inhibiting effect may also be caused by the additional additives required to stabilize the FAME-containing diesel [157].

(a) Influence of FAME on the sulfur breakthrough

(b) FAME and sulfur breakthrough
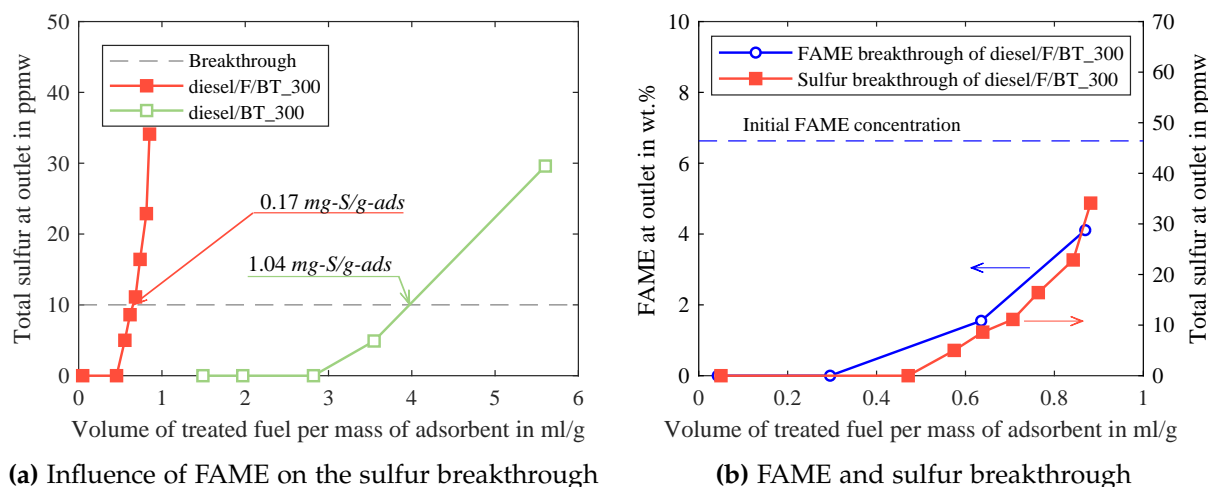
Figure 5.8.: Influence of FAME on the breakthrough capacity of Ag-Al$_2$O$_3$ (adsorbent: Ag-Al$_2$O$_3$; fuel: diesel/BT_300, diesel/F/BT_300; adsorption temperature: $20\,^\circ C$; LHSV: $0.2\,h^{-1}$) [96].

In this work, the adsorption dynamic of FAME adsorbing on Ag-Al$_2$O$_3$ was studied by performing dynamic breakthrough experiments and simultaneously analyzing the FAME concentration at the adsorber outlet. Figure 5.8b shows the breakthrough curves of FAME and sulfur using Ag-Al$_2$O$_3$ to desulfurize diesel/F/BT_300 at an LHSV of $0.2\,h^{-1}$. The FAME concentration in the first sample was $< 10\,ppmw$, and increased in the following samples. The results in Figure 5.8b show the close relationship between sulfur breakthrough and blockage of the active sites by FAME molecules. The probability that a FAME molecule will adsorb before BT is higher because the FAME concentration of $6.63\,wt.\%$ is 220 times the sulfur concentration ($300\,ppmw$). Once a FAME molecule adsorbs on an active site, that site is blocked for BT molecules.

The following result further indicates that the deactivating effect of FAME is enhanced by limiting the diffusion of fuel within the porous structure of the adsorbent. A preliminary breakthrough test with diesel/F/BT_300 and a LHSV of $0.8\,h^{-1}$ led to an immediate break-through of sulfur at the outlet. This diffusion limitation seems to be caused by the long carbon chains of FAME. The FAME molecules are in the range of $2.3\,nm$, compared to the mean pore diameter of $9.6\,nm$. When a long-chain FAME molecule adsorbs on the Ag-Al$_2$O$_3$ surface, it can easily narrow (or even block) pore mouths, resulting in diffusion resistance [208]. In addition, diesel/F/BT_300 has a higher viscosity than FAME-free diesel [209]. This higher viscosity increases the diffusional resistance of the external fluid film covering each adsorbent particle in the adsorber [208]. Desulfurization's diffusion limitation was also observed by H. Chen et al. [105], where the sulfur molecules were in the same range as the pore size of a CuY zeolite.

These results show that both the type of fuel and its non-sulfuric compounds can have a significant influence on the dynamic desulfurization performance of Ag-Al$_2$O$_3$. Consequently, it is essential to investigate and quantify the different phenomena involved in the adsorption mechanisms and dynamics. The results presented above describe and quantify the influence of different types of fuels and their related fuel compounds on the adsorption mechanisms involved, and further quantify the desulfurization performance of Ag-Al$_2$O$_3$, and thus provide answers to research question 3: how is the mechanism influenced by different types of liquid hydrocarbon-based fuels? In addition, the results further show that the breakthrough performance of Ag-Al$_2$O$_3$ can be greatly reduced in the presence of FAME. However, this study is purely of scientific interest, because diesel is only blended with FAME in the EU and US for automotive diesel fuel where the sulfur content is limited by $\leq 15\,ppmw$. This level of sulfur does not present a challenge for the reforming process of a fuel-cell-based APU, in which all hydrocarbons are converted to syngas and H$_2$S (cf. Section 1.3). To achieve the $\leq 10\,ppmw$ sulfur threshold limit for the SOFC stack, adsorptive desulfurization in the gas phase downstream of the reformer is advised.

5.3.3. Influence of the LHSV

The LHSV has a great influence on the breakthrough performance, as pointed out in Section 5.3.1. This influence was further studied and quantified for both jet A-1 and diesel fuel in order to provide reasonable data for the final basic design of a Ag-Al$_2$O$_3$ based on-board desulfurization unit, as will be presented in Section 7.2.

The adsorption kinetics of PASHs is faster in jet A-1 than in diesel fuel, as discussed in Section 5.3.2. This can be clearly seen by the breakthrough curves in Figure 5.7 for an LHSV of $0.85\,h^{-1}$, where the sulfur breakthrough at the adsorber outlet occurred significantly later in the case of jet/DBT_900 (red line) in comparison to diesel/DBT_900 (green line). This indicates that it is possible to operate the adsorptive desulfurization unit at lower LHSVs when jet A-1 is desulfurized in comparison to diesel fuel, while still achieving similar adsorption capacities for both types of fuels. Hence, additional breakthrough experiments were carried out with jet A-1 at an LHSV of $1.7\,h^{-1}$ in order to quantify the influence of the LHSV on the fuel's breakthrough capacity. The breakthrough curves of jet/BT_900 are illustrated for both LHSVs in Figure 5.9. The corresponding breakthrough capacities in mg-S/g-ads were calculated according to Equation 3.3.

As can be calculated from Figure 5.7, the original breakthrough capacity of $1.63\,mg$-S/g-ads at $LHSV = 0.85\,h^{-1}$ dropped to $0.50\,mg$-S/g-ads when the LHSV was increased to $1.7\,h^{-1}$. This result indicates that the breakthrough capacity is reduced by a factor of 3.2 when the LHSV of $0.85\,h^{-1}$ is increased by a factor of 2; hence, the breakthrough capacity is not directly proportional to the LHSV. This is in agreement with the results of the kinetic experiments,
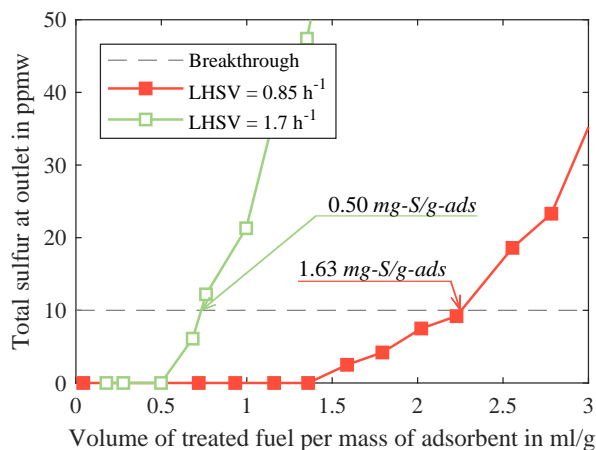
Figure 5.9.: Breakthrough curves of jet/BT_900 at different LHSVs (adsorbent: Ag-Al$_2$O$_3$; fuel: jet/BT_900; adsorption temperature: 20 °C; LHSV: 0.85, 1.7 h^{-1}).

which showed that the adsorption of BT obeys pseudo-second order kinetics (cf. Section 5.2). As known from previous results and discussions, the breakthrough behavior at $LHSV \geq 0.85\,h^{-1}$ corresponds to the kinetic time scale of $t < 1.3\,h$ of the kinetic experiments (cf. Figure 5.2c). This is also apparent from the exponential reduction of the breakthrough capacity from 1.63 to 0.50 mg-S/g-ads when the LHSV was increased to 1.7 h^{-1}. As shown by the kinetic analysis, the overall adsorption within the first 1.3 h of the kinetic experiments is characterized by two different stages (A-B and B-C in Scheme 5.1). In the first stage, the film-diffusion is the rate-limiting step. In the second stage, the overall adsorption is limited by IPD. It thus can be concluded that, in the case of breakthrough experiments, the reduction of the breakthrough capacity from 1.63 to 0.50 mg-S/g-ads, as shown in Figure 5.9, is related to diffusion resistance. However, from these results it is not possible to distinguish whether film-diffusion or IPD is the dominant type of diffusion resistance.

The breakthrough capacity of Ag-Al$_2$O$_3$ observed for diesel/DBT_900 is 1.0 mg-S/g-ads at an LHSV of 0.85 h^{-1}, and thus at the lower end compared to the breakthrough capacities observed for jet A-1 fuels. In order to obtain reasonable breakthrough capacities for diesel fuel, the LHSV was decreased to 0.34 h^{-1}. The breakthrough curves of diesel/DBT_900 for both LHSVs are shown in Figure 5.10. The corresponding breakthrough capacities in mg-S/g-ads can be calculated according to Equation 3.3.

The original breakthrough capacity of 1.0 mg-S/g-ads at $LHSV = 0.85\,h^{-1}$ significantly increased when the LHSV was reduced, as seen in Figure 5.10; this result correlates with the expected behavior. At $LHSV = 0.34\,h^{-1}$, the observed breakthrough capacity of diesel/DBT_900 was 2.59 mg-S/g-ads and thus 2.6 times higher compared to the breakthrough capacity at $LHSV = 0.85\,h^{-1}$. This shows that the LHSV strongly influences breakthrough capacity, and is thus an important design parameter for real applications. This is particularly relevant when fuels with high PAHs concentrations are desulfurized, a process in which the substitution of adsorbed PAHs with PASHs is one of the limiting steps of the overall adsorption mechanism.
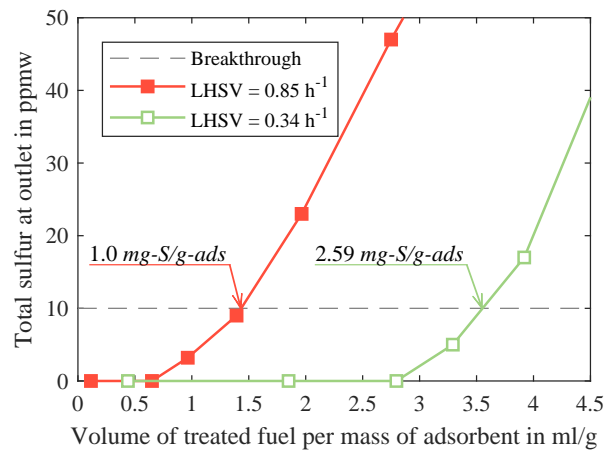
Figure 5.10.: Breakthrough curves of diesel/DBT_900 at different LHSVs (adsorbent: Ag-Al$_2$O$_3$; fuel: diesel/DBT_900; adsorption temperature: $20\,^\circ C$; LHSV: 0.34, 0.85 h^{-1}).

The findings presented above not only confirm the accuracy of the adsorption mechanisms proposed in Section 4.1, but also demonstrate the influence of different parameters on the desulfurization performance of Ag-Al$_2$O$_3$ in a qualitative and quantitative manner. In particular, the characterization of the influence of PAHs on dynamic adsorption behavior is essential to be able to describe and predict the desulfurization performance of Ag-Al$_2$O$_3$. In addition, the ability to quantify the influence of the LHSV on breakthrough performance is essential in order to design an optimized adsorber for real applications (cf. Chapter 7).

6

Adsorbent Regeneration

This chapter discusses the thermal regeneration of spent Ag-Al$_2$O$_3$ adsorbent in oxidizing atmospheres at different final temperatures, in the range of 450 - 525 $°C$. Both ambient air and synthetic off-gas from an SOFC-based APU with different moisture contents were used as regeneration gases, with an gas hourly space velocity (GHSV) of 6771 - 16927 h^{-1}. All of the experiment parameters were set so as to represent reasonable and practical values for real applications. The results of these experiments are discussed in a comprehensive manner and provide deeper insight into the desorption and overall regeneration mechanism of adsorbed PASHs. This understanding is crucial in order to develop an efficient on-board regeneration strategy for mobile desulfurization units that can be integrated into SOFC-based APUs. Hence, this chapter is intended to provide the findings that will make it possible to answer research question 4: what is the service/regeneration interval of this desulfurization approach?

6.1. Introduction

The on-board desulfurization of liquid fuels is essential in order to operate fuel-cell-based APUs with commercial hydrocarbon-based fuels containing 10 - 5000 $ppmw$ of total sulfur [10]. In the last decades, different desulfurization technologies have been investigated for mobile applications. Of all of these technologies, adsorptive desulfurization is the most promising for mobile applications, as was discussed in Section 2.2. However, due to the low adsorption capacities of adsorbents, on-board regeneration of the adsorbent is essential in order to operate the APU continuously, without constantly needing to replace the adsorbent. There are two main categories of strategies for adsorbent regeneration, as illustrated in Figure 6.1: these are (i) solvent-based and (ii) thermal regeneration.

Solvent-based regeneration is based on the elution of adsorbed compounds by a solvent. Different types of polar solvents, including benzene, toluene, and diethyl ether, have been investigated and reported on so far [103, 137, 171]. One of the main drawbacks of solvent-based
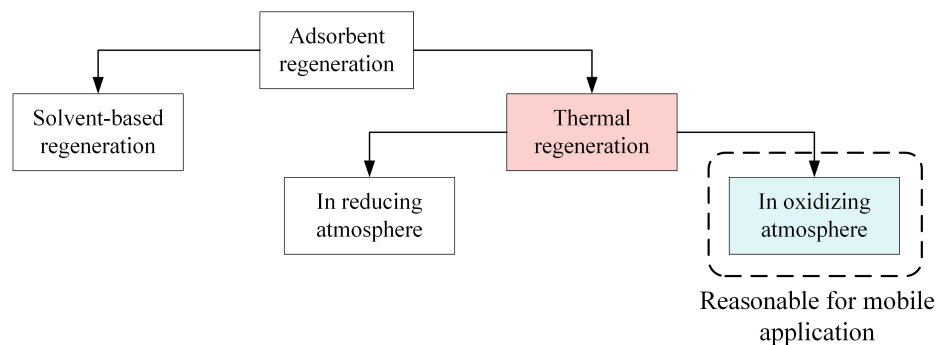
Figure 6.1.: The two main adsorbent regeneration strategies where only thermal regeneration in oxidizing atmosphere is reasonable for mobile applications.

regeneration is the large amount of solvent required for regeneration [103, 112]. Furthermore, the loaded solvent needs to be regenerated, and thus requires an additional operation step. This is why solvent-based regeneration strategies are not considered to be suitable for on-board applications, as this approach would require large tanks to store both the fresh and used solvent. Because this work focuses on mobile applications, only thermal regeneration in an oxidizing atmosphere is discussed in the following sections.

6.2. On-Board Regeneration with Ambient Air[1]

In mobile desulfurization units, thermal regeneration in ambient air is the most common regeneration approach for adsorbents that are active in their oxidized form. Promising results for thermal regeneration with ambient air have been reported in Ref. [94, 101, 102, 105] for a final regeneration temperature of 200 - 450 °C. However, specific heating rates and total regeneration times are missing [100–102, 123, 126, 154]. The heating rate during regeneration is a very important parameter since slow heating rates demand large desulfurization units in order to overcome the long regeneration time. For example, a total regeneration time of 24 h was reported in Ref. [105]. Such long regeneration times are unexceptionable for real applications.

Within this work, thermal regeneration in ambient air (referred to as AIR_g) was carried out with a final regeneration temperature of $T_{final} = 450$ °C. During heat up, the temperature inside the adsorber was kept at 120, 250, and 450 °C for 1, 2, and 1 h, respectively, combined with heating rates of 3.5 - 8.8 K/min. These high heating rates led to a total regeneration time of around 6 h, including heat up and cool down. A more detailed description of this process, including the flow rates used during regeneration, is provided in Section 3.4.

---

[1]Parts of this section were published in *Energy & Fuels* under the title "Adsorptive Desulfurization: Fast On-Board Regeneration and the Influence of Fatty Acid Methyl Ester on Desulfurization and in Situ Regeneration Performance of a Silver-Based Adsorbent" [96].

Figure 6.2 shows the temperature profile measured inside the adsorber as well as the CO_2 concentration profile at the adsorber outlet during regeneration with AIR_g after the desulfurization of diesel/BT_300. The temperature and CO_2 peaks at 1.5 h clearly indicate an exothermic reaction, which led to a sharp temperature peak of $> 800\,°C$. The small time gap between the temperature and CO_2 peak is caused by the experimental set-up, as described in Section 3.6.
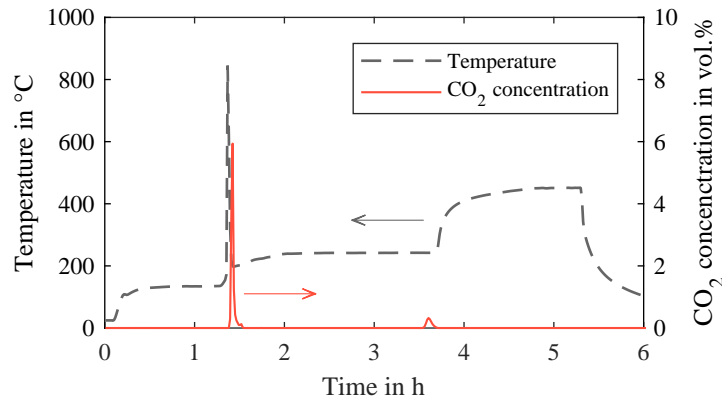
Figure 6.2.: Measured temperature profile within the adsorber and the corresponding CO_2 concentration at the adsorber outlet during regeneration after desulfurizing diesel/BT_300 (adsorbent: Ag-Al$_2$O$_3$; fuel: diesel/BT_300; adsorption temperature: 20 $°C$; regeneration: AIR_g; final regeneration temperature: 450 $°C$) [96].

Further analysis was carried out to measure the concentration of C_xH_y in the off-gas in order to scrutinize whether autoignition took place. The corresponding C_xH_y concentration profile during the uncontrolled exothermic reaction is shown in Figure 6.3. At 1.5 h, a high peak in the C_xH_y concentration can clearly be seen in Figure 6.3, which reinforces the assumption of an autoignition at 1.5 h.
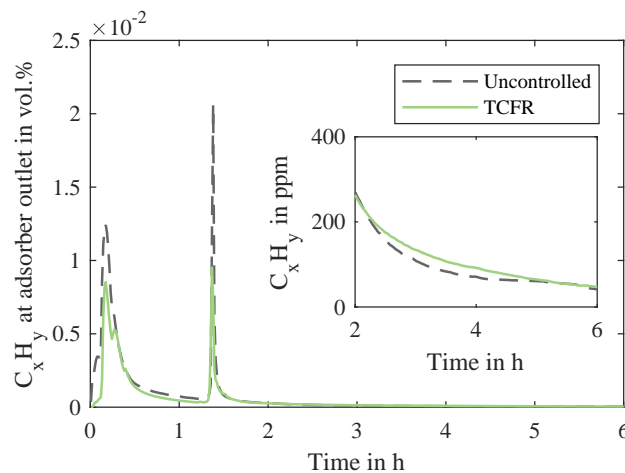
Figure 6.3.: C_xH_y concentration in the off-gas during regeneration using an uncontrolled and temperature-controlled flow rate of AIR_g (adsorbent: Ag-Al$_2$O$_3$; fuel: diesel/BT_300; adsorption temperature: 20 $°C$; regeneration: AIR_g; final regeneration temperature: 450 $°C$) [96].

6.2.1. Temperature Controlled Flow Rate (TCFR) during Regeneration[2]

Thermal regeneration in an oxidizing atmosphere (e.g. ambient air) carries the risk of un-controlled autoignition at elevated temperatures, as shown in Section 6.2. Such uncontrolled autoignition has to be avoided for the following reasons: (i) due to safety issues and (ii) because it causes the thermal destruction of the adsorbent. Autoignition was not mentioned in any of the related works, but neither were any specific heating rates or total regeneration times, as mentioned above. Only S. A. Hussain and Tatarchuk reported a slow heating rate [94]. The problem of vague and incomplete regeneration reports was pointed out by Dasgupta et al. [210]. To avoid autoignition, a slow heating rate would be necessary in order to reduce the volume flow rate of the evaporating fuel. However, slow heating rates require larger desulfurization units in order to overcome the long regeneration time, which would significantly increase the size and weight of mobile desulfurization units.

In this work, the dynamic flow rate of AIR_g was investigated as a means to avoid uncontrolled autoignition. Via this approach, the flow rate of AIR_g is a function of the bed temperature. When the bed temperature exceeded a certain threshold, the flow rate of AIR_g was reduced. Further, the maximum bed temperature was set to $500\,°C$ to protect the adsorbent from thermal destruction. This novel approach is dubbed regeneration with a temperature-controlled flow rate (TCFR). The effect of the TCFR on the temperature within the adsorber is illustrated in Figure 6.4a, while the corresponding flow rates of AIR_g are shown in Figure 6.4b.

(a) Temperature within the adsorber   **(b)** Flow rate of AIR_g during regeneration
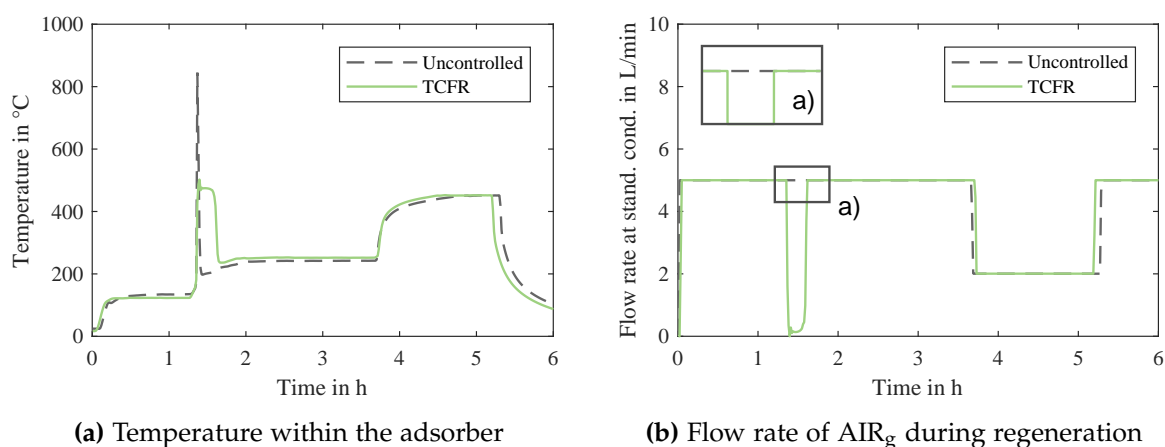
Figure 6.4.: (a) Temperature profile within the adsorber and (b) flow rate of AIR_g during uncontrolled and TCFR regeneration approaches after desulfurizing diesel/BT_300 (adsorbent: Ag-Al$_2$O$_3$; fuel: diesel/BT_300; adsorption temperature: $20\,°C$; regeneration: AIR_g; final regeneration temperature: $450\,°C$) [96].

As can be seen in Figure 6.4a, the bed temperature exceeded $800\,°C$ when the flow rate of AIR_g was uncontrolled. In comparison, when TCFR was used, the flow rate of AIR_g was significantly reduced at around $1.5\,h$. This approach makes it possible to keep the temperature within the adsorber below the prescribed temperature of $500\,°C$, as shown in Figure 6.4a. At $3.75\,h$,

---

the flow rate of AIR_g was reduced from 5 to $2\,L/min$ during both uncontrolled and TCFR regeneration in order to obtain high heating rates (cf. Figure 6.4b). The C_xH_y concentration in the off-gas was also analyzed in the case of TCFR. As shown in the magnified area of Figure 6.3, the C_xH_y concentration at the end of regeneration was the same for TCFR as for the uncontrolled case. This is important since the ineffective removal of hydrocarbons can lead to carbon deposition.

The likelihood of autoignition during regeneration depends on the type of fuel used, as well as its boiling range and composition. The experimental investigations conducted for this work showed that autoignition was observed for all types of diesel fuels, but not for jet fuels (cf. Table 3.3). Regardless of the type of fuel, the TCFR approach makes it possible to regenerate adsorbents in a controlled manner with high heating rates. This is important for desulfurization units integrated into fuel-flexible APU systems. Furthermore, the TCFR approach also allows for fast regeneration cycles, and thus, compact design of on-board desulfurization units. Consequently, this approach was used in all of the regeneration experiments that are presented and discussed in the following sections.

6.2.2. Regeneration Efficiency: Ambient Air (AIR_g)[3]

This section presents the experimental results of thermal in situ regeneration with ambient air (AIR_g) for different types of fuels. During regeneration, the temperature was increased in a step-wise manner with a final regeneration temperature of $T_{final} = 450\,°C$. This approach was chosen in order to prevent the thermal destruction of the adsorbent's micro-structure. A detailed account of the regeneration procedure is provided in Table 6.1. In all of these regeneration experiments, the flow rate of AIR_g was controlled by means of the TCFR approach, which was discussed in the previous section.

Table 6.1.: Temperatures and corresponding gas flow rates during thermal in situ regeneration with AIR_g.

Temperature ($°C$)	Gas flow rate (L/min)	Hold time (h)
20 - 160	5	-
160	5	1
160 - 300	4	-
300	4	1.5
300 - 450	2	-
450	2	1
450 - 20 (cool down)	5	-

---

[3]Parts of this section were published in *Energy & Fuels* under the title "Thermal in Situ and System-Integrated Regeneration Strategy for Adsorptive On-Board Desulfurization Units" [98].

Regeneration efficiency was evaluated by comparing the breakthrough capacities of the first and second desulfurization cycles. Figure 6.5 shows the average breakthrough capacities of both fresh and regenerated Ag-Al$_2$O$_3$ using AIR$_g$ as the regeneration medium and $T_{final} = 450\,^{\circ}C$ as final regeneration temperature. The results show high regeneration efficiencies of $\geq 90\%$ for all types of fuels, except in the case of jet/DBT_900, where the regeneration efficiency was $< 55\%$.
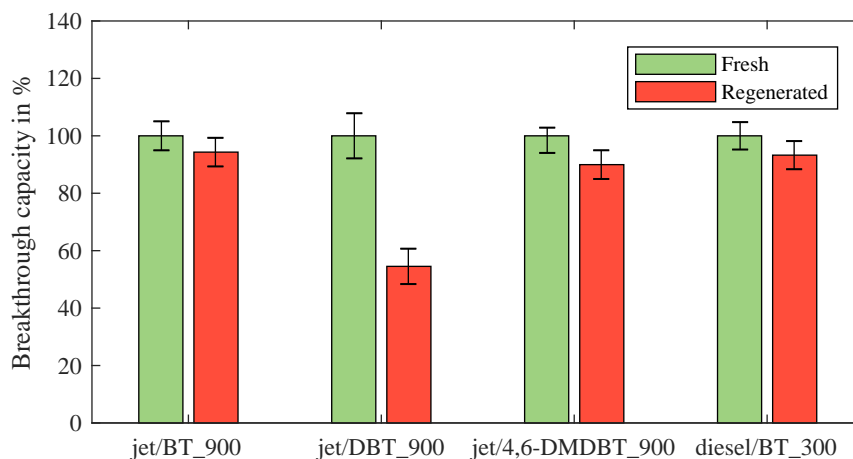
Figure 6.5.: Regeneration efficiency for different types of fuel after one cycle of regeneration using thermal regeneration in AIR$_g$ (adsorbent: Ag-Al$_2$O$_3$; fuel: jet/BT_900, jet/DBT_900, jet/4,6-DMDBT_900, diesel/BT_300; adsorption temperature: $20\,^{\circ}C$; LHSV: $0.85\,h^{-1}$; regeneration: AIR$_g$; final regeneration temperature: $450\,^{\circ}C$).

These results show that AIR$_g$-based regeneration combined with a final regeneration temperature of $T_{final} = 450\,^{\circ}C$ is only effective for fuels containing no DBT. When DBT is present, the regeneration efficiency significantly decreases at these conditions. This conclusion is in agreement with those found in literature: Several promising results were reported with regard to the adsorption of thiophene and BT using ambient air as the regeneration medium. For example, S. Nair and Tatarchuk [101] used Ag/TiO$_2$ to desulfurize jet fuel (JP5, containing no DBT or any of its derivatives) with a total sulfur concentration of $1172\,ppmw$. Thermal regeneration in flowing air at $450\,^{\circ}C$ showed high regenerability over 10 cycles. However, only a few publications deal with thermal regeneration after adsorption of DBT, and none of them reported full regeneration [74, 211]. The difference between DBT and BT regeneration is in the stronger adsorption of DBT, as discussed in Section 4.2.1. This effect is especially relevant when the adsorption is based on π-complexation and direct metal sulfur (S-M) interaction [97].

Additional regeneration experiments were carried in order to investigate whether a final regeneration temperature of $525\,^{\circ}C$ would be sufficient to fully regenerate Ag-Al$_2$O$_3$ after the adsorption of DBT. For these experiments, the temperature profile was slightly modified in comparison one shown in Table 6.1. The slightly modified regeneration procedure with an increased final regeneration temperature of $525\,^{\circ}C$ is displayed in Table 6.2. In order to reduce the chances of the thermal destruction of the adsorbent, the hold time at the final regeneration temperature of $525\,^{\circ}C$ was set to be only $0.33\,h$.

Table 6.2.: Temperatures and corresponding gas flow rates during thermal in situ regeneration with AIR_g at $T_{final} = 525\,°C$.

Temperature ($°C$)	Gas flow rate (L/min)	Hold time (h)
20 - 160	5	-
160	5	1
160 - 300	4	-
300	4	1.5
300 - 450	2	-
450	2	0.33
450 - 525	2	-
525	2	0.33
525 - 20 (cool down)	5	-

The results of the experiments with a final regeneration temperature of $525\,°C$ are shown in Figure 6.6. The observed breakthrough capacities of fresh and regenerated $Ag-Al_2O_3$ were 2.18 and 2.21 $mg\text{-}S/g\text{-}ads$, and thus achieved 100% regeneration of the breakthrough capacity at a final regeneration temperature of $525\,°C$. To the best of the author's knowledge, this is the first time that full thermal regeneration in an oxidative atmosphere has been reported after the adsorption of DBT.
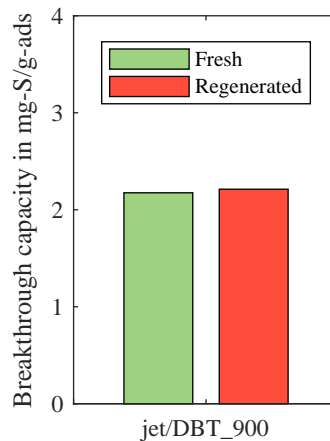
Figure 6.6.: Regeneration efficiency in AIR_g at $525\,°C$ (adsorbent: $Ag-Al_2O_3$; fuel: jet/DBT_900; adsorption temperature: $20\,°C$; LHSV: $0.85\,h^{-1}$; regeneration: AIR_g; final regeneration temperature: $525\,°C$).

The problem with regeneration after the adsorption of DBT is the higher adsorption energy of the two main adsorption mechanisms (π-Ag and S-Ag interaction) in comparison to those of other PASHs, such as BT [97]. DBT is also a more stable compound than BT [54], and thus requires higher temperatures to decompose. These obstacles are the reasons that full thermal regeneration in an oxidizing atmosphere after adsorption of DBT had not previously been reported for any type of adsorbent. For example, Han, H. Lin, and Y. Zheng [74] reported a 23% capacity loss in the second desulfurization cycle for DBT in a model diesel fuel (763 $ppmw$ of

sulfur) after thermal regeneration in air. This capacity loss was related to a significant reduction of the BET surface and the incomplete removal of sulfur from that surface. Xiao and colleagues [123, 127] also performed their regeneration experiments in air, and reported a regenerability of 90 - 95% for a TiO_2-CeO_2 based adsorbent. In their experiments, an ultralow-sulfur diesel was used with 15 $ppmw$ of total sulfur. However, the type of sulfur was not further specified. Hence, the results shown in Figure 6.6 are very promising since they demonstrate that the breakthrough capacity of Ag-Al_2O_3 can be fully restored by means of thermal treatment in an oxidizing atmosphere, even after the adsorption of DBT. However, preheating the ambient air to $525\,°C$ requires large heat exchangers or even additional electric heating. This is why a novel system-integrated thermal on-board regeneration strategy was developed and investigated within this work.

6.3. System-Integrated On-Board Regeneration using Hot APU Off-Gas[4]

Within in this work, a novel system-integrated thermal on-board regeneration strategy, based on hot off-gas from a SOFC-driven APU was developed and investigated. This innovation is important because there is a lack of efficient on-board regeneration strategies for mobile desulfurization units. So far, reasonable regeneration experiments have been carried out in reducing atmospheres (N_2, H_2, or He) or ambient air. However, N_2, H_2, or He are not available on-board, and experiments with ambient air failed to recover 100% of the initial adoption capacity after adsorption of DBT (cf. Section 6.2.2). This is why a novel and reasonable regeneration approach for adsorptive on-board desulfurization units is urgently needed. The schematic flow sheet of the novel approach is illustrated in Figure 6.7. This approach, based on hot APU off-gas, requires no additional regeneration medium, no additional tanks, and no additional bulky equipment and can thus be fully integrated into the concept of an SOFC-operated APU for on-board electricity supply.

6.3.1. Basic Regeneration Performance under APU Off-Gas (APU_g) Conditions[5]

This section presents the results of thermal in situ regeneration with hot APU off-gas (APU_g). The fuel jet/DBT_900 with DBT as a representative PASH was used in most of the experiments. This is because DBT has the strongest adsorption energy compared to other relevant sulfur

---

[4]Parts of this section were published in *Energy & Fuels* and *Journal of Power Sources* under the titles "Thermal in Situ and System-Integrated Regeneration Strategy for Adsorptive On-Board Desulfurization Units" [98] and "Adsorptive on-board desulfurization over multiple cycles for fuel-cell-based auxiliary power units operated by different types of fuels" [99].

[5]Parts of this section were published in *Energy & Fuels* under the title "Thermal in Situ and System-Integrated Regeneration Strategy for Adsorptive On-Board Desulfurization Units" [98].
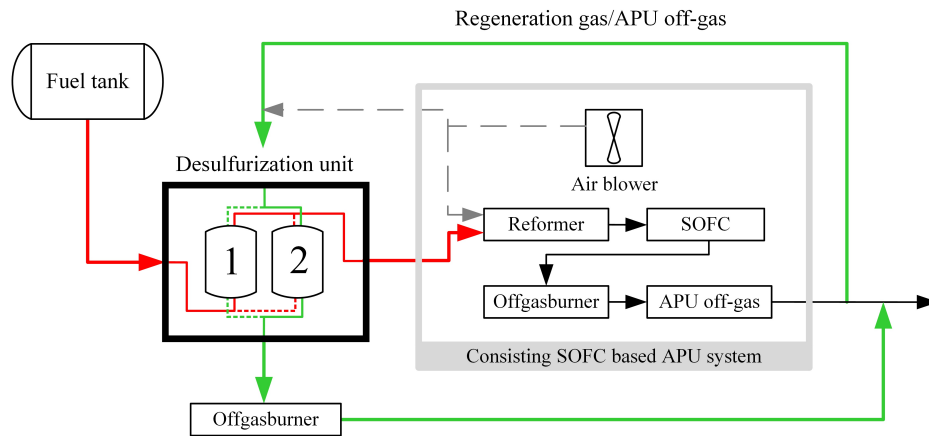
Figure 6.7.: Schematic flow sheet of the novel system-integrated thermal on-board regeneration strategy, based on hot off-gas from an SOFC-operated APU [99].

heterocycles [97, 110], and thus presents a significant challenge for the thermal on-board regeneration of used adsorbent (cf. Figure 6.5). After breakthrough experiments with diesel/DBT_900, the test rig was switched into the regeneration mode described in Section 3.4. For regeneration, the adsorber was flushed with APU_g. The composition of the APU_g is shown in detail in Table 6.3, and is similar to real, hot APU off-gases from an SOFC-based APU [19].

Table 6.3.: Detailed composition of the hot off-gas from an auxiliary power unit with 4.5 mol% H_2O (APU_g) used as regeneration medium.

	APU off-gas (APU_g) composition in (mol/mol)
N_2	0.763
O_2	0.168
CO_2	0.024
H_2O	0.045

For the first regeneration experiments with APU_g, the same temperature profile with a final regeneration temperature of $T_{final} = 525\,°C$ was applied as was used for regeneration with AIR_g (cf. Table 6.2). The regeneration procedure is described in detail in Table 6.4. In all of the regeneration experiments, the flow rate of APU_g was controlled using the TCFR approach presented in Section 6.2.1.

The breakthrough curves of jet/DBT_900 and the average breakthrough capacities of DBT in the first and second desulfurization cycles are shown in panels (a) and (b), respectively, of Figure 6.8. A breakthrough capacity of 2.21 mg-S/g-ads was observed in the first desulfurization cycle. After regeneration with APU_g, the breakthrough capacity was 2.20 mg-S/g-ads, thus indicating 100% recovery. This is a very promising result since it highlights the fact that the hot off-gas from SOFC-based APUs can be used as a regeneration medium for the in situ on-board regeneration of spent adsorbent. Accomplishing the regeneration of the adsorbent on-board is essential in order to keep the whole APU small and light. Additional comprehensive

Table 6.4.: Temperatures and corresponding gas flow rates during thermal in situ regeneration with APU_g at a final regeneration temperature of $T_{final} = 525\,°C$.

Temperature ($°C$)	Gas flow rate (L/min)	Hold time (h)
20 - 160	5	-
160	5	1
160 - 300	4	-
300	4	1.5
300 - 450	2	-
450	2	0.33
450 - 525	2	-
525	2	0.33
525 - 20 (cool down)	5	-

investigations were carried out in order to investigate the influence of the gas composition of the hot APU off-gas on the overall desorption and regeneration mechanism. These results are presented and discussed in the following section.
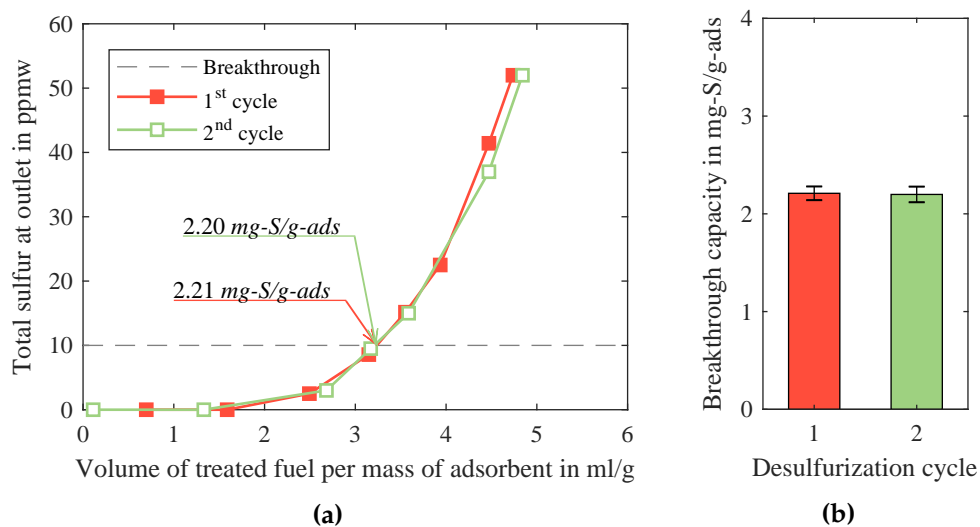
Figure 6.8.: (a) Breakthrough curve of jet/DBT_900 in the first and second desulfurization cycles and (b) the corresponding average breakthrough capacities of DBT in the first and second cycles using APU_g as regeneration medium (adsorbent: $Ag-Al_2O_3$; fuel: jet/DBT_900; adsorption temperature: $20\,°C$; LHSV: $0.85\,h^{-1}$; regeneration: APU_g; final regeneration temperature: $525\,°C$) [98].

6.3.2. Regeneration Mechanism under APU Off-Gas Conditions[6]

The experimental investigation with hot APU off-gas showed excellent regeneration performance. In order to better understand the positive effect of the APU off-gas composition in

---

[6]Parts of this section were published in *Energy & Fuels* under the title "Thermal in Situ and System-Integrated Regeneration Strategy for Adsorptive On-Board Desulfurization Units" [98].

comparison to ambient air, effort was made to gain deeper insight into the overall regeneration mechanisms under APU off-gas conditions. The regenerated adsorbent was therefore analyzed using several different techniques, and the results of these analyses will be compared and discussed in depth. All of the types of analysis and their corresponding positions in the overall experimental process are illustrated in Figure 6.9a. The results of all of the analyses shown in Figure 6.9a will be presented and discussed consecutively in the following paragraphs.

(a) Overall procedure

(b) Elemental sulfur
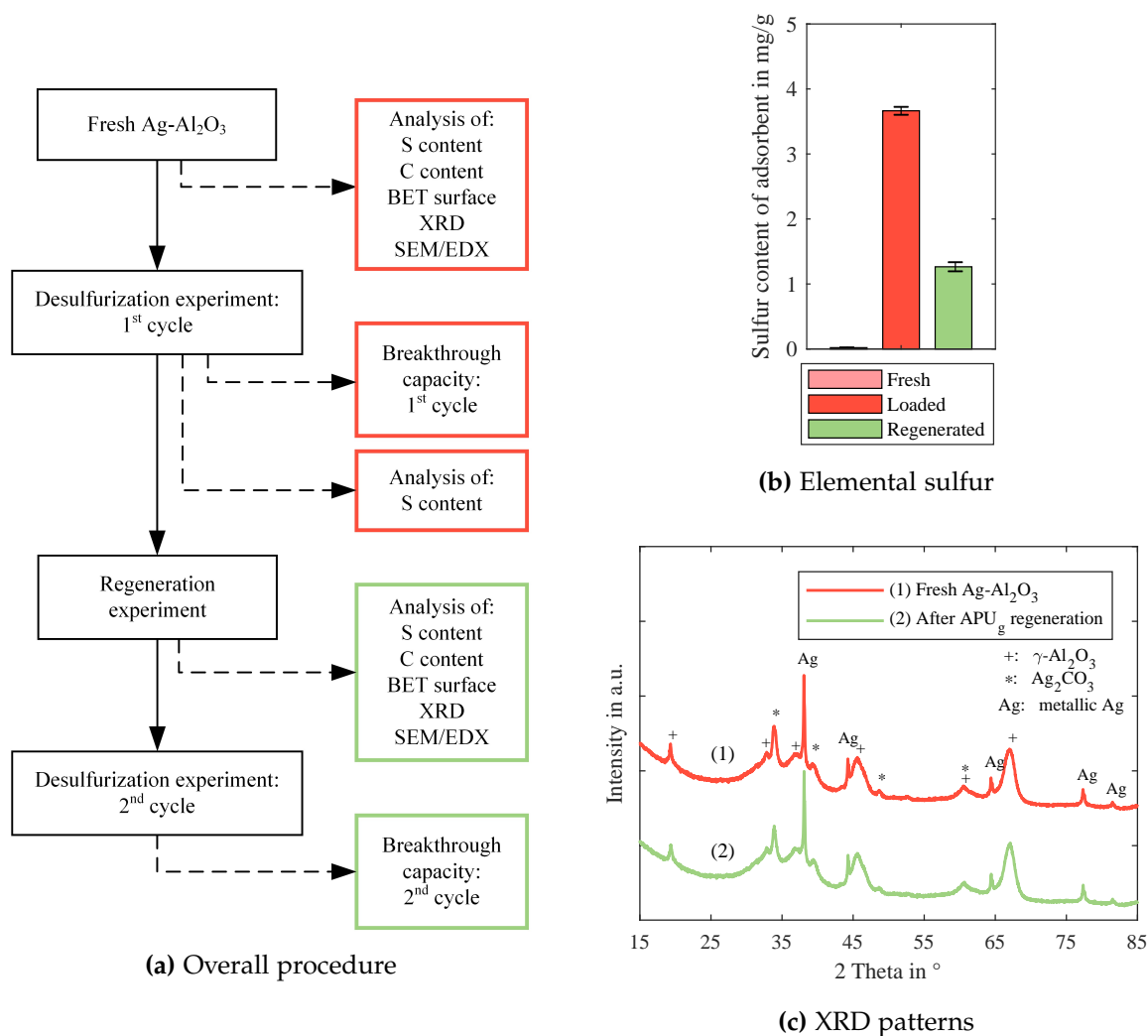
(c) XRD patterns

Figure 6.9.: (a) Overall experimental and analytic procedure, (b) elemental sulfur contents of fresh, loaded, and APU$_g$-regenerated Ag-Al$_2$O$_3$, and (c) XRD patterns of (1) fresh Ag-Al$_2$O$_3$ and (2) after APU$_g$ regeneration (adsorbent: Ag-Al$_2$O$_3$; fuel: jet/DBT$_-$900; adsorption temperature: 20 °C; regeneration: APU$_g$; final regeneration temperature: 525 °C) [98].

The results of the elemental sulfur analysis of fresh Ag-Al$_2$O$_3$, Ag-Al$_2$O$_3$ after the first desulfurization experiment, and Ag-Al$_2$O$_3$ after the regeneration experiment (cf. Figure 6.9a) are presented in Figure 6.9b. The sulfur content of fresh Ag-Al$_2$O$_3$ was below 0.02 mg/g. After the first breakthrough cycle, the sulfur content increased to 3.6 mg/g (loaded) due to the adsorption of DBT on the adsorbent surface. This sulfur content was measured at the end of the experiment (not at breakthrough), and is thus above the total sulfur breakthrough capacity. After APU$_g$ regeneration, the sulfur content dropped to 1.2 mg/g. This result shows that not

all of the sulfur was removed during regeneration. This latter point is of great interest: the breakthrough capacity was $2.2\,mg/g$ in the first desulfurization cycle, and in the subsequent regeneration step, not all of the sulfur was removed. However, in the second desulfurization cycle, the breakthrough adsorption capacity of Ag-Al$_2$O$_3$ was again $2.2\,mg/g$ (cf. Figure 6.8b), thus indicating that 100% of the adsorption sites had regenerated. Similar results were also observed in the case of jet/BT_900 (not shown), indicating the same overall regeneration mechanism for both types of PASHs.

The carbon content of the adsorbent was determined in order to investigate whether the remaining sulfur was an organic or inorganic compound. The carbon-to-sulfur ratio (C/S weight ratio) of DBT is 4.5. The C/S weight ratio for the regenerated Ag-Al$_2$O$_3$ was 0.7, and thus well below the C/S weight ratio of DBT. These results indicate the formation of inorganic rather than organic sulfur compounds during regeneration. Similar results were reported by Samokhvalov et al. [212], who investigated the thermally induced desorption of thiophene from Ag-modified titania under a high vacuum. In their work, surface sulfur content dropped by one-half after the adsorbent was annealed at $525\,°C$ under X-ray photoelectron spectroscopy (XPS) conditions (working pressure of 10^{-8} - $10^{-6}\,Torr$, which is equal to 10^{-11} - $10^{-9}\,bar$). The sulfur compound detected on the surface was assigned to Ag$_2$S [212]. After the addition of O$_2$ ($10^{-2}\,Torr$, which is equal to $10^{-5}\,bar$) at $525\,°C$, all of the sulfur completely disappeared, according to the XPS analysis. Bezverkhyy et al. [213] also observed the formation of Ag$_2$S at temperatures above $200\,°C$. However, Ag$_2$S was also detected by XRD after thermal regeneration in flowing N$_2$ at $300\,°C$.

In the present work, XRD analysis was carried out to identify any changes in the active silver phase. The XRD patterns of fresh and regenerated Ag-Al$_2$O$_3$ are presented in Figure 6.9c. The XRD pattern of the fresh adsorbent (1) was identical to the XRD pattern after APU$_g$ regeneration (2). These results indicate proper regeneration and correlate with the desulfurization results, in which the breakthrough capacity was $2.2\,mg/g$ in both the first and second desulfurization cycles. Aside from γ-Al$_2$O$_3$ (ICSD database; PDF 10-425) metallic silver [186] was also detected by XRD analysis. This metallic silver is related to the small Ag particles on the surface of the adsorbent that are formed during preparation, as discussed in Section 4.1.3. The active silver phase in the XRD analysis is represented by Ag$_2$CO$_3$ (not metallic silver, cf. Section 4.1.3) which was clearly detected in both samples. The same XRD patterns were also observed in the case of jet/BT_900 and are shown in Figure A.2, in Appendix A.3. The similar XRD patterns for BT and DBT indicate that the overall regeneration mechanism is the same for both types of PASH. However, no crystalline Ag$_2$S was detected in any sample.

Figure 6.10a and Figure 6.10b show the SEM images and the corresponding EDX patterns of the fractured surface of fresh and regenerated Ag-Al$_2$O$_3$ particles, respectively. Both EDX patterns clearly show the presence of Ag and C which are related to the Ag$_2$CO$_3$ phase.

(a) Fresh Ag-Al$_2$O$_3$ **(b)** Ag-Al$_2$O$_3$ after one cycle of regeneration
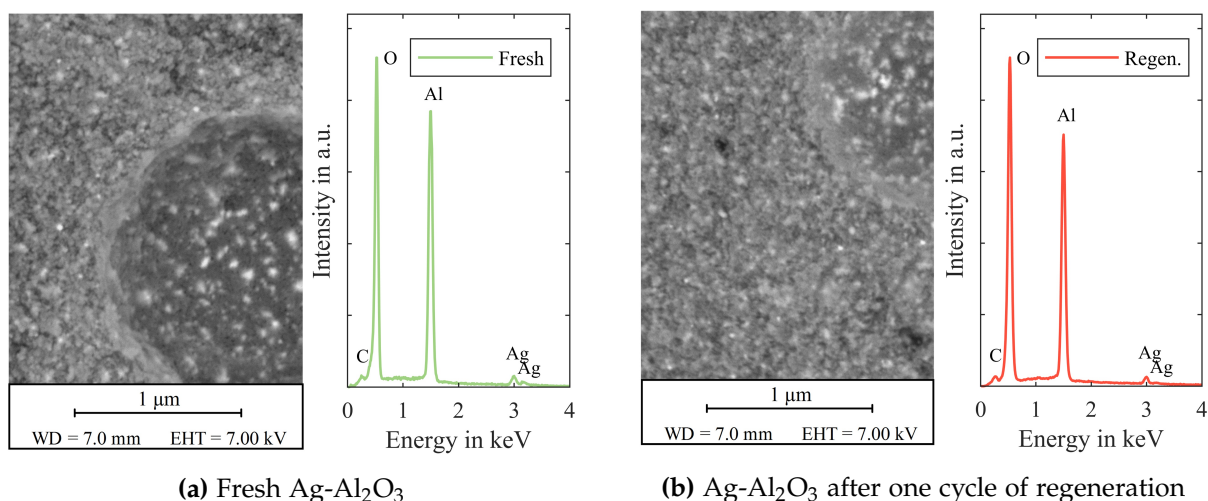
Figure 6.10.: SEM images and EDX patterns of the fractured surfaces of (a) fresh Ag-Al$_2$O$_3$ and (b) after one cycle of regeneration with APU$_g$ (adsorbent: Ag-Al$_2$O$_3$; fuel: jet/DBT_900; adsorption temperature: 20 °C; regeneration: APU$_g$; final regeneration temperature: 525 °C) [98].

The SEM images of both fractured surfaces in Figure 6.10 show a homogeneous and nanodispersed active silver phase (bright dots) within the porous structure of the adsorbent, but no Ag agglomeration was observed during regeneration. Both the XRD and SEM-EDX analyses confirmed a stable active silver phase under APU off-gas conditions, which is in agreement with the experimental results presented in Section 6.3.1. However, the EDX pattern in Figure 6.10b shows no evidence of sulfur, indicating its homogeneous distribution within the bulk phase, and hence, a sulfur level that is below the EDX detection limit (detection limit of 0.1 - 0.2 $wt\%$).

On the basis of the results presented and discussed so far, the following overall desorption mechanism for PASHs in APU off-gas atmosphere is proposed and illustrated in Scheme 6.1. The adsorption of PASHs is favored by the strong π-Ag and S-Ag interactions on silver cations (cf. Chapter 4), as illustrated in Scheme 6.1. At the beginning of regeneration, CO$_2$ from the APU off-gas adsorbs on γ-Al$_2$O$_3$ at temperatures below 60 °C. At temperatures above 60 °C, the CO$_2$ desorbs from the surface [214], and further acts as an inert compound. As the temperature increases (from 90 - 200 °C), weakly bound (physisorbed) PASHs evaporate. More strongly bound (by π-Ag and S-Ag interactions) PASHs start to decompose at temperatures above 200 °C, with the formation of "coke" [215, 216] and Ag$_2$S in the presence of silver (cf. step 1 in Scheme 6.1). The formation of Ag$_2$S was also observed by both Samokhvalov et al. [212] and Bezverkhyy et al. [213], who used Ag-modified titania and Ag-modified zeolite as adsorbents, respectively.

Ag$_2$S is a relatively stable chemical compound, and thus requires higher temperatures to decompose. The straightforward oxidation of Ag$_2$S by molecular O$_2$ according to Equation 6.1 is a possible reaction pathway at temperatures between 400 and 525 °C [217, 218]. At the same time (300 - 525 °C), the thermal decomposition of "coke" takes place [85, 219]. Both processes
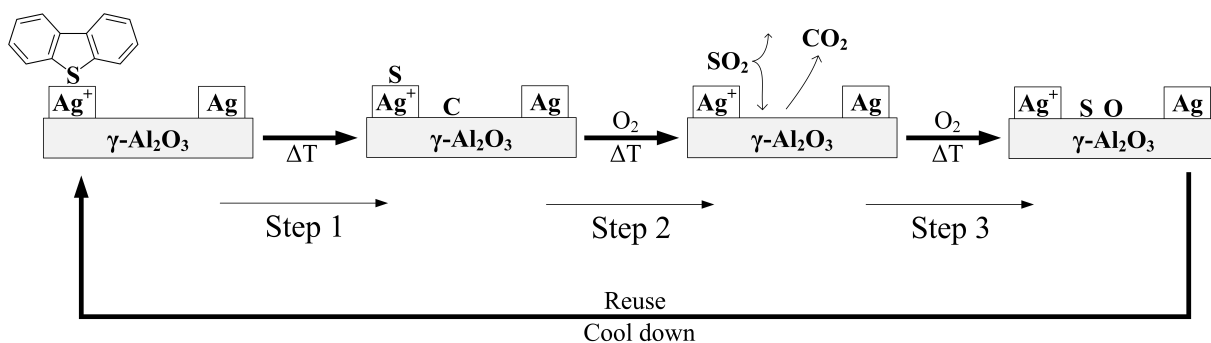
Scheme 6.1: Desorption/regeneration mechanism of DBT from the surface of Ag-Al$_2$O$_3$ during thermal regeneration under APU off-gas conditions [98].

are illustrated in step 2 in Scheme 6.1. A second reaction of Ag$_2$S could proceed according to Equation 6.2, which has sufficiently fast reaction kinetics at temperatures above 300 °C [220]. This reaction requires Ag$_2$O, which was definitively not detected in this work (cf. Figure 6.9c), nor reported by Heinzel [114], who investigated the active phase of silver in Ag-TiO$_2$ and Ag-SiO$_2$. Consequently, Equation 6.2 is not involved in the case of thermal regeneration of Ag-Al$_2$O$_3$ under APU off-gas conditions. However, the preservation of Ag$_2$S, as reported by Bezverkhyy et al. [213], is caused by a lack of O$_2$, as the regeneration was performed in N$_2$, and thus no reaction according to Equation 6.1 could occur. In addition, the reaction of Ag$_2$S according to Equation 6.2 was suppressed because of the insufficient residence time at 300 °C before cool down.

$$Ag_2S + O_2 \longrightarrow 2Ag + SO_2 \tag{6.1}$$

$$2Ag_2O + Ag_2S \longrightarrow 6Ag + SO_2 \tag{6.2}$$
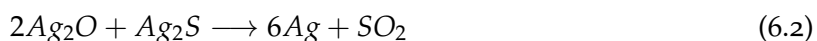
The role of SO$_2$ still needs to be understood to explain the remaining sulfur in the present work. This is particularly interesting because the results showed that the remaining inorganic sulfur compounds neither block nor react with the active adsorption sites under APU off-gas conditions. The final products of all reactions are Ag and SO$_2$. Consequently, SO$_2$ must be the educt of any further reaction. Alumina (Al$_2$O$_3$), mostly in its γ form, is a common catalyst in the Claus process. As is known from the Claus process, even small amounts of O$_2$ results in performance degradation through the formation of aluminum sulfates [221]. The formation of aluminum sulfates upon SO$_2$ adsorption on γ-Al$_2$O$_3$ has also been reported in the presence of O$_2$ at temperatures above 400 °C by Saur et al. [222] and Chang [223]. Gradual thermal decomposition of aluminum sulfates is reported to start above > 600 °C, including complete conversion of the anhydrous sulfate at about 920 °C [224]. SO$_2$ adsorption on γ-Al$_2$O$_3$ at 200 °C was also reported in a N$_2$ atmosphere [225], which, in turn, led to the formation of surface sulfite [223] rather than sulfate. However, increasing the temperature to 500 °C led to the

desorption of SO_2 [225]; only negligible amounts of SO_2 stayed on the surface, which can be attributed to strongly chemisorbed SO_2 [226]. It is important to highlight the fact that, in the presence of O_2, the adsorption of SO_2 on γ-Al_2O_3 was significantly increased [225]. This phenomenon was reported for the whole temperature range of 200 - 500 °C and is one explanation for the different results that were observed by Samokhvalov et al. [212] in a high vacuum, where no sulfur remained on the adsorbent.

SO_2 adsorption on porous TiO_2 has yielded similar results in literature. In the presence of O_2, SO_2 leads to the formation of $TiOSO_4$, which is thermally stable up to 650 °C [222]. However, a lack of O_2 leads only to the formation of sulfite, which decreases significantly upon heating to 500 °C. This explains the results reported by Samokhvalov et al. [212], where O_2 was available only at 525 °C and 10^{-5} bar to oxidize Ag_2S according to Equation 6.1. Hence, the adsorption of SO_2 and the subsequent formation of sulfite or sulfate, as reported in Ref. [222] and [227], is prevented by providing O_2 only at a high temperature of 525 °C.

In this work, all of the regeneration gas mixtures used had O_2 contents in the range of 15 - 21 mol% (cf. Table 3.4). From the results discussed above, it is most likely that the emission of SO_2 during regeneration partly leads to the formation of highly thermally stable aluminum sulfates, which is illustrated in step 3 in Scheme 6.1. The fact that no aluminum sulfates were detected by XRD analysis (cf. Figure 6.9c) indicates that the aluminum sulfates are formed as bulk aluminum sulfates. This was also reported by Hamzehlouyan et al. [228], who provide a more detailed account of the mechanisms and thermodynamic data for the formation of bulk aluminum sulfates by adsorption of SO_2 on γ-Al_2O_3. In addition, She et al. [229] also observed the formation of aluminum sulfates on a Ag/Al_2O_3 catalyst for the selective catalytic reduction (SCR) of NO with methane. The formation of aluminum sulfates on Ag/Al_2O_3 was observed when SO_2 (and O_2) was present in the gas stream at 625 °C. All of these results confirm the validity of the proposed overall desorption mechanism illustrated in Scheme 6.1.

The adsorption of PASHs in subsequent desulfurization cycles is not affected by the formation of aluminum sulfates. This becomes apparent by comparing the first and last stages presented in Scheme 6.1. PASHs are adsorbed primarily through silver cations (cf. Section 4.1), whereas aluminum sulfates are formed on the alumina surface. This is why the full adsorption capacity of Ag-Al_2O_3 was regenerated, as shown in Figure 6.8b. The overall regeneration mechanism proposed in Scheme 6.1 can bee seen as an essential finding in order to improve the novel and system-integrated regeneration strategy based on hot APU off-gas. In addition, this overall regeneration mechanism provides the fundamental understanding necessary to answer research question 4: what is the service/regeneration interval of this desulfurization approach?. However, further discussion is needed regarding the thermal stability of the active silver phase in order to predict the long-term stability of the Ag-Al_2O_3 adsorbent.

According to She et al. [229], Ag clustering of the dispersed silver phase on the surfaces of Ag/Al_2O_3 SCR catalyst was observed at an operating temperature of 625 °C in a gas

stream of CH_4, NO, and O_2. This phenomenon is well known for various supports, including SiO_2, TiO_2, and Al_2O_3 [229, 230]. Within $60\,h$ on stream, the highly dispersed Ag phase (nanoparticles with a particle size $< 20\,nm$) of the Ag/Al_2O_3 SCR catalyst started to form large silver agglomerates with a particle size of up to $> 1\,\mu m$. In the present work, no Ag agglomeration was observed during the first regeneration cycle, which had a final regeneration temperature of $525\,°C$, as shown by the SEM images in Figure 6.10. However, additional long-term experiments and comprehensive material analyses were carried out in order to exclude the possibility of Ag agglomeration in the long run. The results of these long-term experiments are presented and discussed in Section 6.4.2. Prior to the long-term experiments, comprehensive studies were carried out to investigate the role of H_2O during thermal regeneration in an oxidizing atmosphere as well as the influence of different types of PASHs, fuels, and LHSVs on regeneration performance.

6.3.3. The Role of H_2O during Thermal Regeneration in Oxidizing Atmosphere[7]

One difficulty posed by thermal on-board regeneration is finding a source of hot regeneration gas. For mobile applications in particular, preheating the ambient air with a heat exchanger or electrical heating device requires additional bulky equipment and is inefficient. Using the freely available, hot off-gas from an SOFC-driven APU as regeneration gas not only significantly increases the overall efficiency of this approach, but also makes it possible for the desulfurization unit to be smaller and lighter in design. The APU off-gas differs in composition from ambient air in that it contains CO_2 and significantly higher amounts of water (about $4.5\,vol.\%$ [19]). The increased H_2O content of the APU off-gas implies the increased heat capacity of the regeneration gas, which has a positive effect on the thermal decomposition of PASHs. The higher H_2O content of the APU off-gas also inhibits carbon deposition. This is known from the fields of steam reforming [30] and the internal reforming of hydrocarbons in SOFCs [25, 26, 231, 232]. One negative aspect of this higher heat capacity of the regeneration medium would be thermal destruction of the adsorbent. This is why the physical properties of both fresh and regenerated $Ag\text{-}Al_2O_3$ were analyzed by means of N_2 physisorption. The results in Table 6.5 depict the thermal stability of $Ag\text{-}Al_2O_3$ at $525\,°C$ under APU_g conditions.

Table 6.5.: Physical properties of fresh $Ag\text{-}Al_2O_3$ and $Ag\text{-}Al_2O_3$ after regeneration with APU_g at a final temperature of $525\,°C$ (adsorbent: $Ag\text{-}Al_2O_3$; fuel: jet/DBT_900; regeneration: APU_g; final regeneration temperature: $525\,°C$).

Adsorbent	BET surface (m^2/g)	BJH pore volume (cm^3/g)	BJH mean pore diameter (nm)
Fresh	145	0.42	9.5
APU_g-regenerated	143	0.42	9.4

---

[7]Parts of this section were published in *Energy & Fuels* under the title "Thermal in Situ and System-Integrated Regeneration Strategy for Adsorptive On-Board Desulfurization Units" [98].

Only a minor surface reduction, from 145 to $143\,m^2/g$, was observed for the regenerated adsorbent in comparison to the fresh material. This surface reduction of 1.7% was not thermally induced, but was rather the result of aluminum sulfate forming during regeneration. This conclusion is based on the fact that the same surface reduction was observed for Ag-Al$_2$O$_3$ when the final regeneration temperature was $450\,°C$ and thus equal to the calcination temperature of the adsorbent, as reported in Ref. [96]. No analysis of the BET surface was carried out after regeneration in AIR$_g$ since the focus was placed on APU$_g$.

Additional experiments were carried out with an APU off-gas containing $12.4\,mol\%$ H$_2$O, which is three times higher than that of APU$_g$. Thus, this gas is referred to as APU$_{g/wet}$; its composition is provided in detail in Table 3.4. The final regeneration temperature for these experiments was set to $T_{final} = 450\,°C$, and is thus the same as that of regeneration experiments performed with AIR$_g$. The experiments were set up in this way in order to study the influence of the increased H$_2$O content in the regeneration gas since regeneration with AIR$_g$ at $T_{final} = 450\,°C$ failed to fully restore the initial adsorption capacity after adsorption of DBT. Figure 6.11 shows the results of the breakthrough experiments using APU$_{g/wet}$ and AIR$_g$ as regeneration gases at a final regeneration temperature of $450\,°C$.
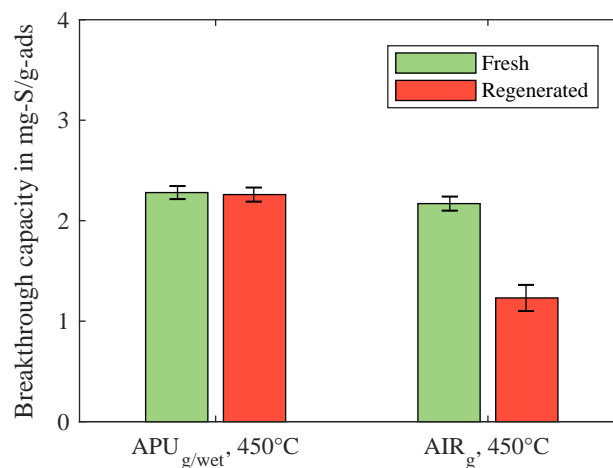
Figure 6.11.: Breakthrough capacity of DBT for fresh and regenerated Ag-Al$_2$O$_3$ using APU$_{g/wet}$ and AIR$_g$ as regeneration gas with a final regeneration temperature of $T_{final} = 450\,°C$ (adsorbent: Ag-Al$_2$O$_3$; fuel: jet/DBT_900; adsorption temperature: $20\,°C$; LHSV: $0.85\,h^{-1}$; regeneration: APU$_{g/wet}$, AIR$_g$; final regeneration temperature: $450\,°C$) [98].

In the case of AIR$_g$, the average breakthrough capacity dropped from 2.17 to $1.23\,mg\text{-}S/g\text{-}ads$, and thus, only 57% of the breakthrough capacity was recovered in the second cycle after regeneration. In contrast, 100% of the breakthrough capacity was recovered when APU$_{g/wet}$ was used as the regeneration gas. This is a very promising result, and this finding highlights the positive impact of the APU$_g$ gas's composition on regeneration. In addition, the regeneration temperature can be significantly reduced when the H$_2$O content of the regeneration gas is increased to $12.4\,mol\%$, which leads to 100% regeneration after DBT adsorption even at $450\,°C$. It is important to note that it seems possible to lower the final regeneration temperature for

regeneration with APU$_{g/wet}$ even further; however, in the present work, these experiments were only carried out to highlight the positive effect of H_2O in a more qualitative manner.

The positive effect of H_2O is not only related to its higher heat input. Its ability to displace adsorbed compounds such as PASHs should also be taken into account. The reaction kinetics of the thermal decomposition of PASHs also seems to increase in the presence of H_2O, as this effect was also observed for other polycyclic aromatic compounds [233]. Further, the presence of H_2O reduces the adsorption of SO_2 and, consequently, can impede the formation of aluminum sulfates. This effect was reported by S. Andersson, Pompe, and Vannerberg [225], who found that SO_2 adsorption on γ-Al_2O_3 significantly decreased in the presence of humidified air over the whole temperature range of 200 - 500 $°C$. These results are supported by a DFT study, which found that SO_2 preferentially adsorbs on a water-free surface of γ-Al_2O_3 [226]. However, the results obtained so far have indicated that neither the adsorption of SO_2, nor the subsequent formation of aluminum sulfates have a negative influence on the desulfurization performance of Ag-Al_2O_3.

6.4. Regeneration Efficiency: Hot APU Off-Gas (APU$_g$)

This section presents an experimental investigation of the regeneration efficiency of APU$_g$ at a final regeneration temperature of $T_{final} = 500 °C$. The detailed temperature profile and corresponding gas flow rates are shown in Table 6.6. A heating rate in the range of 4.2 - 8.2 $°C/min$ and the TCFR approach were used. This regeneration procedure is a first step towards the creation of an optimized regeneration profile in comparison to the basic investigation of APU$_g$ regeneration that was presented and discussed in Section 6.3.1.

Table 6.6.: Optimized temperatures and corresponding gas flow rates during regeneration with APU$_g$.

Temperature ($°C$)	Gas flow rate (L/min)[a]	Hold time (h)
20 - 160	5	-
160	5	1.0
160 - 300	4	-
300	4	1.0
300 - 450	2	-
450	2	0.33
450 - 500	2	-
500	2	0.33
500 - 20 (cool-down)[b]	5	-

[a] At standard conditions

[b] Cool-down with ambient air

In this section, the slightly optimized regeneration profile that is presented and used for all experiments is based on a shorter hold time of only $1\,h$ at $300\,°C$. Moreover, the final regeneration temperature was reduced by $25\,K$ to $T_{final} = 500\,°C$. This reduction in temperature decreases the amount of time necessary for both heat up and cool down, which is important for a fast overall regeneration cycle. The following section presents the results of regeneration efficiency experiments for different scenarios.

6.4.1. Influence of the Type of Fuel, Type of PASH, and LHSV[8]

State of the art regeneration with ambient air has several disadvantages, including the bulky equipment required for preheating. Furthermore, the efficiency of regeneration with ambient air significantly decreases after the desulfurization of a DBT-rich fuel, as shown in Figure 6.5, while regeneration using APU$_g$ achieved full regeneration after desulfurization of a DBT-rich fuel (cf. Section 6.3.1). In this section, regeneration with APU$_g$ was investigated more comprehensively in order to evaluate its regeneration efficiency in different scenarios.

Figure 6.12 shows the average breakthrough capacities of jet/BT_900, jet/DBT_900, and diesel/DBT_900 for the first and the second desulfurization cycles. The results of the regeneration experiments showed that APU off-gas is an ideal regeneration medium. In all cases, breakthrough capacity was restored to 100% after regeneration with APU$_g$, showing excellent reproducibility, as seen in Table 6.6.
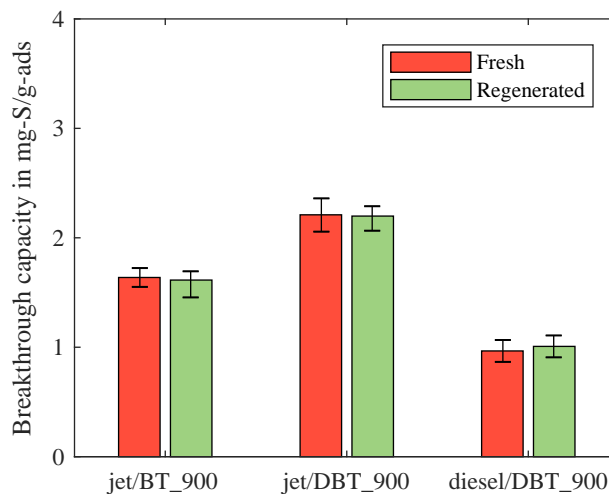
Figure 6.12.: Breakthrough capacities of different types of fuels for fresh and regenerated Ag-Al$_2$O$_3$ adsorbent using APU$_g$ as regeneration gas with a final regeneration temperature of $T_{final} = 500\,°C$ (adsorbent: Ag-Al$_2$O$_3$; fuel: jet/BT_900, jet/DBT_900, diesel/DBT_900; adsorption temperature: $20\,°C$; LHSV: $0.85\,h^{-1}$; regeneration: APU$_g$; final regeneration temperature: $500\,°C$) [99].

---

[8]Parts of this section were published in *Journal of Power Sources* under the title "Adsorptive on-board desulfurization over multiple cycles for fuel-cell-based auxiliary power units operated by different types of fuels" [99].

These results confirm that hot APU off-gas is able to fully regenerate breakthrough capacity at a final regeneration temperature of $T_{final} = 500\,°C$ regardless of the type of fuel or the type of PASH adsorbed. This finding is crucial for real applications because it provides them with high fuel flexibility.

Additional breakthrough experiments were carried out at LHSVs of 0.85 and $0.34\,h^{-1}$ over 5 cycles to investigate whether or not regeneration efficiency was independent of the fuel residence time. This investigation was carried out with diesel/DBT_900, as this fuel was the most challenging in terms of regeneration. Additionally, diesel/DBT_900 showed the lowest breakthrough capacity at $LHSV = 0.85\,h^{-1}$ as shown in Figure 6.12. Consequently, the influence of the LHSV on the breakthrough capacity is of special interest in the case of diesel/DBT_900. The results in Figure 6.13 show that, during the breakthrough experiment, the LHSV has no influence on regeneration performance. Consequently, the efficiency of on-board regeneration with hot APU off-gas is independent of all relevant adsorption parameters, including type of fuel, type of PASH, and LHSV, which thus highlights the extreme efficiency and flexibility of this system-integrated regeneration strategy. Figure 6.13 shows that the breakthrough capacity at $LHSV = 0.34\,h^{-1}$ (green bars) significantly increased in comparison to the breakthrough capacity at $LHSV = 0.85\,h^{-1}$ (red bars), but is still about $0.8\,mg\text{-}S/g\text{-}ads$ below the average equilibirum saturation capacity (dotted line). A more detailed discussion of the influence and importance of the LHSV on the desulfurization performance can be found in Section 5.3.3.
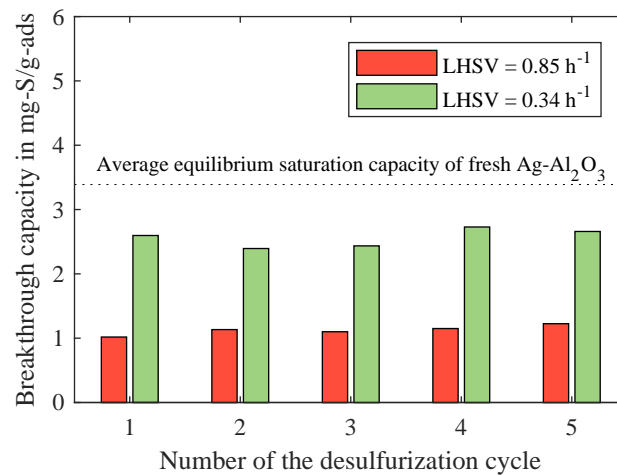
Figure 6.13.: Breakthrough capacity of diesel/DBT_900 over 5 cycles at different LHSVs using APU$_g$ as the regeneration medium at a final regeneration temperature of $T_{final} = 500\,°C$ (adsorbent: Ag-Al$_2$O$_3$; fuel: diesel/DBT_900; adsorption temperature: $20\,°C$; LHSV: 0.85, $0.34\,h^{-1}$ regeneration: APU$_g$; final regeneration temperature: $500\,°C$) [99].

The breakthrough capacity slightly fluctuated over the 5 cycles of desulfurization at an LHSV of $0.34\,h^{-1}$ with an average breakthrough capacity of $2.6\,mg\text{-}S/g\text{-}ads$. This slight fluctuation can be linked to the uncertainty of the experimental procedure and analysis, but it is within the range of fluctuation that was also observed for the repeated saturation experiments (cf. average saturation capacity in Figure 4.10). In the case of $LHSV = 0.85\,h^{-1}$, the average breakthrough capacity was $1.1\,mg\text{-}S/g\text{-}ads$. However, no fluctuation was observed, but rather a slight increase

in the breakthrough capacity. This increase in the breakthrough capacity, however, is again within the uncertainty of the experimental procedure and analysis. The stronger fluctuation at $LHSV = 0.34\,h^{-1}$ can be related to the long duration of the experiment ($14\,h$) in comparison to a duration of only $3\,h$ at $LHSV = 0.85\,h^{-1}$, since deviations in the flow rate are added up over the experiment's duration. Nonetheless, no tendency towards the of degradation of the breakthrough capacity was obtained in either experiment. This is a very promising result that indicates stable desulfurization performance over multiple cycles, and thus long service intervals (meaning that the adsorbent seldom has to be replaced) for the mobile desulfurization unit. Further long-term experiments were carried out over 14 cycles in order to study the long-term stability of the adsorbent. The results of these investigations are presented and discussed in the following section.

6.4.2. Long-Term Regeneration Performance with Hot APU Off-Gas[9]

Additional breakthrough experiments were carried out over 14 cycles using APU$_\text{g}$ as the regeneration medium in order to investigate the long-term desulfurization and regeneration performance of Ag-Al$_2$O$_3$. The results of these experiments are illustrated in Figure 6.14 and depict full thermal regeneration over 14 cycles of operation. An additional equilibrium saturation experiment was carried out after 14 cycles of operation to investigate the chemical and thermal stability of Ag-Al$_2$O$_3$ from an experimental point of view. This experiment was performed with the Ag-Al$_2$O$_3$ adsorbent that had been regenerated 14 times, according to the procedure described in Section 3.3.1. The equilibrium saturation capacity observed was $3.3\,mg/g$, and is given as the 15$^{\text{th}}$ desulfurization cycle in Figure 6.14. This is the same level as the average equilibrium saturation capacity of fresh Ag-Al$_2$O$_3$ ($3.4\,^{+0.06}_{-0.14}\,mg$-$S/g$-$ads$, cf. Figure 4.12) and thus confirms both the thermal and chemical stability of all relevant active adsorption sites under APU off-gas conditions over 14 cycles of operation. To the best of this author's knowledge, this is the first time that the adsorbent has been successfully regenerated after desulfurization of a DBT-rich fuel over 14 cycles without degeneration.

Comprehensive material analyses, including N$_2$ physisorption and an elemental analysis, were carried out to investigate the thermal and chemical stability of the Ag-Al$_2$O$_3$ adsorbent in more detail. The physical properties of fresh Ag-Al$_2$O$_3$, Ag-Al$_2$O$_3$ after 1 cycle of operation, and Ag-Al$_2$O$_3$ after 14 cycles are shown in Table 6.7. The initial surface area of $141.7\,m^2/g$ decreased only by 1.3% after one cycle of operation. After the first cycle, the surface area remained stable over the following 13 cycles of operation. These results confirm the excellent thermal stability of the porous structure of the Ag-Al$_2$O$_3$ adsorbent under APU$_\text{g}$ conditions at $500\,^\circ C$. The minor

---

[9]Parts of this section were published in *Journal of Power Sources* under the title "Adsorptive on-board desulfurization over multiple cycles for fuel-cell-based auxiliary power units operated by different types of fuels" [99].
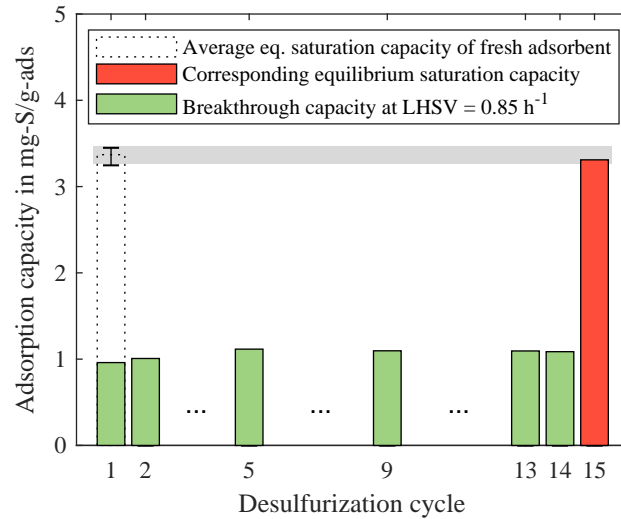
Figure 6.14.: Breakthrough capacity of diesel/DBT_900 over 14 cycles of operation and comparison of the equilibrium saturation capacity of fresh and 14 times used Ag-Al$_2$O$_3$ (adsorbent: Ag-Al$_2$O$_3$; fuel: diesel/DBT_900; adsorption temperature: 20 °C; LHSV: 0.85 h^{-1} regeneration: APU$_g$; final regeneration temperature: 500 °C) [99].

deviations in the BET surface, BJH pore volume, and BJH mean pore diameter from Table 6.7 in comparison to Table 6.5 are the result of different batches of adsorbents.

Table 6.7.: Physical properties of fresh Ag-Al$_2$O$_3$, Ag-Al$_2$O$_3$ after 1 cycle, and Ag-Al$_2$O$_3$ after 14 cycles of operation with diesel/DBT_900 (adsorbent: Ag-Al$_2$O$_3$; fuel: diesel/DBT_900; adsorption temperature: 20 °C; LHSV: 0.85 h^{-1}; regeneration: APU$_g$; final regeneration temperature: 500 °C).

Adsorbent	BET surface (m^2/g)	BJH pore volume (cm^3/g)	BJH mean pore diameter (nm)
Fresh	141.7	0.42	9.5
After 1 cycle	139.9	0.42	9.9
After 14 cycles	139.6	0.42	9.9

Further element analyses of both fresh and regenerated Ag-Al$_2$O$_3$ were also performed, and their results are illustrated in Figure 6.15. The average carbon content of the adsorbent (Figure 6.15a) increased only slightly in the first cycle from 1.4 to 1.5 mg/g and did not increase further over the following 13 cycles. This result correlates with the BET surfaces observed for fresh and regenerated Ag-Al$_2$O$_3$ (cf. Table 6.7) and indicate the efficient decomposition of DBT during regeneration with APU$_g$. The average sulfur content (Figure 6.15b) increased from < 0.015 to 1.4 mg/g after the first cycle. This phenomenon is related to the formation of bulk aluminum sulfates, where SO$_2$ from decomposed PASHs adsorbs and reacts with the γ-Al$_2$O$_3$ support, as discussed in Section 6.3.2. These bulk aluminum sulfates are stable under APU off-gas conditions and only begin to decompose at higher temperatures (800 °C) [223]. This highlights the importance of long-term experiments to investigate whether the chemical stability of the adsorbent is preserved over multiple cycles. The subsequent analysis of the adsorbent used in 14 cycles of operation showed that the average sulfur content was stable after cycle 1 (cf. Figure 6.15b). It can thus be concluded that the formation of bulk aluminum

sulfates is restricted to a limited number of adequate adsorption sites for SO$_2$, which correlates with results reported in Ref. [228]. These potential sites are saturated within the first cycle of regeneration, after which stable conditions were observed over multiple cycles.
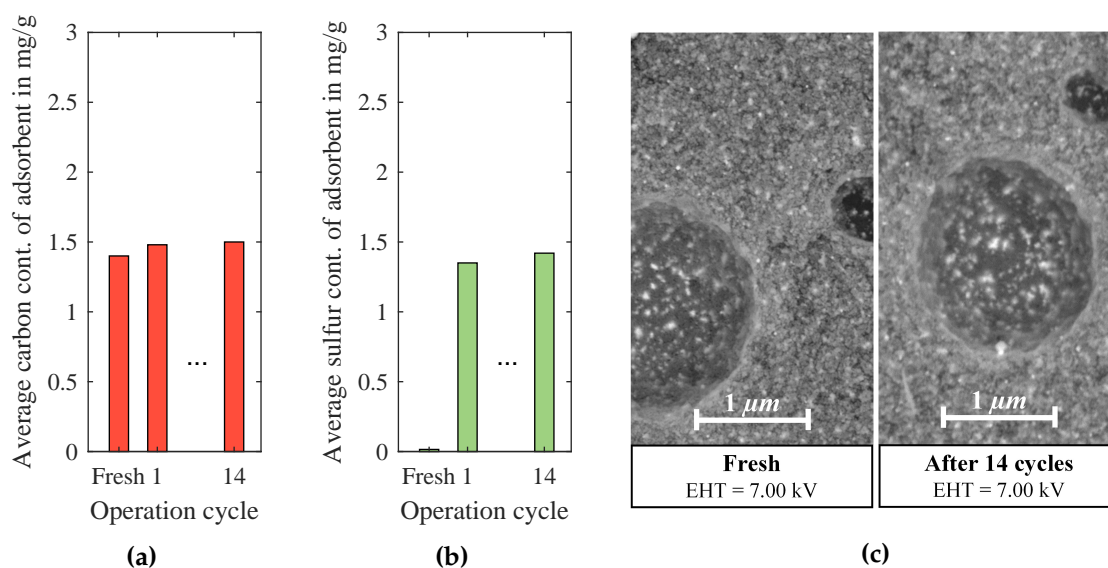
Figure 6.15.: (a) Average carbon content, (b) average sulfur content, and (c) SEM image of the fractured surface of fresh and regenerated Ag-Al$_2$O$_3$ (adsorbent: Ag-Al$_2$O$_3$; fuel: diesel/DBT_900; adsorption temperature: 20 °C; LHSV: 0.85 h^{-1}; regeneration: APU$_g$; final regeneration temperature: 500 °C) [99].

The main adsorption mechanisms of PASHs on Ag-Al$_2$O$_3$ are π-Ag, S-Ag, and S-H interactions, as described in Section 4.1. Consequently, the thermal and chemical stability of the active Ag sites (π-Ag and S-Ag interaction) as well as the acidic surface groups (S-H interaction) are important to describe and predict the long-term desulfurization performance of Ag-Al$_2$O$_3$ under realistic conditions. Additional analyses were carried out to investigate the thermal and chemical stability of the relevant Ag-Al$_2$O$_3$ adsorption sites. The SEM images of the fractured surface of fresh Ag-Al$_2$O$_3$ and Ag-Al$_2$O$_3$ after 14 cycles of operation are depicted in Figure 6.15c. Both SEM images show the uniform distribution of the active Ag phase (bright dots), indicating that no thermal induced clustering takes place after 14 cycles of operation.

Figure 6.16 illustrates the XRD patterns of fresh Ag-Al$_2$O$_3$ and Ag-Al$_2$O$_3$ after 14 cycles of operation. The XRD patterns of both fresh and 14-times regenerated Ag-Al$_2$O$_3$ showed the same relevant peaks of γ-Al$_2$O$_3$ (ICSD database; PDF: 10-425) and Ag$_2$CO$_3$ [185], representing the active Ag phase for PASH adsorption [109]. Thus, both the SEM and the XRD analysis confirm the results of all desulfurization experiments, indicating a stable active Ag phase under APU off-gas conditions over 14 cycles of operation.

The breakthrough capacity slightly increased within the first 5 cycles of operation and was stable in the subsequent 9 cycles of operation, as can be seen in Figure 6.14. This is interesting to note, as this result suggests an increase in potential adsorption sites, even if the increase in breakthrough capacity is only a tendency and not significant. The long-term results presented in Figure 6.14 show the breakthrough capacity for DBT at $LHSV = 0.85\,h^{-1}$. At these parameters,
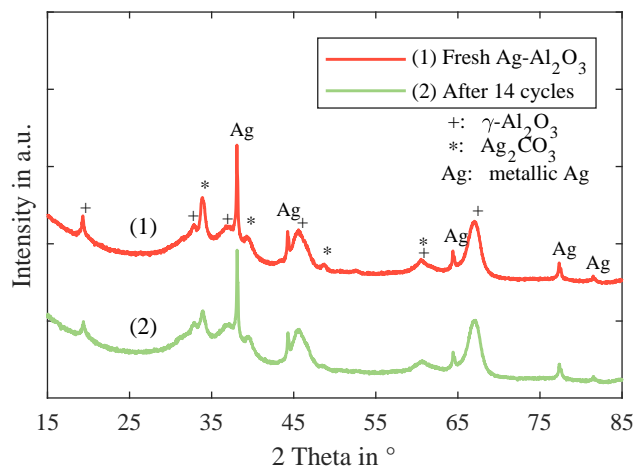
Figure 6.16.: XRD patterns of fresh Ag-Al$_2$O$_3$ and Ag-Al$_2$O$_3$ after 14 cycles of operation (adsorbent: Ag-Al$_2$O$_3$; fuel: diesel/DBT_900; adsorption temperature: $20\,^\circ C$; LHSV: $0.85\,h^{-1}$ regeneration: APU$_g$; final regeneration temperature: $500\,^\circ C$) [99].

only the silver involved π-Ag and S-Ag interactions are relevant, as discussed in Section 5.2. Consequently, the assumption of an increase in potential adsorption sites indicates the thermally activated dispersion of the active Ag phase during regeneration under APU$_g$ conditions, even if this phenomenon runs counter to the well-known phenomenon of Ag agglomeration at higher temperatures. The well-known case of thermally activated Ag agglomeration was reported by She et al. [229] for a Ag-Al$_2$O$_3$ SCR catalyst in a gas stream of CH$_4$, NO, and O$_2$ at $625\,^\circ C$. However, exactly the same phenomenon of the thermally activated dispersion of the active Ag phase was observed by She et al. [229] when the same Ag-Al$_2$O$_3$ SCR catalyst was operated in the presence of 250 - 1070 ppm of SO$_2$ (gas stream of CH$_4$, NO, O$_2$, and SO$_2$) at $625\,^\circ C$. This stabilizing and re-dispersing effect of SO$_2$ for Ag-Al$_2$O$_3$ has not yet been fully understood, but a more detailed discussion of the observed phenomena as well as possible explanations thereof are provided in Ref. [229]. The results reported by She et al. [229] support the conclusion that the increase in breakthrough capacity is related to the thermally activated dispersion of the active Ag phase of the Ag-Al$_2$O$_3$ adsorbent during regeneration with hot APU off-gas.

In the present work, the increase in the breakthrough capacity, and thus in the thermally activated dispersion of the active Ag, was only observed at a very low level, close to the uncertainty allowance of the experimental procedure and analysis. This can be related to the significantly lower SO$_2$ concentrations ($< 60\,ppm$) during the thermal regeneration of the adsorbent [219], which weaken the dispersive effect of SO$_2$ [229]. Nevertheless, the results show that the active Ag phase is stable over multiple cycles. This is an excellent result and highlights the efficiency of regeneration with APU off-gas, which showed no degradation in desulfurization performance over multiple cycles. Apart from Ag$_2$CO$_3$, both XRD patterns in Figure 6.16 also show the presence of metallic silver [186] related to small Ag particles on the surface of the adsorbent, which are formed during preparation as reported and discussed in Section 4.1.3. This metallic silver phase is not included in the overall adsorption mechanisms of

PASHs [97, 109].

The weaker S-H interaction involves surface acidic functional groups from the Ag-Al$_2$O$_3$ adsorbent [97]. Temperature programmed desorption (TPD) of ammonia was used to analyze the thermal chemical stability of the relevant surface acidity of fresh and regenerated Ag-Al$_2$O$_3$. The NH$_3$-TPD profiles of fresh Ag-Al$_2$O$_3$ and Ag-Al$_2$O$_3$ after 14 cycles of operation are illustrated in Figure 6.17. Both NH$_3$-TPD profiles show a similar peak at 200 $^\circ$C indicating a large number of weak acid sites on both materials. These weak acid sites are mainly related to -OH groups [102], which are formed during the preparation of Ag-Al$_2$O$_3$ [97]. The NH$_3$-TPD profile of Ag-Al$_2$O$_3$ after 14 cycles of operation levels off at a slightly higher temperature of around 400 $^\circ$C. This result indicates a slightly lower number of strong acid sites after 14 cycles of operation. The strong acid sites are not relevant for the three main adsorption mechanisms of PASHs (cf. Section 4.1).
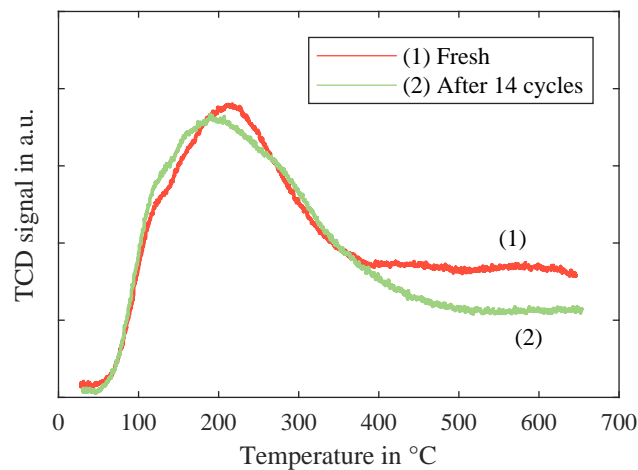
Figure 6.17.: NH$_3$-TPD profiles of fresh Ag-Al$_2$O$_3$ and after 14 cycles of operation (adsorbent: Ag-Al$_2$O$_3$; fuel: diesel/DBT$_-$900; adsorption temperature: 20 $^\circ$C; LHSV: 0.85 h^{-1}; regeneration: APU$_g$; final regeneration temperature: 500 $^\circ$C) [99].

It is thus possible to concluded that the decrease in strong acid sites is related to the formation of bulk aluminum sulfates within the first cycle of operation, as discussed above. However, the relevant weak acid sites are stable under APU$_g$ conditions over multiple cycles. Consequently, all of the results from the N$_2$ physisorption, elemental analyses, SEM and XRD analyses, and NH$_3$-TPD analysis prove that the relevant adsorption sites (active Ag phase and weak acid sites) are both thermally and chemically stable in APU off-gas conditions over multiple cycles; this finding also correlates with all of the experimental results performed within the scope of this work.

6.5. Alternative Regeneration Strategy for Low-Temperature, Fuel-Cell Based APUs[10]

A desulfurization unit based on highly thermally stable $Ag-Al_2O_3$ is a promising technology for stationary applications, and for mobile applications, in particular. The ability to efficiently desulfurize liquid fuels via adsorption and 100% regeneration of the $Ag-Al_2O_3$ adsorbent means that it is also possibility to operate fuel cell systems, such as auxiliary power units or hybrid vehicles, with commercial hydrocarbon-based fuels. The novel regeneration strategy, as introduced in Section 6.3, highlights the synergy between high-temperature fuel cell systems and the thermal on-board regeneration of spent adsorbent using hot APU off-gas.

Additional regeneration experiments were carried out with $APU_{g/wet}$, which contains $12.4\,mol\%$ of H_2O. At this level of H_2O, a regeneration temperature of only $450\,°C$ is required to achieve the full regeneration of $Ag-Al_2O_3$, as shown by the results presented in Figure 6.11. This H_2O content of $12.4\,mol\%$ is similar to the H_2O content of typical exhaust gases of combustion engines [234], which present an alternative option for use as the regeneration gas for hybrid applications. The schematic flow sheet of such a hybrid application is illustrated in Figure 6.18. In this application, the fuel (red line) is desulfurized upstream of the APU. For regeneration, the hot exhaust gas from the combustion engine is used as the regeneration medium (green line,) where the temperature is adjusted through the admixing of ambient air.
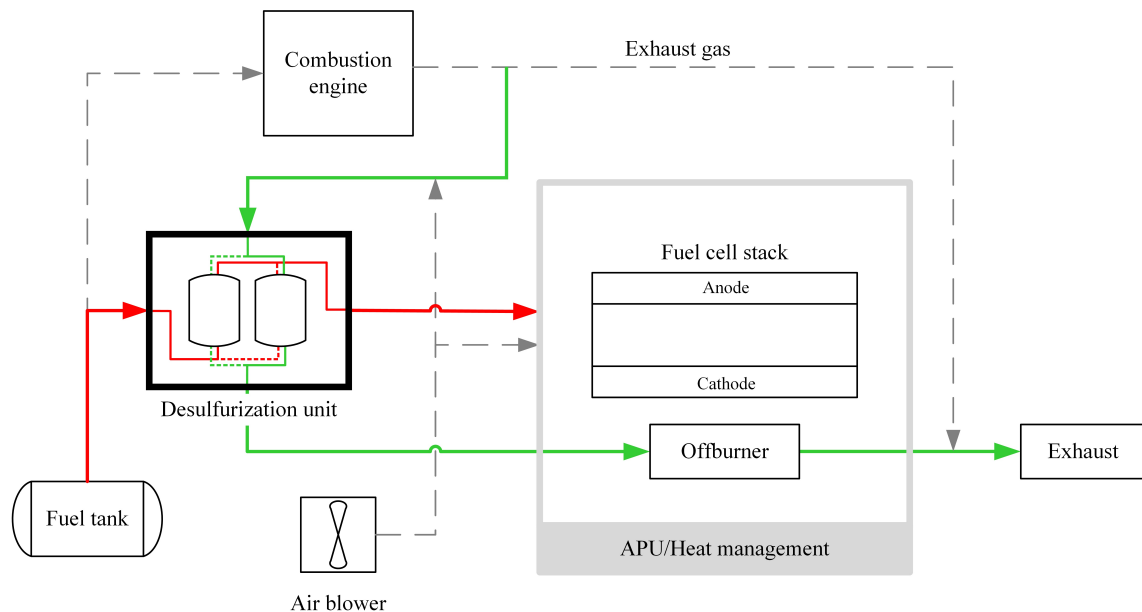
Figure 6.18.: Flow sheet diagram of APU process intensification by means of adsorbent regeneration with hot exhaust gas from a combustion engine [98].

In such a hybrid application (combustion engine and fuel cell system), not only high-temperature, but also low-temperature fuel cell systems can be operated with the hot regeneration gas pro-

---

[10]Parts of this section were published in *Energy & Fuels* under the title "Thermal in Situ and System-Integrated Regeneration Strategy for Adsorptive On-Board Desulfurization Units" [98].

vided by the combustion engine. The hot exhaust gas can then be mixed with ambient air to adjust the regeneration temperature, as shown in Figure 6.18. The higher CO_2 concentrations found in combustion exhaust gases do not have a negative influence on regeneration performance because CO_2 desorbs from the surface of γ-Al_2O_3 at temperatures above $60\,°C$ [214]. This alternative regeneration strategy was not further investigated in this work, but should underline the flexibility of the on-board regeneration of spent Ag-Al_2O_3 adsorbent using hot off-gases from combustion engines.

6.6. Summary of Reasonable On-Board Regeneration Strategies

Adsorptive desulfurization is a promising technology for on-board desulfurization units that make it possible to operate mobile fuel cell systems with commercial hydrocarbon-based fuels from petroleum feedstocks. The main drawback of the adsorptive desulfurization approach is the low adsorption capacity of adsorbents, which further requires the cyclic regeneration of the adsorbent in order to operate the desulfurization unit in a cost-effective manner.

Two main regeneration approaches are available: (i) solvent-based and (ii) thermal regeneration. According to several publications [73, 149, 235], regeneration with solvents is very efficient. Within this approach, the adsorbed sulfur heterocycles are eluted by polar solvents. However, large amounts of solvents are necessary to fully regenerate the adsorbent [103, 112]. In contrast, thermal regeneration is based on the thermal decomposition of adsorbed sulfur heterocycles, which are subsequently flushed out by a gas stream. This approach can be performed in both reducing and oxidizing atmospheres. Regeneration in reducing atmospheres has several advantages, including the ability to use a wide range of very selective adsorbents. Common reducing atmospheres for adsorbent regeneration and activation are H_2, N_2, or He [35, 72, 90]. However, none of these reducing gases are available on-board.

Regeneration in oxidizing atmospheres has the advantage that ambient air can be used as the regeneration medium. Promising results have been reported for different adsorbent desulfurizing jet fuels, which contain thiophene, BT, and their derivatives [69, 94]. Similar results were obtained within this work, and showed the high regeneration efficiency of Ag-Al_2O_3 after adsorption of BT or 4,6-DMDBT and its subsequent regeneration in ambient air at a final temperature of $450\,°C$. However, when DBT was present during the desulfurization cycle, regeneration efficiency dropped by $55\,\%$. There are only a few other publications that deal with thermal regeneration in ambient air after DBT adsorption, and none of them reported full regeneration [74, 211]. Besides inefficient regeneration after DBT adsorption, regeneration with ambient air also requires an external source of heat or a bulky heat exchanger to heat up ambient air to the final regeneration temperature of about $450\,°C$. This presents a major obstacle since it leads to larger desulfurization units and decreases the APU's overall efficiency.

Within this work, a novel and system-integrated regeneration strategy was developed, presented and discussed in Section 6.3. This regeneration strategy is based on reusing hot APU off-gas as the regeneration medium. To adjust the temperature, ambient air is admixed with the hot APU off-gas, which makes it possible to fully integrate the desulfurization unit into a SOFC-based APU system. The main advantages of this novel approach are the following:

- No external source of heat
- No bulky heat exchanger
- No additional tanks or pressurized container
- Regeneration temperature is controlled by admixing of ambient air
- No additional reagents, e.g. solvents or gases
- Reduced final regeneration temperature

Comprehensive investigations were carried out in order to study the desorption mechanisms and the overall regeneration efficiency of this approach under APU off-gas conditions. The water content in the off-gas of an SOFC-base APU is about $4.5\,mol\%$. The results showed that this increased water content has a positive effect on the thermal decomposition of adsorbed PASHs, and thus makes it possible to have a lower final regeneration temperature compared to the temperature necessary for regeneration with ambient air. The presence of CO_2 in the hot APU off-gas had no negative influence on regeneration performance. This can be related to the fact that CO_2 desorbs from the adsorbent surface at temperatures above $60\,^{\circ}C$ [214], and further acts as an inert compound. This insight also highlights the possibility of using hot off-gas from a combustion engine as a regeneration gas when an APU is based on a low-temperature fuel cell rather than an SOFC.

The regeneration experiments with hot APU off-gas achieved full regeneration for different types of fuels and PASHs, including the challenging DBT compound. This is an excellent result since, to the best of the author's knowledge, 100% regeneration after the adsorption of DBT has not yet been reported for thermal regeneration in an oxidizing atmosphere. Additional long-term experiments did not show any sign that the adsorption capacity degraded over 15 cycles of operation. This result was confirmed by comprehensive material analyses, which demonstrated the full thermal and chemical stability of the $Ag\text{-}Al_2O_3$ adsorbent and its related active adsorption sites.

7

Basic Design

This chapter presents the basic design of an Ag-Al$_2$O$_3$-based on-board desulfurization unit. All of the boundary conditions used for this basic design were obtained from the results presented and discussed in previous chapters of this work. This chapter is intender to provide an answer to research question 4 - what is the service/regeneration interval of this desulfurization approach? - in the context of real applications, such as an SOFC-based APU operated with sulfur-rich diesel fuel.

7.1. Introduction

The basic design of the desulfurization unit is based on the flow sheet provided in Figure 7.1, which used hot APU off-gas (red line) as its regeneration medium. As indicated in Figure 7.1, a two-adsorber concept is used to enable the continuous desulfurization of the liquid fuel, as the two adsorbers are operated in alternation. This basic design depicts only one adsorber since the concept is based on the use of two identical adsorbers.
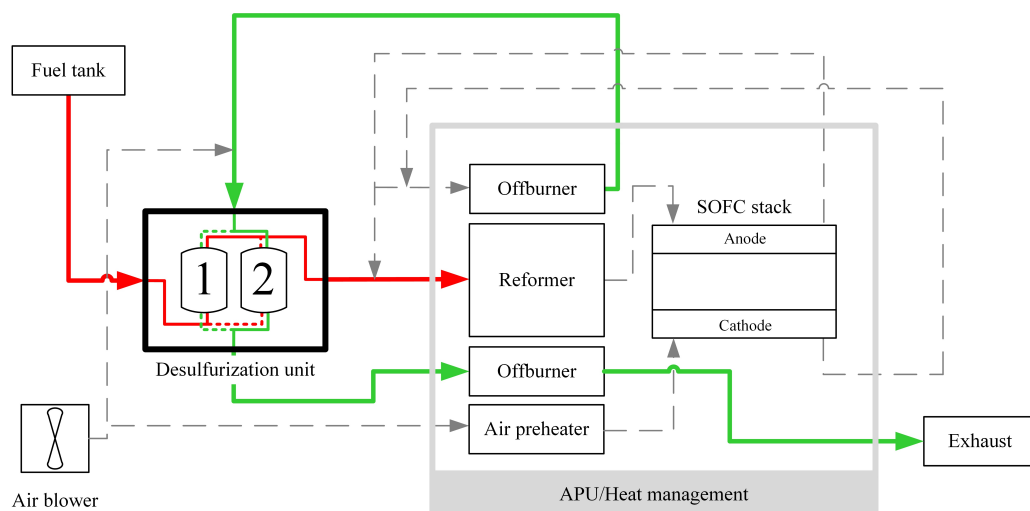
Figure 7.1.: Conceptual system design of an SOFC-operated APU with an integrated on-board desulfurization unit based on a two-adsorber concept [98].

The calculations of the basic concept presented above were carried out for the simulated and optimized $5.5\,kW_{el}$ SOFC-based APU reported in Ref. [8]. The relevant parameters of this SOFC-based APU are provided in Table 7.1. The simulation of the APU in Ref. [8] is based on the use of n-dodecane as fuel, which is a typical compound of diesel fuel. Hence, the experimental results obtained in Section 6.4 of this work for diesel/DBT_900 were used in order to design a suitable on-board desulfurization unit.

Table 7.1.: Relevant parameters of the simulated $5.5\,kW_{el}$ SOFC-based APU reported in Ref. [8].

APU parameters [8]:	
Electrical Power	$5.5\,kW$ [a]
Fuel consumption $\dot{V}_{fuel}$	$1.6\,L/h$ [a]
APU off-gas flow rate $\dot{V}_{off\text{-}gas}$	$450\,L/min$ [a,b]
APU off-gas temperature $\vartheta_{off\text{-}gas}$	$506\,°C$
APU off-gas density $\rho_{off\text{-}gas}$	$1.282\,kg/m^3$ [b]

[a] At full load

[b] At standard conditions

The calculations for the basic design are based on the results obtained from the lab-scale desulfurization experiments with diesel/DBT_900 presented in Section 6.4. The important results of these experiments are provided again in Figure 7.2. As indicated by the dashed line in Figure 7.2a, an average breakthrough capacity of $q_{break} = 2.6\,mg\text{-}S/g\text{-}ads$ was observed for diesel/DBT_900 at an LHSV of $0.34\,h^{-1}$. Regeneration was performed using APU$_g$ as the regeneration medium, with the detailed gas composition seen in Table 7.2. The corresponding temperature profile and the GHSV of APU$_g$ during regeneration can be seen in Figure 7.2b as $\vartheta_{set}(t)$ and $GHSV_{exp}(t)$, respectively.

(a) Average breakthrough capacity

(b) Temperature and flow rate during regeneration
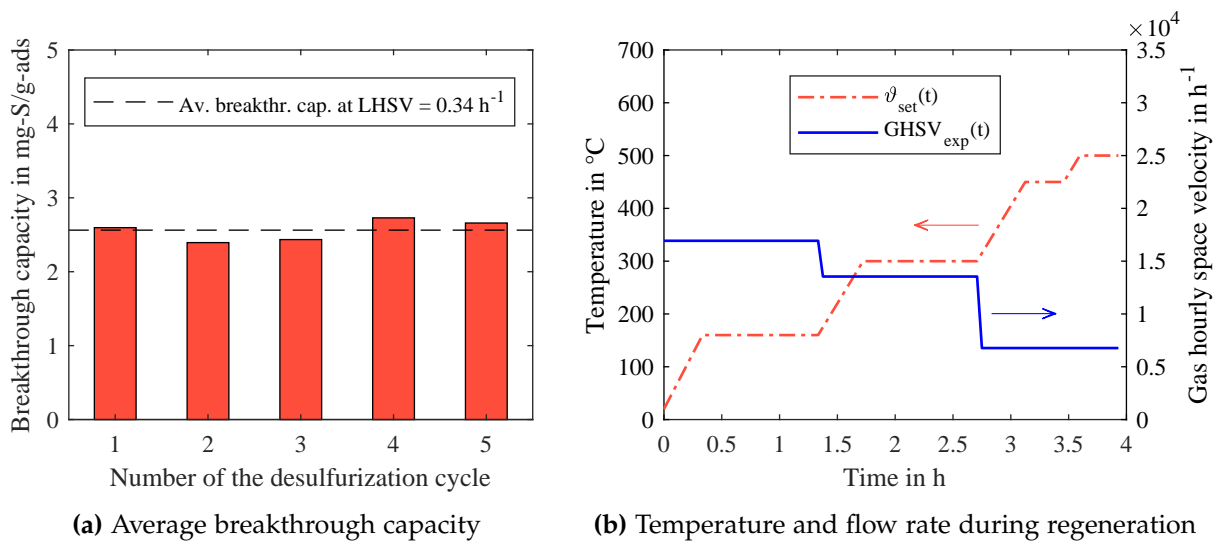
Figure 7.2.: Boundary conditions for the basic design: (a) Average breakthrough capacity of diesel/DBT_900 at an LHSV of $0.34\,h^{-1}$ and (b) temperature profile and the corresponding GHSV for the adsorbent regeneration (adsorbent: Ag-Al$_2$O$_3$; fuel: diesel/BT_900; adsorption temperature: $20\,°C$; LHSV: $0.34\,h^{-1}$; regeneration: APU$_g$; final regeneration temperature: $500\,°C$).

Table 7.2.: Detailed composition of hot off-gas from an auxiliary power unit with 4.5 $mol\%$ H_2O (APU_g) used as regeneration medium.

	APU off-gas (APU_g) composition in (mol/mol)
N_2	0.763
O_2	0.168
CO_2	0.024
H_2O	0.045

For the scale up, the space velocity (SV) was kept constant, as seen in Equation 7.1. This makes it possible to use the breakthrough capacity q_{break} from the lab-scale experiments (cf. Figure 7.2a) as the boundary condition in the basic design since q_{break} is a function of the LHSV. The same approach was used for the GHSV of the hot APU off-gas during regeneration.

$$SV_{scale\,up} \stackrel{!}{=} SV_{exp} \tag{7.1}$$

The discussion of the basic design of the on-board desulfurization unit is divided into two sections. Section 7.2 discusses the design of the adsorber in desulfurization mode. Section 7.3 contains an integration study that discusses the regeneration of the aforementioned adsorber with the available APU off-gas.

7.2. Basic Design of the Desulfurization Cycle

This section discusses the basic design of the adsorber's desulfurization mode for the simulated and optimized $5.5\,kW_{el}$ SOFC-based APU reported in Ref. [8]. As described in the previous section, the calculations for the adsorber are based on the same LHSV of $0.34\,h^{-1}$ that was used in the experiments presented above (cf. Figure 7.2a). The LHSV during adsorption is defined as the ratio of the fuel flow rate to the volume of the adsorber: $LHSV_{fuel} = \dot{V}_{fuel}/V_{adsorber}$. Rearrangement of this definition leads to Equation 7.2, which can be used to determine the volume of the adsorber $V_{adsorber}$ (L) at a given LHSV (h^{-1}) and a given APU fuel consumption $\dot{V}_{fuel}$ (L/h).

$$V_{adsorber} = \frac{\dot{V}_{fuel}}{LHSV_{fuel}} \tag{7.2}$$

The operation time of the given adsorber with $V_{adsorber}$ can be calculated according to Equation 7.3. Within Equation 7.3, the operation time $t_{operation}$ is defined as the time during which the total sulfur concentration in the effluent fuel is $\leq 10\,ppmw$ at the adsorber outlet and at a constant fuel flow rate of $\dot{V}_{fuel}$. The $10\,ppmw$ sulfur threshold limit in Equation 7.3 is considered by the breakthrough capacity q_{break} (cf. Equation 3.3), which itself is a function of the LHSV and strongly depends on the type of fuel as wella as its initial sulfur concentration $c_{S,0}$, as discussed in Sections 5.3.1 - 5.3.3. Hence, all three parameters of q_{break}, ρ_{fuel}, and $c_{S,0}$ relate to one experiment performed at an LHSV of $0.34\,h^{-1}$.

$$t_{operation} = \frac{q_{break}(LHSV)}{\dot{V}_{fuel}\rho_{fuel}c_{S,0}}V_{adsorber}\rho_{bulk,ads} \tag{7.3}$$

The first and second parts of Table 7.3 provide the relevant parameters of the $5.5\,kW_{el}$ SOFC-based APU as well as the experimental and physical boundary conditions necessary in order to determine the adsorber volume $V_{adsorber}$ and the related operation time $t_{operation}$ according to Equation 7.2 and Equation 7.3. The values given in the second part of Table 7.3 correspond to the experimental results shown in Figure 7.2a. The results of the basic design of the desulfurization mode are given in the last part of Table 7.3.

Table 7.3.: Relevant parameters, experimental/physical boundary conditions, and results of the basic adsorber design for the simulated $5.5\,kW_{el}$ SOFC-based APU reported in Ref. [8].

APU parameters [8]:	
Fuel consumption $\dot{V}_{fuel}$	$1.6\,L/h$ [a]
Experimental/physical boundary conditions:	
Assumed LHSV during adsorption $LHSV_{fuel}$	$0.34\,h^{-1}$
Breakthrough adsorption capacity q_{break}	$2.6\,mg\text{-}S/g\text{-}ads$ [b,c]
Fuel density ρ_{fuel}	$826.7\,kg/m^3$ [c]
Initial total sulfur concentration $c_{S,0}$	$900\,ppmw$
Adsorbent bulk density $\rho_{bulk,ads}$	$790\,kg/m^3$
Results of basic adsorber design	
Adsorber volume $V_{adsorber}$	$4.7\,L$
Operation time of adsorber $t_{operation}$	$8.1\,h$ [a]

[a] At full load

[b] At an LHSV of $0.34\,h^{-1}$

[c] At a temperature of $20\,°C$

The basic design of the desulfurization mode shows that an adsorber volume of $V_{adsorber} = 4.7\,L$ provides sulfur-free diesel fuel with $\leq 10\,ppmw$ of total sulfur that is suitable for the operation

of a $5.5\,kW_{el}$ SOFC-based APU with diesel/DBT_900 for $t_{operation} = 8.1\,h$ at full load. The sulfur threshold limit of $10\,ppmw$ is essential in order to protect the SOFC stack from sulfur poisoning (cf. Section 1.3). As discussed in the previous chapters, desulfurization performance strongly depends on the type of fuel used and its composition. Further experimental investigations with real sulfur rich fuels and different total sulfur concentrations are necessary in order to carry out more detailed calculations. However, the most important design parameters are provided given in Equation 7.2. In addition, the desulfurization performance of an adsorber is significantly influenced by its overall aspect ratio, as reported by Velu et al. [36], which is defined according to Equation 7.4:

$$A_o = \frac{H_{adsorber}}{D_{adsorber}} \tag{7.4}$$

where $H_{adsorber}$ is the height of the adsorber and $D_{adsorber}$ is the diameter of the adsorber. The desulfurization performance of an adsorber significantly improves as the overall aspect ratio increases, until $A_o = 40$ [36]. In the present work, the calculated operation time of $t_{operation} = 8.1\,h$ (cf. Table 7.3) is based on an overall aspect ratio of $A_o = 0.83$ ($H_{adsorber} = 160.3\,mm$, $D_{adsorber} = 193.2\,mm$). Hence, the operation time of the adsorber with a volume of $V_{adsorber} = 4.7\,L$ could be significantly increased by increasing the overall aspect ratio. However, aspect ratios of $A_o > 8$ lead to undesirable adsorber geometries that are not practical for real applications.

The results calculated above further highlight the importance of on-board regeneration since reasonable adsorber volumes are not sufficient to operate the APU for more than a few days. In order to continuously operate the $5.5\,kW_{el}$ SOFC-based APU, a second adsorber is necessary to provide the possibility of regeneration, as schematically shown in Figure 7.1. In addition, the operation time $t_{operation}$ of one adsorber has to be longer than the corresponding regeneration time t_{reg} to keep the system running. Hence, Equation 7.5 has to be fulfilled.

$$t_{operation} > t_{reg} \tag{7.5}$$

The regeneration experiments carried out within this work have shown that the regeneration time t_{reg} of one adsorber is $6.3\,h$. These $6.3\,h$ include cool down of the adsorber from the final regeneration temperature of 500 to $50\,°C$ with ambient air ($\vartheta_{air} = 20\,°C$) at a GHSV of $16930\,h^{-1}$. This final adsorber temperature of $50\,°C$ is within the optimal operating temperature of $-10 < 60\,°C$ for the subsequent desulfurization cycle (cf. Section 4.2.1 and 4.2.2). Consequently, the regeneration time $t_{reg} = 6.3\,h$ is significantly shorter in comparison to the operation time of

$t_{operation} = 8.1\,h$, and thus Equation 7.5 is fulfilled. This result shows that only two Ag-Al$_2$O$_3$-based adsorbers with a volume of $4.7\,L$ each are necessary to continuously operate a $5.5\,kW_{el}$ SOFC-based APU with high sulfuric diesel at full electric load. Such a small desulfurization unit can easily be integrated into an SOFC-based APU, which highlights the potential of adsorptive desulfurization for mobile applications. The following section discusses the basic design of the regeneration mode in order to determine whether the required amount of regeneration gas can be provided by the hot APU off-gas from the $5.5\,kW_{el}$ SOFC-based APU reported in Ref. [8].

7.3. Basic Design of the Regeneration Cycle

A novel, system-integrated on-board regeneration strategy was developed and investigated on a lab scale, as described in Section 6.3, and hot APU off-gas was used as the regeneration medium. The outcome of this investigation is a proposed temperature profile combined with a related GHSV for the hot APU off-gas, shown in Figure 7.3 as $\vartheta_{set}(t)$ and $GHSV_{exp}(t)$, respectively. The integration study presented in this section will be carried out for the adsorber designed in Section 7.2 for the $5.5\,kW_{el}$ SOFC-based APU that was reported in Ref. [8]. The volume of adsorber and the corresponding operation time can be seen in the last part of Table 7.3. For the regeneration of the scaled-up adsorber, the same temperature profile of $\vartheta_{set}(t)$ from the lab scale experiments was applied (cf. Figure 7.2b).

In order to regenerate the adsorber according to the prescribed temperature profile $\vartheta_{set}(t)$, the hot off-gas from the APU ($\vartheta_{off\text{-}gas} = 506\,°C$) has to be cooled down. This can be done by mixing the hot APU off-gas with cool ambient air, as indicated in Figure 7.1. The flow rate of ambient air required for admixing can be calculated according to Equation 7.6. This time-dependent air flow rate $\dot{V}_{air}(t)$ is based on the heat flux necessary to cool down the hot APU off-gas $\dot{V}_{off\text{-}gas}$ from a temperature of $T_{off\text{-}gas}$ to the prescribed temperature $T_{set}(t)$. Within Equation 7.6, the temperature dependency of the specific molar heat capacities of $C_{m,p_{off\text{-}gas}}$ and $C_{m,p_{air}}$ are considered by Equation 7.7 where ϑ_1 and ϑ_2 represent the relevant temperatures in $°C$. The specific molar heat capacities of ambient air and APU off-gas (composition according to Table 7.2) for the temperature range of $\vartheta = 0$ to ϑ_1 are calculated by means of polynomial fits (Equations A.3 and A.5 on pages 114 and 115) obtained from the software EES^{TM} [236].

$$\dot{V}_{air}(t) = \frac{\dot{V}_{off\text{-}gas}\rho_{off\text{-}gas}M_{air}C_{m,p_{off\text{-}gas}}\Big|_{\vartheta_{set(t)}}^{\vartheta_{off\text{-}gas}}(T_{off\text{-}gas} - T_{set}(t))}{\rho_{air}M_{off\text{-}gas}C_{m,p_{air}}\Big|_{\vartheta_{air}}^{\vartheta_{set(t)}}(T_{set}(t) - T_{air})} \tag{7.6}$$

$$C_{m,p_i}\Big|_{\vartheta_1}^{\vartheta_2} = \frac{C_{m,p_i}\Big|_{\vartheta=0}^{\vartheta_2}\vartheta_2 - C_{m,p_i}\Big|_{\vartheta=0}^{\vartheta_1}\vartheta_1}{\vartheta_2 - \vartheta_1} \tag{7.7}$$

By admixing ambient air to the hot APU off-gas, the possible flow rate of regeneration gas from the APU increases according to Equation 7.8. Because the regeneration temperature increases over time (cf. $\vartheta_{set}(t)$ in Figure 7.2b), the required flow rate of ambient air $\dot{V}_{air}(t)$ decreases over time, and thus, the available flow rate of regeneration gas $\dot{V}_{reg}(t)$ also decreases.

$$\dot{V}_{reg}(t) = \dot{V}_{air}(t) + \dot{V}_{off\text{-}gas} \tag{7.8}$$

In order to determine whether the time-dependent regeneration gas flow rate $\dot{V}_{reg}(t)$ from the APU (according to Equation 7.8) is sufficient for regeneration, the GHSV can be calculated according to Equation 7.9 where $V_{adsorber}$ is the volume of the adsorber designed in Section 7.2.

$$GHSV_{scale\,up}(t) = \frac{\dot{V}_{reg}(t)}{V_{adsorber}} \tag{7.9}$$

Table 7.4 provides the relevant parameters of the $5.5\,kW_{el}$ SOFC-based APU as well as the physical boundary conditions required to determine the necessary flow rate of ambient air $\dot{V}_{air}(t)$ and the possible GHSV of regeneration gas $GHSV_{scale\,up}(t)$, according to Equation 7.6 and Equation 7.9, respectively.

Table 7.4.: Relevant parameters and physical boundary conditions for the integration study of on-board regeneration integrated into the simulated $5.5\,kW_{el}$ SOFC-based APU reported in Ref. [8].

APU parameters [8]:	
APU off-gas flow rate $\dot{V}_{off\text{-}gas}$	$450\,L/min$ [a,b]
APU off-gas temperature $\vartheta_{off\text{-}gas}$	$506\,°C$
Adsorber volume $V_{adsorber}$ (cf. Section 7.2)	$4.7\,L$
Physical boundary conditions:	
Molecular weight of APU off-gas $M_{off\text{-}gas}$	$28.61\,kg/mol$
Molecular weight of ambient air M_{air}	$28.96\,kg/mol$
Density of APU off-gas $\rho_{off\text{-}gas}$	$1.282\,kg/m^3$ [b]
Density of ambient air ρ_{air}	$1.292\,kg/m^3$ [b]
Temperature of ambient air ϑ_{air}	$20\,°C$

[a] At full load

[b] At standard conditions

The results of the integration study are shown in Figure 7.3. The same temperature profile of $\vartheta_{set}(t)$ was applied for both the lab-scale experiments and the scaled-up adsorber, as shown by the red dash-dotted line in Figure 7.3 . The corresponding GHSV of the lab-scale experiments

$GHSV_{exp}(t)$ and the scaled up adsorber $GHSV_{scale\,up}(t)$ are also shown in Figure 7.3 as a solid and dashed blue lines, respectively.
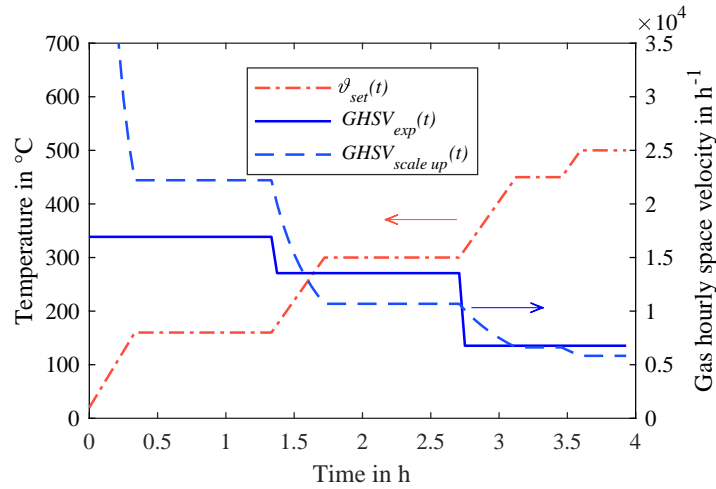
Figure 7.3.: Prescribed temperature profile and GHSV during regeneration of the lab-scale experiment and the basic scale up design for the $5.5\,kW_{el}$ SOFC-based APU reported in Ref. [8].

For the first temperature ramp (20 - 160 °C) in Figure 7.3, the achievable $GHSV_{scale\,up}$ is higher than that used in the lab-scale experiment. Within this ramp, the main target of the regeneration cycle is to evaporate and flush out the weakly bound PASHs and fuel that remain after the gravimetric discharge of the adsorber. Consequently, higher values of the $GHSV$ would increase the evaporation and mass transfer rates, thus shortening the regeneration time. At this stage, the gas composition of the regeneration gas has no impact on regeneration efficiency since no relevant chemical reactions are taking place (cf. Section 6.3.2). However, reasonable GHSVs during the first ramp are limited by the pressure drop of the adsorber.

Within the second ramp (160 - 300 °C) in Figure 7.3, the more strongly bound PASHs and high boiling compounds from the fuel start to decompose and evaporate. As can be seen in Figure 7.3, the achievable $GHSV_{scale\,up}$ in the second ramp is below that of the lab-scale experiment. Within this second ramp, the GHSV of the regeneration medium is not as important as in the first. This is due to the fact that the amount of high boiling compounds, even for diesel fuel, are limited, as can be seen by the C_xH_y profile shown in Figure 6.3. Hence, only the few high boiling compounds need to be evaporated and flushed out. Consequently, the slightly lower $GHSV_{scale\,up}$ has a negligible influence on the regeneration efficiency. In addition, the C_xH_y concentration peak in Figure 6.3 is very sharp, indicating that the hold time at 300 °C could potentially be reduced.

In the last ramp (300 - 500 °C) in Figure 7.3, the value of $GHSV_{scale\,up}(t)$ is at the same level as in the lab-scale experiments. Within this last ramp, the silver-based adsorption sites are activated, and any carbon depositions that formed during the second ramp are burned off. These processes must be performed in an oxidative atmosphere. As indicated by the low CO_2 profile in Figure 6.2 (where the temperature is above 300 °C), the required amount of O_2 and

thus the GHSV can be very low to burn off the carbon depositions. Hence, it might be possible to reduce the GHSV even further.

The results show that the temperature profile $\vartheta_{set}(t)$, developed and proposed for regeneration, is not only suitable for full adsorbent regeneration, but is also operable within the temperature range of hot APU off-gas from an SOFC-based APU. This means that a desulfurization unit using the novel regeneration strategy proposed in this work could easily be fully integrated into an SOFC-based APU. This integration study has outlined the synergy between high-temperature fuel cell systems and the thermal on-board regeneration of spent adsorbent via hot APU off-gas. The achievable GHSV of this regeneration medium is close to that investigated in the lab-scale experiments, and thus validates the conceptual system design of an SOFC-based APU with an integrated desulfurization unit as presented in Figure 7.1.

These results further provide an answer to research question 4, in terms of real applications: what is the service/regeneration interval of this desulfurization approach? As demonstrated by the integration study above, this novel and efficient regeneration strategy based on hot APU off-gas can be fully integrated into SOFC-based APUs. Furthermore, the experimental investigations showed no degradation in the desulfurization performance of Ag-Al$_2$O$_3$ over 15 cycles and confirmed the full chemical and thermal stability of the adsorption sites involved. Based on these findings, one adsorber for the $5.5\,kW_{el}$ SOFC-based APU can be operated for $8.1\,h$ before it needs to be regenerated. Both adsorbers are capable of performing at least 15 cycles of operation. Thus, the $5.5\,kW_{el}$ SOFC-based APU can be operated continuously for $243\,h$ at full electric load ($2\,adsorber \times 8.1\,h/adsorber \times 15\,cycles = 243\,h$). Neither the experimental investigations nor the theoretical background of the overall regeneration mechanism (cf. Section 6.3.2) showed any indication that performance degradation would occur, and thus that it may be possible to operate the SOFC-based APU for significantly longer than $243\,h$ before the adsorbent needs to be replaced. The real number of achievable operating cycles will have to be examined by means of long-term experimental investigations, which are a recommended topic for future research. Further recommendations for future studies will be discussed and outlined in the following chapter.

8

Conclusions and Recommendations for Future Works

8.1. Conclusion

The on-board desulfurization of hydrocarbon-based fuels is a challenging and interdisciplinary field of research. This thesis has aimed to provide answers to the research question that were stated in the Introduction of this work:

- Which desulfurization approach fulfills the specific requirements of on-board applications?
- What is the mechanism behind this desulfurization process?
- How is this mechanism influenced by different types of liquid hydrocarbon-based fuels?
- What is the maintenance interval of this desulfurization approach?

This chapter will provide condensed answers to the above questions, and its structure follows the same order as the research questions.

Which desulfurization approach fulfills the specific requirements of on-board applications?

Commercial hydrocarbon-based fuels from petroleum feedstocks contain 10 - 5000 ppm of total sulfur, depending on the class of fuel and its purpose of use [10]. Fuel-cell-based APUs are especially attractive when commercial, hydrocarbon-based on-board fuel can be used to produce hydrogen-rich syngas via reforming, which is subsequently fed to the fuel cell. This approach requires no additional tanks or pressured container and keeps the fuel logistics simple. However, the electrodes and catalysts of both the fuel cells and the reformer can easily be poisoned by sulfur-based impurities. Hence, most suppliers of fuel cells (including proton-exchange membrane, molten-carbonate, and solid oxide fuel cells) recommend to using feed gas

with well below 1 *ppmw* of total sulfur [16]. This requires a maximum total sulfur concentration of 1 - 10 *ppmw* in the hydrocarbon feed upstream of the reformer. This requirement means that on-board desulfurization is essential.

Thus the answer to the first research question is as follows: Adsorptive desulfurization in the liquid phase appears to be the most promising approach; its simplicity, in particular, makes it attractive for on-board applications. Other desulfurization approaches, such as oxidative desulfurization or extraction, have multiple stages and often require additional reagents (e.g. oxidants or solvents). Because it requires only one stage, adsorptive desulfurization allows for the design of a compact desulfurization unit. This thesis has shown that adsorptive desulfurization, in its current state, provides a fuel-flexible approach that can be used to hydrocarbon-based fuels, such as jet and diesel fuels, down to $\leq 10\,ppmw$ of total sulfur, and thus fulfills the specific requirements of on-board applications in SOFC-based APUs.

What is the mechanism behind this desulfurization process?

Adsorptive desulfurization is based on the selective adsorption of sulfuric compounds. The adsorption mechanisms involved therein strongly depend on the composition of the adsorbent as well as the active adsorption sites. One major challenge of adsorptive desulfurization is its selectivity towards certain sulfuric compounds. This challenge is due to the fact that sulfuric compounds are similar to other major compounds in hydrocarbon-based fuels. Intensive research has been carried out, and is still ongoing, in the effort to increase the selectivity of adsorption. Several promising adsorbents have been reported in recent years. However, most of these adsorbents are not practical for mobile applications since they need activation in reducing atmospheres, which would require additional tanks and reagents, and thus negate the advantages of the adsorptive desulfurization approach.

Silver-based adsorbents are one of the few materials that are active in their oxidized state. This characteristic makes silver-based adsorbents very attractive for on-board applications since no activation is necessary. Incorporating the active silver phase into the porous structure of metal oxides provides both a thermally and chemically stable adsorbent. γ-Al_2O_3 and TiO_2 are promising metal oxides as they provide additional active adsorption sites.

To answer the second research question: According to the current state of knowledge, three main adsorption mechanisms are involved in the overall adsorption of sulfur heterocycles on the surface of Ag-Al_2O_3. The strongest adsorption interaction is based on a π-complexation between the sulfur heterocycle and the silver cation, which is referred to as the π-Ag interaction. The second interaction is an acid-base interaction, in which the sulfur atom of the sulfur heterocycle directly interacts with the silver cation; hence, it is referred to as the S-Ag interaction. This S-Ag interaction is only slightly weaker in comparison to the π-Ag interaction. The third adsorption mechanism is also an acid-base interaction, but it does not involve any active silver phase.

Within this third adsorption mechanism, the sulfur atom of the sulfur heterocycle interacts with an acidic surface group, which can be related to active hydroxyl groups. This third adsorption mechanism is referred to as the S-H interaction and is significantly weaker compared to the π-Ag and S-Ag interactions. As stated above, the S-H interaction does not involve any active silver phase; however, the results obtained within this thesis and in related publications indicate that the incorporation of silver has a strong influence on the formation of active hydroxyl groups.

How is this mechanism influenced by different types of liquid hydrocarbon-based fuels?

The adsorption capacity and thus the adsorption selectivity of Ag-Al$_2$O$_3$ is strongly influenced by the fuel composition. Transportation fuels, such as gasoline, jet fuel, and diesel fuel, are related to the three main refining streams: naphtha (gasoline), kerosene (jet fuel), and gas oil (diesel fuel). It is thus apparent that the fuel compositions of gasoline, jet fuel, and diesel fuel differ in both the concentrations and the types of hydrocarbons and sulfuric compounds they contain (e.g. benzothiophene (BT) and dibenzothiophene (DBT)). The strength of the interaction is not only dependent on the adsorption mechanism, but is also influenced by the type of sulfur heterocycle and the correlated electron density in the relevant orbitals.

The answer to the third research question is as follows: The two stronger π-Ag and S-Ag interactions have a higher adsorption energy for DBT in comparison to BT. This is different than the weak S-H interaction, in which the selectivity of adsorption is BT > DBT. As was demonstrated by the comprehensive experimental investigations carried out for this work, the weak S-H interaction becomes more relevant when the adsorptive concentration within the pores increases. Consequently, the selectivity order of adsorption depends on the state of equilibrium. The initial selectivity order is DBT > BT. With increasing time, the S-H interaction becomes more relevant and changes the selectivity order to BT > DBT. In addition to the sulfuric compounds, the non-sulfuric compounds also have a strong influence on the adsorption performance of Ag-Al$_2$O$_3$. Within these non-sulfuric compounds, the polycyclic aromatic hydrocarbons (PAHs), in particular, need to be taken into account. These PAHs have similar molecular structures in comparison to the most relevant sulfuric compounds. Consequently, PAHs and sulfuric compounds compete for adsorption, and thus, high PAH concentrations decrease the adsorption kinetics. This is why adsorptive desulfurization via Ag-Al$_2$O$_3$ is more challenging for diesel fuel in comparison to jet fuel, since diesel fuel generally has a higher content of PAHs than jet fuel, for example (cf. Table 2.1). This work further shows that the selectivity of the weak S-H interaction does not decrease its selectivity in the presence of aromatics at $20\,^{\circ}C$. This is different in the case of the two stronger π-Ag and S-Ag interactions, which seem to slightly lose their selectivity in the presence of aromatic compounds. However, at $60\,^{\circ}C$, the contribution of the S-H interaction to the overall adsorption mechanism is significantly decreased. In addition, at this temperature the selectivities of both the π-Ag

and S-Ag interactions towards PASHs also significantly decrease in the presence of high PAH concentrations.

What is the service/regeneration interval of this desulfurization approach?

In the case of real fuels, the sulfur adsorption capacity is low, even for the most selective adsorbents. Consequently, an adsorber of a reasonable size is only able to operate for a few days before the adsorbent needs to be replaced. This highlights the importance of regenerable adsorbents as well as reasonable on-board regeneration strategies to make the adsorptive desulfurization approach a successful story.

Adsorbent regeneration strategies can be categorized into two main approaches: (i) solvent-based and (ii) thermal regeneration strategies. As their description indicates, solvent-based regeneration strategies use different types of solvents to restore adsorption capacity. However, this approach requires additional tanks and reagents, and thus negates the inherent advantages of the adsorptive desulfurization approach. Thermal regeneration can be carried out in different atmospheres; however, in terms of mobile applications, only an oxidizing atmosphere (e.g. ambient air, or off-gas from APU/combustion engine) is reasonable for regeneration since reducing gases are not available on-board. Several promising results have been published showing high regeneration efficiencies for thermal regeneration with ambient air. Nonetheless, only a few studies have used thermal regeneration with ambient air after adsorption of DBT, and none of them have reported full regeneration. This failure to completely regenerate the adsorbent was also confirmed by the experiments carried out within this work, which showed similar results. The difficulty of adsorbent regeneration after adsorption of DBT can be linked to the high adsorption energy of the two strong π-Ag and S-Ag interactions in the case of DBT. In addition, regeneration with ambient air requires cool air to be heated via electricity or a bulky heat exchanger in order to reach regeneration temperatures $\geq 450\,°C$.

This thesis presebts a novel and system-integrated regeneration strategy based on hot off-gas for an SOFC-based APU. The results show full regeneration regardless of the type of fuel. This is an excellent result since 100% regeneration after adsorption of DBT has not yet been reported for thermal regeneration in oxidizing atmospheres. Further studies of this novel regeneration strategy confirmed its constant performance as well as the thermal and chemical stability of the Ag-Al$_2$O$_3$ adsorbent and its active adsorption sites over 14 cycles of operation.

To answer the last research question: The results reported herein prove that the Ag-Al$_2$O$_3$ adsorbent can be regenerated over 14 cycles without showing any tendency towards degradation. However, both the identified adsorption and regeneration mechanisms, as well as theoretical considerations and material analyses, lead one to assume that a significantly higher number of regeneration cycles would be feasible; from the current state of knowledge, there is no reason why the desulfurization performance of the Ag-Al$_2$O$_3$ adsorbent should significantly

degrade over multiple cycles when this novel regeneration strategy is applied. Furthermore, this strategy, based on hot APU off-gas, does no require any additional reagents, tanks, or pressurized containers, and can thus be fully integrated into SOFC-based APUs.

The answers to all of the research questions investigated in this thesis show that the adsorptive desulfurization of liquid hydrocarbon-based fuels is both feasible and a very promising concept for on-board applications. This approach provides the possibility of operating fuel-cell systems - as one of the most effective technologies for energy conversion - with the most common types of fuels. The concept presented in this thesis proves the feasibility of a $5.5\,kW_{el}$ SOFC-driven APU with an integrated on-board desulfurization unit based on $Ag-Al_2O_3$ and provides a fundamental understanding of the adsorption and regeneration mechanisms involved in the adsorptive desulfurization approach.

8.2. Recommendations for Future Works

Improvement and development of new materials

The synthesized $Ag-Al_2O_3$ adsorbent in this thesis shows great potential for improvement. As shown by the SEM and XRD analyses, high amounts of metallic silver are not transformed into the active Ag phase during calcination. Consequently, the amount of silver could potentially be reduced without decreasing the adsorption performance. Such optimizations have also been reported for other silver-based adsorbents [94, 106]. In addition, deeper insight into the incorporation mechanisms of the active Ag phase would make it possible to further optimize the dispersion rate of active silver during synthesis. At the same time, the role of SO_2 on the re-dispersion of the active Ag phase during regeneration has not yet been fully understood. The $Ag-Al_2O_3$ adsorbent has shown good performance in desulfurizing commercial jet and diesel fuels containing BT, DBT, and/or 4,6-DMDBT. Additional experiments with commercial sulfur-rich fuels are advised in order to fully understand the impact of different sulfur heterocycles and PAHs on the desulfurization performance of $Ag-Al_2O_3$. This is also important in order to further quantify the desulfurization performance under realistic conditions. The possibility also remains that other support materials, or even other adsorbent formulations, could increase the desulfurization capacity. For example, ZrO_2, MgO, and mixed metal oxides are other potential support materials. From the current state of knowledge, however, such improvements would not replace the importance of on-board regeneration.

Improvement and development of on-board regeneration strategies

The novel regeneration strategy presented herein is both a very efficient and very effective approach. However, the regeneration profile was not optimized in terms of regeneration

temperature and time. The overall regeneration mechanism identified within this work provides an ideal basis for further improvement of the regeneration cycle. The final regeneration temperature and hold time in particular seem to have great potential to be reduced.

Within this thesis, emphasis has been placed on understanding desulfurization and regeneration mechanisms. Additional long-term experiments over more than 500 cycles of operation are advised in order to scrutinize the presented findings and the thermal and chemical stability of Ag-Al_2O_3 in particular. Further investigations should consider the process design of practical desulfurization units. The process conditions should be thoroughly optimized in terms of adsorbent particle sizes, flow rates, and adsorber design, with a focus on both the desulfurization and regeneration modes. For desulfurization, the adsorber should be designed to achieve a sharper breakthrough since this is more desirable in a real application. For regeneration, the flow rate and temperature should be adjusted so as to enable full system-integration into the APU concept. As shown by Göll, Samsun, and Peters [8], reduced off-gas temperatures and intensive heat exchange within the APU system do not necessarily imply higher system efficiency. For regeneration, reduced flow rates of the regeneration medium are also desirable in order to reduce the pressure drop within the adsorber. The integration study and the development of the overall process control could thereby be assisted by a process simulation software. Finally, investigations should be undertaken on a full-size scale (1 - 10 kW_{el} APU) for real applications.

A

Supplementary Data and Analyses

A.1. Supports Used for Adsorbent Preparation

Different support materials based on γ-Al$_2$O$_3$ and anatase TiO$_2$ were used to synthesize adsorbents according to the preparation method described in Section 3.1. The following Table A.1 provides the product name and vendor of all blank support materials used within this work.

Table A.1.: Additional information to Table 3.1 regarding the various γ-Al$_2$O$_3$ and anatase TiO$_2$-based support materials used within this work.

Designation	Support	Product name	Vendor
Al$_2$O$_3$/1	γ-Al$_2$O$_3$	γ-Alumina	Strem Chemicals
Al$_2$O$_3$/2	γ-Al$_2$O$_3$	SA 6173	Saint-Gobain-NorPro
Al$_2$O$_3$/3	γ-Al$_2$O$_3$	SA 6175	Saint-Gobain-NorPro
Al$_2$O$_3$/4	γ-Al$_2$O$_3$	SA 6176	Saint-Gobain-NorPro
Al$_2$O$_3$/5	γ-Al$_2$O$_3$ (92.8%)	SA 61169	Saint-Gobain-NorPro
TiO$_2$/1	anatase TiO$_2$	ST 31119	Saint-Gobain-NorPro
TiO$_2$/2	anatase TiO$_2$	ST 61120	Saint-Gobain-NorPro

A.2. Pseudo-First Order Equation

Equation A.1 shows the differential form of the pseudo-first order equation proposed by Lagergren [195]. Integration of Equation A.1 with the boundary conditions $q_{t,(t=0)} = 0$ and rearrangement leads to the linearized form of the pseudo-first order equation as shown by Equation A.2.

$$\frac{dq_t}{dt} = k_1(q_{eq} - q_t) \tag{A.1}$$

$$\ln(q_{eq} - q_t) = \ln q_{eq} - k_1 t \tag{A.2}$$

Figure A.1 shows the linearized plot of $\ln(q_{eq} - q_t)$ versus t according to Equation A.1. The corresponding model parameters are given in Table A.2, which obtains correlation coefficients of $R^2 \leq 0.9916$ for both types of PASHs.
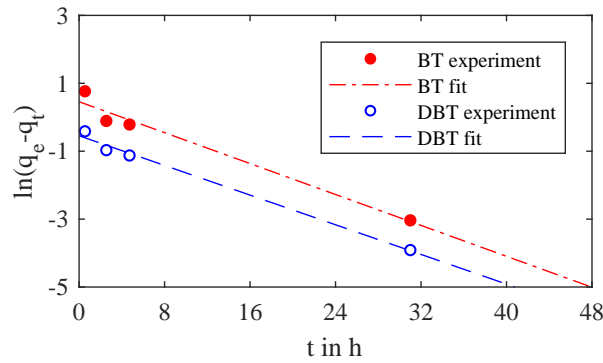
Figure A.1.: Linearized pseudo-first order fit according to Equation A.2 (adsorbent: Ag-Al$_2$O$_3$; fuel: jet/BT_900, jet/DBT_900; adsorption temperature: 20 °C).

Table A.2.: Pseudo-first order model parameters for the adsorption of BT and DBT on Ag-Al$_2$O$_3$ from jet A-1 fuel.

	$q_{eq,exp}$ (mg-S/g-ads)	$q_{eq,calc}$ (mg-S/g-ads)	k_1 (h^{-1})	R^2
jet/BT_900	4.67	1.58	0.114	0.9716
jet/DBT_900	3.65	0.58	0.109	0.9916

A.3. Additional XRD Analysis of the Adsorbent

Figure A.2 shows the XRD patterns of fresh and regenerated Ag-Al$_2$O$_3$ after desulfurizing jet/BT_900. The regeneration was carried out using APU$_g$ as the regeneration medium at a final regeneration temperature of 525 °C. The regeneration procedure is described in detail in Section 6.3.1. The XRD patterns are identical to those observed in the case of jet/DBT_900 (cf. Figure 6.9c).
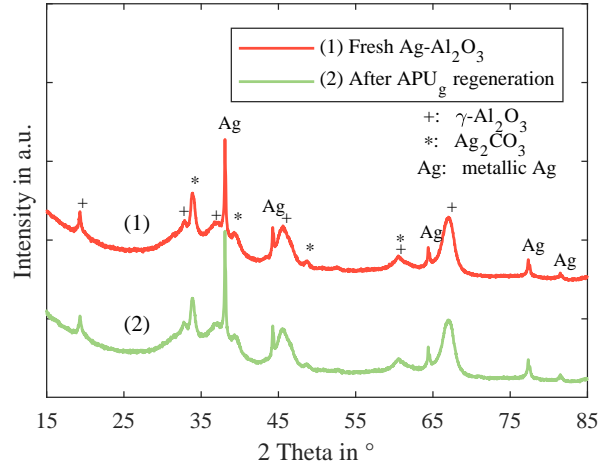
Figure A.2.: XRD patterns of (1) fresh Ag-Al₂O₃ and (2) after APU$_g$ regeneration (adsorbent: Ag-Al₂O₃; fuel: jet/BT_900; adsorption temperature: $20\,^{\circ}C$; regeneration: APU$_g$; final regeneration temperature: $525\,^{\circ}C$).

A.4. Specific Heat Capacities

Specific Heat Capacity of Ambient Air

The temperature dependency of the specific heat capacity of ambient air $C_{m,p_{air}}(\vartheta)$ is taken into account by Equation A.3.

$$C_{m,p_{air}}\Big|_{\vartheta=0}^{\vartheta_1} = p_{0,air} + p_{1,air}\vartheta_1 + p_{2,air}\vartheta_1{}^2 + p_{3,air}\vartheta_1{}^3 \tag{A.3}$$

The parameters for the polynomial fit and the corresponding correlation coefficient are provided in Table A.3. This polynomial fit is based on the thermodynamic data for dry air as calculated by the EES^{TM} software [236], and has a range of validity from 20 - 550 $^{\circ}C$.

Table A.3.: Fit parameters for Equation A.3.

Fit parameter	Value
$p_{0,air}$	1.00601834921903
$p_{1,air}$	$-2.51591370364829 \times 10^{-6}$
$p_{2,air}$	$5.79677755017655 \times 10^{-7}$
$p_{3,air}$	$-4.57138912067958 \times 10^{-10}$
R^2	0.999903

Specific Heat Capacity of APU off-gas

The specific molar heat capacity of the APU off-gas is calculated according to Equation A.4, where x_i is the mole fraction of the component i and C_{m,p_i} the corresponding specific molar heat capacity. The mole fractions of all components of APU off-gas are provided in Table A.4.

$$C_{m,p_{off\text{-}gas}}\Big|_{\vartheta=0}^{\vartheta_1} = \sum_{i=1}^{k} x_i C_{m,p_i}\Big|_{\vartheta=0}^{\vartheta_1} \tag{A.4}$$

Table A.4.: Detailed composition of hot off-gas from an auxiliary power unit with $4.5\,mol\%$ H_2O (APU_g) used as regeneration medium.

	Mole fractions of APU off-gas (mol/mol)
N_2	0.763
O_2	0.168
CO_2	0.024
H_2O	0.045

The temperature dependency of the specific heat capacity of APU off-gas $C_{m,p_{off\text{-}gas}}(\vartheta)$ is taken into account by Equation A.5.

$$C_{m,p_{off\text{-}gas}}\Big|_{\vartheta=0}^{\vartheta_1} = p_{0,off\text{-}gas} + p_{1,off\text{-}gas}\vartheta_1 + p_{2,off\text{-}gas}\vartheta_1^2 + p_{3,off\text{-}gas}\vartheta_1^3 \tag{A.5}$$

The parameters for the polynomial fit and the corresponding correlation coefficient are provided in Table A.5. This polynomial fit is based on the thermodynamic data for APU off-gas (cf. Table A.4) calculated according to Equation A.4 by the EES^{TM} software [236] and has a range of validity from 20 - 550 $°C$.

Table A.5.: Fit parameters for Equation A.5.

Fit parameter	Value
$p_{0,off\text{-}gas}$	1.05383310926373
$p_{1,off\text{-}gas}$	$8.50010689583036 \times 10^{-6}$
$p_{2,off\text{-}gas}$	$6.10861184907079 \times 10^{-7}$
$p_{3,off\text{-}gas}$	$-4.81207617971745 \times 10^{-10}$
R^2	0.999947

Bibliography

[1] G. E. Boyd, A. W. Adamson, and L. S. Myers Jr. The Exchange Adsorption of Ions from Aqueous Solutions by Organic Zeolites. II. Kinetics. *Journal of the American Chemical Society*, **69** (1) (1948): 2836–2848.

[2] R. G. Pearson. Hard and Soft Acids and Bases. *Journal of the American Chemical Society*, **85** (22) (1963): 3533–3539. DOI: 10.1021/ja00905a001.

[3] A. Cutillo, S. Specchia, M. Antonini, et al. Diesel fuel processor for PEM fuel cells: Two possible alternatives (ATR versus SR). *Journal of Power Sources*, **154** (2) (2006): 379–385. DOI: 10.1016/j.jpowsour.2005.10.065.

[4] P. Engelhardt, M. Maximini, F. Beckmann, et al. Integrated fuel cell APU based on a compact steam reformer for diesel and a PEMFC. *International Journal of Hydrogen Energy*, **37** (18) (2012): 13470–13477. DOI: 10.1016/j.ijhydene.2012.06.080.

[5] R. C. Samsun, J. Pasel, H. Janßen, et al. Design and test of a 5kWehigh-temperature polymer electrolyte fuel cell system operated with diesel and kerosene. *Applied Energy*, **114** (2014): 238–249. DOI: 10.1016/j.apenergy.2013.09.054.

[6] A. Lindermeir, S. Kah, S. Kavurucu, et al. On-board diesel fuel processing for an SOFC-APU-Technical challenges for catalysis and reactor design. *Applied Catalysis B: Environmental*, **70** (1-4) (2007): 488–497. DOI: 10.1016/j.apcatb.2006.02.025.

[7] J. Lawrence and M. Boltze. Auxiliary power unit based on a solid oxide fuel cell and fuelled with diesel. *Journal of Power Sources*, **154** (2) (2006): 479–488. DOI: 10.1016/j.jpowsour.2005.10.036.

[8] S. Göll, R. C. Samsun, and R. Peters. Analysis and optimization of solid oxide fuel cell-based auxiliary power units using a generic zero-dimensional fuel cell model. *Journal of Power Sources*, **196** (22) (2011): 9500–9509. DOI: 10.1016/j.jpowsour.2011.07.030.

[9] V. C. Srivastava. An evaluation of desulfurization technologies for sulfur removal from liquid fuels. *RSC Advances*, **2** (2012): 759–783. DOI: 10.1039/c1ra00309g.

[10] A. Samokhvalov and B. J. Tatarchuk. Review of Experimental Characterization of Active Sites and Determination of Molecular Mechanisms of Adsorption, Desorption and Regeneration of the Deep and Ultradeep Desulfurization Sorbents for Liquid Fuels. *Catalysis Reviews*, **52** (3) (2010): 381–410. DOI: 10.1080/01614940.2010.498749.

[11]   R. C. Samsun, J. Pasel, R. Peters, et al. Fuel cell systems with reforming of petroleum-based and synthetic-based diesel and kerosene fuels for APU applications. *International Journal of Hydrogen Energy*, **40** (19) (2015): 6405–6421. DOI: 10.1016/j.ijhydene.2015.03.091.

[12]   T. Aicher, B. Lenz, F. Gschnell, et al. Fuel processors for fuel cell APU applications. *Journal of Power Sources*, **154** (2) (2006): 503–508. DOI: 10.1016/j.jpowsour.2005.10.026.

[13]   N. Armaroli and V. Balzani. The Hydrogen Issue. *ChemSusChem*, **4** (1) (2011): 21–36. DOI: 10.1002/cssc.201000182.

[14]   A. Simson. "Developing an energy efficient steam reforming process to produce hydrogen from sulfur-containing fuels." Ph.D. Dissertation. Columbia University, 2013.

[15]   R. Kaila and a. Krause. Autothermal reforming of simulated gasoline and diesel fuels. *International Journal of Hydrogen Energy*, **31** (13) (2006): 1934–1941. DOI: 10.1016/j.ijhydene.2006.04.004.

[16]   C. Hulteberg. Sulphur-tolerant catalysts in small-scale hydrogen production, a review. *International Journal of Hydrogen Energy*, **37** (5) (2012): 3978–3992. DOI: 10.1016/j.ijhydene.2011.12.001.

[17]   P. Kurzweil. Brennstoffzellentechnik: Grundlagen, Komponenten, Systeme, Anwendungen. 2nd. Wiesbaden: Springer, 2013, 260.

[18]   T. Li, M. F. Rabuni, L. Kleiminger, et al. A highly-robust solid oxide fuel cell (SOFC): Simultaneous greenhouse gas treatment and clean energy generation. *Energy and Environmental Science*, **9** (12) (2016): 3682–3686. DOI: 10.1039/c6ee02562e.

[19]   T. Tanim, D. J. Bayless, and J. P. Trembly. Modeling of a 5 kWe tubular solid oxide fuel cell based system operating on desulfurized JP-8 fuel for auxiliary and mobile power applications. *Journal of Power Sources*, **221** (2013): 387–396. DOI: 10.1016/j.jpowsour.2012.08.024.

[20]   J. Zizelman, S. Shaffer, and S. Mukerjee. Solid oxide fuel cell auxiliary power unit - A development update. *SAE Technical Papers*, (SAE 2002 World Congress) (2002). DOI: 10.4271/2002-01-0411.

[21]   L. Wang, K. Murata, and M. Inaba. Development of novel highly active and sulphur-tolerant catalysts for steam reforming of liquid hydrocarbons to produce hydrogen. *Applied Catalysis A: General*, **257** (1) (2004): 43–47. DOI: 10.1016/S0926-860X(03)00590-8.

[22]   M. Ferrandon, J. Mawdsley, and T. Krause. Effect of temperature, steam-to-carbon ratio, and alkali metal additives on improving the sulfur tolerance of a Rh/La–Al2O3 catalyst reforming gasoline for fuel cell applications. *Applied Catalysis A: General*, **342** (1-2) (2008): 69–77. DOI: 10.1016/j.apcata.2008.03.001.

[23] I. Kang, J. Bae, and G. Bae. Performance comparison of autothermal reforming for liquid hydrocarbons, gasoline and diesel for fuel cell applications. *Journal of Power Sources*, **163** (1) (2006): 538–546. DOI: 10.1016/j.jpowsour.2006.09.035.

[24] J. Rechberger, A. Kaupert, J. Hagerskans, et al. Demonstration of the First European SOFC APU on a Heavy Duty Truck. *Transportation Research Procedia*, **14** (x) (2016): 3676–3685. DOI: 10.1016/j.trpro.2016.05.442.

[25] B. Stoeckl, V. Subotić, D. Reichholf, et al. Extensive analysis of large planar SOFC: Operation with humidified methane and carbon monoxide to examine carbon deposition based degradation. *Electrochimica Acta*, **256** (2017): 325–336. DOI: 10.1016/j.electacta.2017.09.026.

[26] R. M. Ormerod. "Fuels and Fuel Processing." In: *High Temperature Solid Oxide Fuel Cells: Fundamentals, Design and Applications.* Elsevier Ltd, 2003. Chap. 12, 333–361. DOI: 10.1016/B978-185617387-2/50029-5.

[27] V. Subotić, C. Schluckner, H. Schroettner, et al. *Analysis of possibilities for carbon removal from porous anode of solid oxide fuel cells after different failure modes.* 2016. DOI: 10.1016/j.jpowsour.2015.10.071.

[28] D. Papurello, A. Lanzini, D. Drago, et al. Limiting factors for planar solid oxide fuel cells under different trace compound concentrations. *Energy*, **95** (2016): 67–78. DOI: 10.1016/j.energy.2015.11.070.

[29] A. Vita, C. Italiano, L. Pino, et al. Hydrogen-rich gas production by steam reforming of n-dodecane. Part II: Stability, regenerability and sulfur poisoning of low loading Rh-based catalyst. *Applied Catalysis B: Environmental*, **218** (2017): 317–326. DOI: 10.1016/j.apcatb.2017.06.059.

[30] Q. Zheng, C. Janke, and R. Farrauto. Steam reforming of sulfur-containing dodecane on a Rh-Pt catalyst: Influence of process parameters on catalyst stability and coke structure. *Applied Catalysis B: Environmental*, **160-161** (1) (2014): 525–533. DOI: 10.1016/j.apcatb.2014.05.044.

[31] L. Liu and L. Hong. Interactions between CeO_2 and Ni_xP_y for enhancing coking and sulfur resistance in autothermal reforming of liquid hydrocarbons. *Fuel*, **96** (2012): 348–354. DOI: 10.1016/j.fuel.2011.12.055.

[32] C. Xie, Y. Chen, M. H. Engelhard, et al. Comparative Study on the Sulfur Tolerance and Carbon Resistance of Supported Noble Metal Catalysts in Steam Reforming of Liquid Hydrocarbon Fuel. *ACS Catalysis*, **2** (6) (2012): 1127–1137. DOI: 10.1021/cs200695t.

[33] S. L. Lakhapatri and M. a. Abraham. Sulfur poisoning of Rh–Ni catalysts during steam reforming of sulfur-containing liquid fuels. *Catalysis Science & Technology*, **3** (10) (2013): 2755. DOI: 10.1039/c3cy00351e.

[34] K. Murata, M. Saito, M. Inaba, et al. Hydrogen production by autothermal reforming of sulfur-containing hydrocarbons over re-modified Ni/Sr/ZrO2 catalysts. *Applied Catalysis B: Environmental*, **70** (1-4) (2007): 509–514. DOI: 10.1016/j.apcatb.2006.01.012.

[35] X. Xu, S. Zhang, P. Li, et al. Adsorptive desulfurization of liquid Jet-A fuel at ambient conditions with an improved adsorbent for on-board fuel treatment for SOFC applications. *Fuel Processing Technology*, **124** (2014): 140–146. DOI: 10.1016/j.fuproc.2014.03.001.

[36] S. Velu, X. Ma, C. Song, et al. Desulfurization of JP-8 Jet Fuel by Selective Adsorption over a Ni-based Adsorbent for Micro Solid Oxide Fuel Cells. *Energy and Fuels*, **19** (3) (2005): 1116–1125. DOI: 10.1021/ef049800b.

[37] O. van Rheinberg, K. Lucka, H. Köhne, et al. Selective removal of sulphur in liquid fuels for fuel cell applications. *Fuel*, **87** (13-14) (2008): 2988–2996. DOI: 10.1016/j.fuel.2008.03.020.

[38] J. Latz. "Entschwefelung von Mitteldestillaten für die Anwendung in mobilen Brennstoffzellen-Systemen." Ph.D. Dissertation. RWTH Aachen University, Germany, 2008.

[39] S. A. Hussain. "Liquid Phase Desulfurization of Hydrocarbon Fuels under Ambient Conditions using Regenerable Mixed Oxide Supported Silver Adsorbents." Ph.D. Dissertation. Auburn University, 2014.

[40] J. H. Gary, G. E. Handwerk, and M. J. Kaiser. PETROLEUM REFINING: Technology and Economics. 5th ed. Boca Raton: CRC Press, 2007.

[41] S. Nair and B. J. Tatarchuk. Characteristics of sulfur removal by silver-titania adsorbents at ambient conditions. *Adsorption*, **3** (2011): 663–673. DOI: 10.1007/s10450-011-9362-2.

[42] M. Bernabei, R. Reda, R. Galiero, et al. Determination of total and polycyclic aromatic hydrocarbons in aviation jet fuel. *Journal of Chromatography A*, **985** (1-2) (2003): 197–203. DOI: 10.1016/S0021-9673(02)01826-5.

[43] B. H. Cooper and B. B. L. Donnis. Aromatic saturation of distillates: An overview. *Applied Catalysis A: General*, **137** (2) (1996): 203–223. DOI: 10.1016/0926-860X(95)00258-8.

[44] M. S. Rakow. "Petroleum Oil Refining." In: *Fuels and Lubricants Handbook: Technology, Properties, Performance, and Testing*. Ed. by G. E. Totten, S. R. Westbrook, and R. J. Shah. ASTM International, West Conshohocken, 2003. Chap. 1, 3–30. DOI: 10.1520/MNL37WCD-EB.

[45] J. Xiao, C. Song, X. Ma, et al. Effects of aromatics, diesel additives, nitrogen compounds, and moisture on adsorptive desulfurization of diesel fuel over activated carbon. *Industrial and Engineering Chemistry Research*, **51** (8) (2012): 3436–3443. DOI: 10.1021/ie202440t.

[46] T. C. Zannis, D. T. Hountalas, R. G. Papagiannakis, et al. Effect of Fuel Chemical Structure and Properties on Diesel Engine Performance and Pollutant Emissions: Review of the Results of Four European Research Programs. *SAE International Journal of Fuels and Lubricants*, **1** (1) (2009): 384–419. DOI: 10.4271/2008-01-0838.

[47] J. H. Kim, X. Ma, A. Zhou, et al. Ultra-deep desulfurization and denitrogenation of diesel fuel by selective adsorption over three different adsorbents: A study on adsorptive selectivity and mechanism. *Catalysis Today*, **111** (1-2) (2006): 74–83. DOI: 10.1016/j.cattod.2005.10.017.

[48] X. Han, H. Lin, and Y. Zheng. Adsorptive denitrogenation and desulfurization of diesel using activated carbons oxidized by (NH4)2S2O8 under mild conditions. *The Canadian Journal of Chemical Engineering*, **93** (3) (2015): 538–548. DOI: 10.1002/cjce.22132.

[49] R. Hua, J. Wang, H. Kong, et al. Analysis of sulfur-containing compounds in crude oils by comprehensive two-dimensional gas chromatography with sulfur chemiluminescence detection. *Journal of Seperation Science*, **27** (2004): 691–698. DOI: 10.1002/jssc.200301631.

[50] C. Song. An overview of new approaches to deep desulfurization for ultra-clean gasoline, diesel fuel and jet fuel. *Catalysis Today*, **86** (1-4) (2003): 211–263. DOI: 10.1016/S0920-5861(03)00412-7.

[51] Y. S. Al-Degs, A. H. El-Sheikh, Z. A. Al Bakain, et al. Conventional and Upcoming Sulfur-Cleaning Technologies for Petroleum Fuel : A Review. *Energy Technology*, **4** (2016): 679–699. DOI: 10.1002/ente.201500475.

[52] M. H. Ibrahim, M. Hayyan, M. A. Hashim, et al. The role of ionic liquids in desulfurization of fuels: A review. *Renewable and Sustainable Energy Reviews*, **76** (November 2016) (2017): 1534–1549. DOI: 10.1016/j.rser.2016.11.194.

[53] K. G. Knudsen, B. H. Cooper, and H. Topsøe. Catalyst and process technologies for ultra low sulfur diesel. *Applied Catalysis A: General*, **189** (1999): 205–215.

[54] C. Song. New Approaches to Deep Desulfurization for Ultra- Clean Gasoline and Diesel Fuels: An Overview. *Division of Fuel Chemistry Preprints*, **47** (2) (2002): 438–444.

[55] P. S. Kulkarni and C. A. M. Afonso. Deep desulfurization of diesel fuel using ionic liquids: current status and future challenges. *Green Chemistry*, **12** (7) (2010): 1139. DOI: 10.1039/c002113j.

[56] E. Ito and J. A. R. van Veen. On novel processes for removing sulphur from refinery streams. *Catalysis Today*, **116** (4) (2006): 446–460. DOI: 10.1016/j.cattod.2006.06.040.

[57] C. Asumana, R. Haque, L. Yu, et al. Desulfurization of Real Fuel Oils by Extraction with Ionic Liquids. *Separation Science and Technology*, **48** (17) (2013): 2582–2588. DOI: 10.1080/01496395.2013.804559.

[58] H. Zhao, G. A. Baker, D. V. Wagle, et al. Tuning Task-Specific Ionic Liquids for the Extractive Desulfurization of Liquid Fuel. *ACS Sustainable Chemistry and Engineering*, **4** (9) (2016): 4771–4780. DOI: 10.1021/acssuschemeng.6b00972.

[59] B. Saha and S. Sengupta. Extraction of thiophenic sulfur compounds from model fuel using a water-based solvent. *Energy and Fuels*, **31** (1) (2017): 996–1004. DOI: 10.1021/acs.energyfuels.6b01842.

[60] Y. S. Al-Degs and M. A. Al-Ghouti. Influence of diesel acidification on dibenzothiophene removal: A new desulfurization practice. *Separation and Purification Technology*, **139** (2015): 1–4. DOI: 10.1016/j.seppur.2014.10.027.

[61] A. M. Dehkordi, Z. Kiaei, and M. A. Sobati. Oxidative desulfurization of simulated light fuel oil and untreated kerosene. *Fuel Processing Technology*, **90** (3) (2009): 435–445. DOI: 10.1016/j.fuproc.2008.11.006.

[62] Y. Zhu, M. Zhu, L. Kang, et al. Phosphotungstic Acid Supported on Mesoporous Graphitic Carbon Nitride as Catalyst for Oxidative Desulfurization of Fuel. *Industrial and Engineering Chemistry Research*, **54** (7) (2015): 2040–2047. DOI: 10.1021/ie504372p.

[63] B. Smitha, D. Suhanya, S. Sridhar, et al. Separation of organic-organic mixtures by pervaporation - A review. *Journal of Membrane Science*, **241** (1) (2004): 1–21. DOI: 10.1016/j.memsci.2004.03.042.

[64] I. Bettermann and C. Staudt. Desulphurization of kerosene: Pervaporation of benzothiophene/n-dodecane mixtures. *Journal of Membrane Science*, **343** (1-2) (2009): 119–127. DOI: 10.1016/j.memsci.2009.07.017.

[65] L. Lin, Y. Zhang, and Y. Kong. Recent advances in sulfur removal from gasoline by pervaporation. *Fuel*, **88** (10) (2009): 1799–1809. DOI: 10.1016/j.fuel.2009.03.031.

[66] I. Bettermann and C. Staudt. Permeation of binuclear, sulphur containing aromatic compounds. *Desalination*, **250** (3) (2010): 1144–1146. DOI: 10.1016/j.desal.2009.09.128.

[67] G. Liu, T. Zhou, W. Liu, et al. Enhanced desulfurization performance of PDMS membranes by incorporating silver decorated dopamine nanoparticles. *Journal of Materials Chemistry A*, **2** (32) (2014): 12907. DOI: 10.1039/C4TA01778A.

[68] Y. Wang, J. Latz, R. Dahl, et al. Liquid phase desulfurization of jet fuel by a combined pervaporation and adsorption process. *Fuel Processing Technology*, **90** (3) (2009): 458–464. DOI: 10.1016/j.fuproc.2008.11.008.

[69] Y. Wang, J. Geder, J. M. Schubert, et al. Optimization of adsorptive desulfurization process of jet fuels for application in fuel cell systems. *Fuel Processing Technology*, **95** (2012): 144–153. DOI: 10.1016/j.fuproc.2011.11.011.

[70] M. Soleimani, A. Bassi, and A. Margaritis. Biodesulfurization of refractory organic sulfur compounds in fossil fuels. *Biotechnology Advances*, **25** (6) (2007): 570–596. DOI: 10.1016/j.biotechadv.2007.07.003.

[71] F. Tian, Z. Fu, H. Zhang, et al. Thiophene adsorption onto metal-organic framework HKUST-1 in the presence of toluene and cyclohexene. *Fuel*, **158** (2015): 200–206. DOI: 10.1016/j.fuel.2015.05.030.

[72] T. Wang, X. Li, W. Dai, et al. Enhanced adsorption of dibenzothiophene with zinc/copper-based metal-organic frameworks. *Journal of Materials Chemistry A*, **3** (42) (2015): 21044–21050. DOI: 10.1039/C5TA05204A.

[73] J. Wang and J. Wei. Selective and simultaneous removal of dibenzothiophene and 4-methyldibenzothiophene using double-template molecularly imprinted polymers on the surface of magnetic mesoporous silica. *Journal of Materials Chemistry A*, **5** (9) (2017): 4651–4659. DOI: 10.1039/C6TA11167J.

[74] X. Han, H. Lin, and Y. Zheng. Regeneration methods to restore carbon adsorptive capacity of dibenzothiophene and neutral nitrogen heteroaromatic compounds. *Chemical Engineering Journal*, **243** (2014): 315–325. DOI: 10.1016/j.cej.2013.12.074.

[75] N. Farzin Nejad, E. Shams, and M. K. Amini. Synthesis of magnetic ordered mesoporous carbon (Fe-OMC) adsorbent and its evaluation for fuel desulfurization. *Journal of Magnetism and Magnetic Materials*, **390** (2015): 1–7. DOI: 10.1016/j.jmmm.2015.04.074.

[76] J. Bu, G. Loh, C. G. Gwie, et al. Desulfurization of diesel fuels by selective adsorption on activated carbons: Competitive adsorption of polycyclic aromatic sulfur heterocycles and polycyclic aromatic hydrocarbons. *Chemical Engineering Journal*, **166** (1) (2011): 207–217. DOI: 10.1016/j.cej.2010.10.063.

[77] S. A. Ganiyu, K. Alhooshani, K. O. Sulaiman, et al. Influence of aluminium impregnation on activated carbon for enhanced desulfurization of DBT at ambient temperature: Role of surface acidity and textural properties. *Chemical Engineering Journal*, **303** (2016): 489–500. DOI: 10.1016/j.cej.2016.06.005.

[78] R. Menzel, D. Iruretagoyena, Y. Wang, et al. Graphene oxide/mixed metal oxide hybrid materials for enhanced adsorption desulfurization of liquid hydrocarbon fuels. *Fuel*, **181** (2016): 531–536. DOI: 10.1016/j.fuel.2016.04.125.

[79] N. Farzin Nejad, E. Shams, M. Amini, et al. Ordered mesoporous carbon CMK-5 as a potential sorbent for fuel desulfurization: Application to the removal of dibenzothiophene and comparison with CMK-3. *Microporous and Mesoporous Materials*, **168** (2013): 239–246. DOI: 10.1016/j.micromeso.2012.10.012.

[80] G. Blanco-Brieva, J. Campos-Martin, S. Al-Zahrani, et al. Effectiveness of metal–organic frameworks for removal of refractory organo-sulfur compound present in liquid fuels. *Fuel*, **90** (1) (2011): 190–197. DOI: 10.1016/j.fuel.2010.08.008.

[81] P. Baltzopoulou, K. X. Kallis, G. Karagiannakis, et al. Diesel Fuel Desulfurization via Adsorption with the Aid of Activated Carbon: Laboratory- and Pilot-Scale Studies. *Energy and Fuels*, **29** (9) (2015): 5640–5648. DOI: 10.1021/acs.energyfuels.5b01133.

[82] G. Blanco-Brieva, J. Campos-Martin, S. Al-Zahrani, et al. Thermal regeneration of the metal organic frameworks used in the adsorption of refractory organosulfur compounds from liquid fuels. *Fuel*, **105** (2013): 459–465. DOI: 10.1016/j.fuel.2012.08.003.

[83] W. Kleist, M. Maciejewski, and A. Baiker. MOF-5 based mixed-linker metal-organic frameworks: Synthesis, thermal stability and catalytic application. *Thermochimica Acta*, **499** (1-2) (2010): 71–78. DOI: 10.1016/j.tca.2009.11.004.

[84] J. M. Kim, J. H. Kwak, S. Jun, et al. Ion exchange and thermal stability of MCM-41. *Journal of Physical Chemistry*, **99** (45) (1995): 16742–16747. DOI: 10.1021/j100045a039.

[85] A. Samokhvalov, E. C. Duin, S. Nair, et al. Adsorption and desorption of dibenzothiophene on Ag-titania studied by the complementary temperature-programmed XPS and ESR. *Applied Surface Science*, **257** (8) (2011): 3226–3232. DOI: 10.1016/j.apsusc.2010.10.142.

[86] P. Jarzombek. "Entwicklung und Charakterisierung von sphärischen γ-Al2O3 Formkörpern und deren Anwendung als Trägermaterial für Goldkatalysatoren." Ph.D. Dissertation. Technische Universität Carolo-Wilhelmina, Germany, 2010, 182.

[87] R. Ullah, P. Bai, P. Wu, et al. Comparison of the Reactive Adsorption Desulfurization Performance of Ni/ZnO-Al2O3 Adsorbents Prepared by Different Methods. *Energy and Fuels*, **30** (4) (2016): 2874–2881. DOI: 10.1021/acs.energyfuels.6b00232.

[88] C. Sentorun-Shalaby, X. Ma, and C. Song. Ultra-deep desulfurization of ultra-low sulfur diesel over nickel-based sorbents in the presence of hydrogen for fuel cell applications. *ACS Symposium Series*, **1088** (2011): 55–62. DOI: 10.1021/bk-2011-1088.ch004.

[89] A. Mansouri, A. A. Khodadadi, and Y. Mortazavi. Ultra-deep adsorptive desulfurization of a model diesel fuel on regenerable Ni-Cu/γ-Al2O3 at low temperatures in absence of hydrogen. *Journal of hazardous materials*, **271** (2014): 120–30. DOI: 10.1016/j.jhazmat.2014.02.006.

[90] S. Aslam, F. Subhan, Z. Yan, et al. Microporous and Mesoporous Materials Rapid functionalization of as-synthesized KIT-6 with nickel species occluded with template for adsorptive desulfurization. *Microporous and Mesoporous Materials*, **214** (2015): 54–63. DOI: 10.1016/j.micromeso.2015.04.032.

[91] A. J. Hernández-Maldonado and R. T. Yang. Desulfurization of Diesel Fuels by Adsorption via π-Complexation with Vapor-Phase Exchanged Cu(I)-Y Zeolites. *Journal of the American Chemical Society*, **126** (4) (2004): 992–993. DOI: 10.1021/ja039304m.

[92] S. Nair, A. H. M. S. Hussain, and B. J. Tatarchuk. The role of surface acidity in adsorption of aromatic sulfur heterocycles from fuels. *Fuel*, **105** (2013): 695–704. DOI: 10.1016/j.fuel.2012.10.005.

[93] H.-Y. Sun, L.-P. Sun, F. Li, et al. Adsorption of benzothiophene from fuels on modified NaY zeolites. *Fuel Processing Technology*, **134** (2015): 284–289. DOI: 10.1016/j.fuproc.2015.02.010.

[94] S. A. Hussain and B. J. Tatarchuk. Adsorptive desulfurization of jet and diesel fuels using Ag/TiOx–Al2O3 and Ag/TiOx–SiO2 adsorbents. *Fuel*, **107** (2013): 465–473. DOI: 10.1016/j.fuel.2012.11.030.

[95] C. Xu, M. Zheng, K. Chen, et al. CeOx doping on a TiO2-SiO2 supporter enhances Ag based adsorptive desulfurization for diesel. *Journal of Fuel Chemistry and Technology*, **44** (8) (2016): 943–953. DOI: 10.1016/S1872-5813(16)30042-1.

[96] R. Neubauer, C. Weinlaender, N. Kienzl, et al. Adsorptive Desulfurization: Fast On-Board Regeneration and the Influence of Fatty Acid Methyl Ester on Desulfurization and in Situ Regeneration Performance of a Silver-Based Adsorbent. *Energy and Fuels*, **30** (6) (2016): 5174–5182. DOI: 10.1021/acs.energyfuels.6b00519.

[97] R. Neubauer, M. Husmann, C. Weinlaender, et al. Acid base interaction and its influence on the adsorption kinetics and selectivity order of aromatic sulfur heterocycles adsorbing on Ag-Al2O3. *Chemical Engineering Journal*, **309** (2017): 840–849. DOI: 10.1016/j.cej.2016.10.094.

[98] R. Neubauer, N. Kienzl, B. Bitschnau, et al. Thermal in Situ and System-Integrated Regeneration Strategy for Adsorptive On-Board Desulfurization Units. *Energy and Fuels*, **31** (11) (2017): 12942–12950. DOI: 10.1021/acs.energyfuels.7b01987.

[99] R. Neubauer, C. Weinlaender, N. Kienzl, et al. Adsorptive on-board desulfurization over multiple cycles for fuel-cell-based auxiliary power units operated by different types of fuels. *Journal of Power Sources*, **385** (2018): 45–54. DOI: 10.1016/j.jpowsour.2018.02.083.

[100] X. Meng, G. Qiu, G. Wang, et al. Durable and regenerable mesoporous adsorbent for deep desulfurization of model jet fuel. *Fuel Processing Technology*, **111** (2013): 78–85. DOI: 10.1016/j.fuproc.2013.02.002.

[101] S. Nair and B. J. Tatarchuk. Supported silver adsorbents for selective removal of sulfur species from hydrocarbon fuels. *Fuel*, **89** (11) (2010): 3218–3225. DOI: 10.1016/j.fuel.2010.05.006.

[102] S. A. Hussain and B. J. Tatarchuk. Mechanism of hydrocarbon fuel desulfurization using Ag/TiO2–Al2O3 adsorbent. *Fuel Processing Technology*, **126** (2014): 233–242. DOI: 10.1016/j.fuproc.2014.05.006.

[103] J. M. Palomino, D. T. Tran, J. L. Hauser, et al. Mesoporous silica nanoparticles for high capacity adsorptive desulfurization. *Journal of Materials Chemistry A*, **2** (2014): 14890–14895. DOI: 10.1039/C4TA02570A.

[104] A. J. Hernández-Maldonado and R. T. Yang. Desulfurization of liquid fuels by adsorption via π complexation with Cu(I)-Y and Ag-Y zeolites. *Industrial and Engineering Chemistry Research*, **42** (1) (2003): 123–129. DOI: 10.1021/ie0301132.

[105]   H. Chen, Y. Wang, F. H. Yang, et al. Desulfurization of high-sulfur jet fuel by mesoporous
        π-complexation adsorbents. *Chemical Engineering Science*, **64** (24) (2009): 5240–5246. DOI:
        10.1016/j.ces.2009.08.031.

[106]   J. M. Palomino, D. T. Tran, A. R. Kareh, et al. Zirconia-silica based mesoporous desul-
        furization adsorbents. *Journal of Power Sources*, **278** (2015): 141–148. DOI: 10.1016/j.
        jpowsour.2014.12.043.

[107]   L. Yang, Y. Wang, D. Huang, et al. Preparation of High Performance Adsorbents by
        Functionalizing Mesostructured Silica Spheres for Selective Adsorption of Organosulfur
        Compounds. *Industrial & Engineering Chemistry Research*, **46** (2) (2007): 579–583. DOI:
        10.1021/ie061174d.

[108]   H. Song, G. Yang, H. L. Song, et al. Kinetic and thermodynamic studies on adsorption
        of thiophene and benzothiophene onto AgCeY Zeolite. *Journal of the Taiwan Institute of
        Chemical Engineers*, **63** (2016): 125–132. DOI: 10.1016/j.jtice.2016.02.020.

[109]   P. Jeevanandam, K. J. Klabunde, and S. H. Tetzler. Adsorption of thiophenes out of
        hydrocarbons using metal impregnated nanocrystalline aluminum oxide. *Microporous
        and Mesoporous Materials*, **79** (1-3) (2005): 101–110. DOI: 10.1016/j.micromeso.2004.10.
        029.

[110]   A. H. M. S. Hussain, M. L. McKee, J. M. Heinzel, et al. Density Functional Theory Study
        of Organosulfur Selective Adsorption on Ag–TiO2 Adsorbents. *The Journal of Physical
        Chemistry C*, **118** (27) (2014): 14938–14947. DOI: 10.1021/jp503097y.

[111]   A. H. M. S. Hussain, H. Yang, and B. J. Tatarchuk. "Investigation of organosulfur
        adsorption pathways from liquid fuels onto Ag/TiOx-Al2O3 adsorbents at ambient
        conditions." In: *Energy and Fuels*. Vol. 27. 8. 2013, 4353–4362. DOI: 10.1021/ef3020266.

[112]   J. L. Hauser, D. T. Tran, E. T. Conley, et al. Plasma Treatment of Silver Impregnated
        Mesoporous Aluminosilicate Nanoparticles for Adsorptive Desulfurization. *Chemistry of
        Materials*, **28** (2) (2016): 474–479. DOI: 10.1021/acs.chemmater.5b03018.

[113]   J. Xiao, Z. Li, B. Liu, et al. Adsorption of benzothiophene and dibenzothiophene on
        ion-impregnated activated carbons and ion-exchanged Y zeolites. *Energy and Fuels*, **22**
        (6) (2008): 3858–3863. DOI: 10.1021/ef800437e.

[114]   J. M. Heinzel. "Identification of Adsorption Mechanisms of Sulfur Heterocycles via
        Surface Analysis of Selected Metal-Doped Adsorbent Materials for Logistics Fuels
        Desulfurization." Ph.D. Dissertation. Auburn University, 2013.

[115]   C.-J. Li, Y.-J. Li, J.-N. Wang, et al. Ag+-loaded polystyrene nanofibrous membranes
        preparation and their adsorption properties for thiophene. *Chemical Engineering Journal*,
        222 (2013): 419–425. DOI: 10.1016/j.cej.2012.09.107.

[116] M. Zheng, C. Xu, H. Hu, et al. A modified homogeneous surface diffusion model for the fixed-bed adsorption of 4,6-DMDBT on Ag-CeOx/TiO2-SiO2. *RSC Advances*, **6** (114) (2016): 112899–112907. DOI: 10.1039/c6ra23967f.

[117] C. He, B. Xu, S. Chen, et al. Facile regeneration and modification of industrial used chelating resin for fuel oil desulfurization. *International Journal of Environmental Science and Technology*, **14** (1) (2017): 165–176. DOI: 10.1007/s13762-016-1135-8.

[118] H. Song, B. L. Jiang, H. L. Song, et al. Preparation of AgY zeolite and study on its adsorption equilibrium and kinetics. *Research on Chemical Intermediates*, **41** (6) (2015): 3837–3854. DOI: 10.1007/s11164-013-1493-5.

[119] G. Bakhtiari, M. Abdouss, M. Bazmi, et al. Optimization of sulfur adsorption over Ag-zeolite nanoadsorbent by experimental design method. *International Journal of Environmental Science and Technology*, **13** (3) (2016): 803–812. DOI: 10.1007/s13762-015-0910-2.

[120] A. A. Olajire, J. J. Abidemi, A. Lateef, et al. Adsorptive desulphuirization of model oil by Ag nanoparticles-modified activated carbon prepared from brewer's spent grains. *Biochemical Pharmacology*, **5** (1) (2017): 147–159. DOI: 10.1016/j.jece.2016.11.033.

[121] D. T. Tran, Z. W. Dunbar, and D. Chu. Regenerable sulfur adsorbent for liquid phase JP-8 fuel using gold/silica based materials. *International Journal of Hydrogen Energy*, **37** (13) (2012): 10430–10434. DOI: 10.1016/j.ijhydene.2012.01.115.

[122] J.-C. Hoguet, G. P. Karagiannakis, J. a. Valla, et al. Gas and liquid phase fuels desulphurization for hydrogen production via reforming processes. *International Journal of Hydrogen Energy*, **34** (11) (2009): 4953–4962. DOI: 10.1016/j.ijhydene.2008.11.043.

[123] J. Xiao, X. Wang, Y. Chen, et al. Ultra-Deep Adsorptive Desulfurization of Light-Irradiated Diesel Fuel over Supported TiO2-CeO2 Adsorbents. *Industrial and Engineering Chemistry Research*, **52** (45) (2013): 15746–15755. DOI: 10.1021/ie402724q.

[124] Y. Shen, X. Xu, and P. Li. A novel potential adsorbent for ultra deep desulfurization of jet fuels at room temperature. *RSC Advances*, **2** (15) (2012): 6155. DOI: 10.1039/c2ra20224g.

[125] J. C. Zhang, L. F. Song, J. Y. Hu, et al. Investigation on gasoline deep desulfurization for fuel cell applications. *Energy Conversion and Management*, **46** (1) (2005): 1–9. DOI: 10.1016/j.enconman.2004.02.005.

[126] X. Xu, S. Zhang, P. Li, et al. Desulfurization of Jet-A fuel in a fixed-bed reactor at room temperature and ambient pressure using a novel selective adsorbent. *Fuel*, **117** (2014): 499–508. DOI: 10.1016/j.fuel.2013.09.074.

[127] J. Xiao, S. Sitamraju, Y. Chen, et al. Air-Promoted Adsorptive Desulfurization of Diesel Fuel Over Ti-Ce Mixed Metal Oxides. *AIChE Journal*, **61** (2) (2015): 631–639. DOI: 10.1002/aic.14647.

[128] H. Song, Y. Chang, X. Wan, et al. Equilibrium , Kinetic , and Thermodynamic Studies on Adsorptive Desulfurization onto Cu I Ce IV Y Zeolite. *Industrial & Engineering Chemistry Research*, **53** (2014): 5701–5708.

[129] X. Xu, S. Zhang, P. Li, et al. Equilibrium and kinetics of Jet-A fuel desulfurization by selective adsorption at room temperatures. *Fuel*, **111** (2013): 172–179. DOI: 10.1016/j.fuel.2013.04.068.

[130] A. L. Santos, R. A. Reis, V. Rossa, et al. Silica-alumina impregnated with cerium, nickel, and molybdenum oxides for adsorption of sulfur and nitrogen compounds from diesel. *Materials Letters*, **83** (2012): 158–160. DOI: 10.1016/j.matlet.2012.06.011.

[131] G. I. Danmaliki and T. A. Saleh. Effects of bimetallic Ce/Fe nanoparticles on the desulfurization of thiophenes using activated carbon. *Chemical Engineering Journal*, **307** (2017): 914–927. DOI: 10.1016/j.cej.2016.08.143.

[132] K. X. Lee and J. A. Valla. Investigation of metal-exchanged mesoporous Y zeolites for the adsorptive desulfurization of liquid fuels. *Applied Catalysis B: Environmental*, **201** (2017): 359–369. DOI: 10.1016/j.apcatb.2016.08.018.

[133] N. A. Khan and S. H. Jhung. Low-temperature loading of Cu+ species over porous metal-organic frameworks (MOFs) and adsorptive desulfurization with Cu+-loaded MOFs. *Journal of hazardous materials*, **237-238** (2012): 180–5. DOI: 10.1016/j.jhazmat.2012.08.025.

[134] Y. Wang, R. T. Yang, and J. M. Heinzel. Desulfurization of Jet Fuel JP-5 Light Fraction by MCM-41 and SBA-15 Supported Cuprous Oxide for Fuel Cell Applications. *Industrial & Engineering Chemistry Research*, **48** (1) (2009): 142–147. DOI: 10.1021/ie800208g.

[135] S. Velu, X. Ma, and C. Song. Selective Adsorption for Removing Sulfur from Jet Fuel over Zeolite-Based Adsorbents. *Industrial & Engineering Chemistry Research*, **42** (21) (2003): 5293–5304. DOI: 10.1021/ie020995p.

[136] X. Ma, S. Velu, J. H. Kim, et al. Deep desulfurization of gasoline by selective adsorption over solid adsorbents and impact of analytical methods on ppm-level sulfur quantification for fuel cell applications. *Applied Catalysis B: Environmental*, **56** (1-2) (2005): 137–147. DOI: 10.1016/j.apcatb.2004.08.013.

[137] Y. Wang, R. T. Yang, and J. M. Heinzel. Desulfurization of jet fuel by π-complexation adsorption with metal halides supported on MCM-41 and SBA-15 mesoporous materials. *Chemical Engineering Science*, **63** (2) (2008): 356–365. DOI: 10.1016/j.ces.2007.09.002.

[138] K.-S. Lin, A. K. Adhikari, and Z.-P. Wang. Desulfurization of Gasoline and Diesel by Adsorption with Cu (I)– Y Zeolite. *Journal of Chemical Engineering of Japan*, **42** (2009): 168–175.

[139] A. J. Hernández-Maldonado, F. H. Yang, G. Qi, et al. Desulfurization of transportation fuels by π-complexation sorbents: Cu(I)-, Ni(II)-, and Zn(II)-zeolites. *Applied Catalysis B: Environmental*, **56** (1-2) (2005): 111–126. DOI: 10.1016/j.apcatb.2004.06.023.

[140] N. A. Khan and S. H. Jhung. Adsorptive removal of benzothiophene using porous copper-benzenetricarboxylate loaded with phosphotungstic acid. *Fuel Processing Technology*, **100** (2012): 49–54. DOI: 10.1016/j.fuproc.2012.03.006.

[141] S. Nuntang, P. Prasassarakich, and C. Ngamcharussrivichai. Comparative study on adsorptive removal of thiophenic sulfurs over Y and USY zeolites. *Industrial and Engineering Chemistry Research*, **47** (19) (2008): 7405–7413. DOI: 10.1021/ie701785s.

[142] W. Li, J. Xing, X. Xiong, et al. Feasibility Study on the Integration of Adsorption/Bioregeneration of pi-complexation adsorbent for desulfurization. *Industrial & engineering chemistry research*, **45** (8) (2006): 2845–2849.

[143] Y. Wang, F. H. Yang, R. T. Yang, et al. Desulfurization of High Sulfur Jet Fuel By Pi-Complexation With Copper and Palladium Halide Sorbents. *Industrial & Engineering Chemistry Research*, **45** (22) (2006): 7649–7655.

[144] Y. Li, F. H. Yang, G. Qi, et al. Effects of oxygenates and moisture on adsorptive desulfurization of liquid fuels with Cu(I)Y zeolite. *Catalysis Today*, **116** (4) (2006): 512–518. DOI: 10.1016/j.cattod.2006.06.037.

[145] N. A. Khan, Z. Hasan, K. S. Min, et al. Facile introduction of Cu+ on activated carbon at ambient conditions and adsorption of benzothiophene over Cu+/activated carbon. *Fuel Processing Technology*, **116** (2013): 265–270. DOI: 10.1016/j.fuproc.2013.07.003.

[146] X. Li, X. Zhang, and L. Lei. Preparation of CuNaY zeolites with microwave irradiation and their application for removing thiophene from model fuel. *Separation and Purification Technology*, **64** (3) (2009): 326–331. DOI: 10.1016/j.seppur.2008.10.016.

[147] G. S. He, L. B. Sun, X. L. Song, et al. Adjusting host properties to promote cuprous chloride dispersion and adsorptive desulfurization sites formation on SBA-15. *Energy and Fuels*, **25** (8) (2011): 3506–3513. DOI: 10.1021/ef200723m.

[148] J. A. Arcibar-Orozco, J. R. Rangel-Mendez, and T. J. Bandosz. Desulfurization of Model Diesel Fuel on Activated Carbon Modified with Iron Oxyhydroxide Nanoparticles: Effect of tert-Butylbenzene and Naphthalene Concentrations. *Energy and Fuels*, **27** (9) (2013): 5380–5387. DOI: 10.1021/ef400999g.

[149] S. S. Shah, I. Ahmad, and W. Ahmad. Adsorptive desulphurization study of liquid fuels using Tin (Sn) impregnated activated charcoal. *Journal of Hazardous Materials*, **304** (2016): 205–213. DOI: 10.1016/j.jhazmat.2015.10.046.

[150] S. Velu, C. Song, M. H. Engelhard, et al. Adsorptive Removal of Organic Sulfur Compounds from Jet Fuel over K-Exchanged NiY Zeolites Prepared by Impregnation and Ion Exchange. *Industrial & Engineering Chemistry Research*, **44** (15) (2005): 5740–5749. DOI: 10.1021/ie0488492.

[151] F. Subhan, B. S. Liu, Q. L. Zhang, et al. Production of ultra-low-sulfur gasoline: An equilibrium and kinetic analysis on adsorption of sulfur compounds over Ni/MMS sorbents. *Journal of Hazardous Materials*, **239-240** (2012): 370–380. DOI: 10.1016/j.jhazmat.2012.09.012.

[152] F. Subhan and B. S. Liu. Acidic sites and deep desulfurization performance of nickel supported mesoporous ALMCM-41 sorbents. *Chemical Engineering Journal*, **178** (2011): 69–77. DOI: 10.1016/j.cej.2011.10.013.

[153] R. Mahmoudi and C. Falamaki. Ni2+-ion-exchanged dealuminated clinoptilolite: A superior adsorbent for deep desulfurization. *Fuel*, **173** (2016): 277–284. DOI: 10.1016/j.fuel.2016.01.048.

[154] F. Subhan, Z. Yan, P. Peng, et al. The enhanced adsorption of sulfur compounds onto mesoporous Ni-AlKIT-6 sorbent, equilibrium and kinetic analysis. *Journal of hazardous materials*, **270** (2014): 82–91. DOI: 10.1016/j.jhazmat.2014.01.046.

[155] A. J. Hernández-Maldonado and R. T. Yang. Desulfurization of Diesel Fuels via π-Complexation with Nickel (II)-Exchanged X- and Y-Zeolites. *Industrial and Engineering Chemistry Research*, **43** (4) (2004): 1081–1089. DOI: 10.1021/ie034206v.

[156] X. Ma, M. Sprague, and C. Song. Deep desulfurization of gasoline by selective adsorption over nickel-based adsorbent for fuel cell applications. *Industrial and Engineering Chemistry Research*, **44** (15) (2005): 5768–5775. DOI: 10.1021/ie0492810.

[157] J. a. Z. Pieterse, S. Van Eijk, H. a. J. Van Dijk, et al. On the potential of absorption and reactive adsorption for desulfurization of ultra low-sulfur commercial diesel in the liquid phase in the presence of fuel additive and bio-diesel. *Fuel Processing Technology*, **92** (3) (2011): 616–623. DOI: 10.1016/j.fuproc.2010.11.019.

[158] S. Rashidi, M. R. Khosravi Nikou, and B. Anvaripour. Adsorptive desulfurization and denitrogenation of model fuel using HPW and NiO-HPW modified aluminosilicate mesostructures. *Microporous and Mesoporous Materials*, **211** (2015): 134–141. DOI: 10.1016/j.micromeso.2015.02.041.

[159] S. K. Thaligari, S. Gupta, V. C. Srivastava, et al. Simultaneous Desulfurization and Denitrogenation of Liquid Fuel by Nickel-Modified Granular Activated Carbon. *Energy and Fuels*, **30** (7) (2016): 6161–6168. DOI: 10.1021/acs.energyfuels.6b00579.

[160] Y. N. Prajapati and N. Verma. Adsorptive desulfurization of diesel oil using nickel nanoparticle-doped activated carbon beads with/without carbon nanofibers: Effects of adsorbate size and adsorbent texture. *Fuel*, **189** (2017): 186–194. DOI: 10.1016/j.fuel.2016.10.044.

[161] C. Sentorun-Shalaby, S. K. Saha, X. Ma, et al. Mesoporous-molecular-sieve-supported nickel sorbents for adsorptive desulfurization of commercial ultra-low-sulfur diesel fuel. *Applied Catalysis B: Environmental*, **101** (3-4) (2011): 718–726. DOI: 10.1016/j.apcatb.2010.11.014.

[162] M. Teymouri, A. Samadi-Maybodi, A. Vahid, et al. Adsorptive desulfurization of low sulfur diesel fuel using palladium containing mesoporous silica synthesized via a novel in-situ approach. *Fuel Processing Technology*, **116** (2013): 257–264. DOI: 10.1016/j.fuproc.2013.07.009.

[163] A. K. O. Rodrigues, J. E. T. Ramos, C. L. Cavalcante Jr., et al. Pd-loaded mesoporous silica as a robust adsorbent in adsorption/desorption desulfurization cycles. *Fuel*, **126** (2014): 96–103. DOI: 10.1016/j.fuel.2014.02.019.

[164] X. Ren, G. Miao, Z. Xiao, et al. Catalytic adsorptive desulfurization of model diesel fuel using TiO2/SBA-15 under mild conditions. *Fuel*, **174** (2016): 118–125. DOI: 10.1016/j.fuel.2016.01.093.

[165] R. T. Yang, A. J. Hernández-Maldonado, and F. H. Yang. Desulfurization of Transportation Fuels with Zeolites Under Ambient Conditions. *Science*, **301** (5629) (2003): 79–81.

[166] A. J. Hernández-Maldonado, G. Qi, and R. T. Yang. Desulfurization of commercial fuels by π-complexation: Monolayer CuCl/γ-Al2O3. *Applied Catalysis B: Environmental*, **61** (3-4) (2005): 212–218. DOI: 10.1016/j.apcatb.2005.05.003.

[167] J. Zhang, G. Qiu, L. Fan, et al. Enhanced sulfur capacity of durable and regenerable mesoporous sorbents for the deep desulfurization of diesel. *Fuel*, **153** (2015): 578–584. DOI: 10.1016/j.fuel.2015.03.056.

[168] K. Liu, C. Song, and V. Subramani. Hydrogen and Syngas Production and Purification Technologies. Hoboken, New Jersey: John Wiley & Sons, 2009, 1–533. DOI: 10.1002/9780470561256.

[169] Y. Mathieu, L. Tzanis, M. Soulard, et al. Adsorption of SOx by oxide materials: A review Yannick. *Fuel Processing Technology*, **114** (2013): 81–100. DOI: 10.1016/j.fuproc.2013.03.019.

[170] X. Han, H. Lin, and Y. Zheng. Understanding capacity loss of activated carbons in the adsorption and regeneration process for denitrogenation and desulfurization of diesel fuels. *Separation and Purification Technology*, **133** (2014): 194–203. DOI: 10.1016/j.seppur.2014.06.020.

[171] J. Xiong, W. Zhu, H. Li, et al. Carbon-doped porous boron nitride: metal-free adsorbents for sulfur removal from fuels. *Journal of Materials Chemistry A*, **3** (24) (2015): 12738–12747. DOI: 10.1039/C5TA01346A.

[172] M. Seredych, J. Rawlins, and T. J. Bandosz. Investigation of the Thermal Regeneration Efficiency of Activated Carbons Used in the Desulfurization of Model Diesel Fuel. *Industrial & Engineering Chemistry Research*, **50** (24) (2011): 14097–14104. DOI: 10.1021/ie202159a.

[173] F. Liang, M. Lu, M. E. Birch, et al. Determination of polycyclic aromatic sulfur heterocycles in diesel particulate matter and diesel fuel by gas chromatography with atomic emission detection. *Journal of Chromatography. A*, **1114** (1) (2006): 145–53. DOI: 10.1016/j.chroma.2006.02.096.

[174] T. Schade and J. T. Andersson. Speciation of alkylated dibenzothiophenes in a deeply desulfurized diesel fuel. *Energy and Fuels*, **20** (4) (2006): 1614–1620. DOI: 10.1021/ef0502507.

[175] J. King. "Separation Processes Based on Reversible Chemical Complexation." In: *Handbook of Separation Process Technology*. Ed. by R. W. Rousseau. New York: John Wiley & Sons, 1987. Chap. 15, 760–774.

[176] R. T. Yang, A. Takahashi, and F. H. Yang. New Sorbents for Desulfurization of Liquid Fuels by π-Complexation. *Ind. Eng. Chem. Res.* **40** (2001): 6236–6239. DOI: 10.1021/ie010729w.

[177] J.-j. Gao, H.-q. Li, H.-x. Zhang, et al. Removal mechanism of thiophenic compounds in model oil by inorganic Lewis acids. *Industrial and Engineering Chemistry Research*, **51** (12) (2012): 4682–4691. DOI: 10.1021/ie202831p.

[178] C. Yu, J. S. Qiu, Y. F. Sun, et al. Adsorption removal of thiophene and dibenzothiophene from oils with activated carbon as adsorbent: Effect of surface chemistry. *Journal of Porous Materials*, **15** (2) (2008): 151–157. DOI: 10.1007/s10934-007-9116-4.

[179] K. Tanabe, M. Misono, Y. Ono, et al. New Solid Acids and Bases: Their Catalytic Properties. Vol. 51. Elsevier, 1989, 364. arXiv: arXiv:1011.1669v3.

[180] M. Digne, P. Sautet, P. Raybaud, et al. Hydroxyl groups on γ-alumina surfaces: A DFT study. *Journal of Catalysis*, **211** (1) (2002): 1–5. DOI: 10.1016/S0021-9517(02)93741-3.

[181] H. Tang, D. Zhang, G. Tang, et al. Low temperature synthesis and photocatalytic properties of mesoporous TiO2 nanospheres. *Journal of Alloys and Compounds*, **591** (2014): 52–57. DOI: 10.1016/j.jallcom.2013.12.176.

[182] K. R. P. Sabu, K. V. C. Rao, and C. G. R. Nair. *A Comparative Study on the Acidic Properties and Catalytic Activities of TiO2, SiO2, Al2O3, SiO2-Al2O3, SiO2-TiO2, Al2O3-TiO2, and TiO2-SiO2-Al2O3*. 1991. DOI: 10.1246/bcsj.64.1920.

[183] R. E. Olsen. "Synthesis, Characterization, and Application of High Surface Area, Mesoporous, Stabilized Anatase TiO2 Catalyst Supports." PhD. Dissertation. Brigham Young University, 2013.

[184] A. Samokhvalov, S. Nair, E. C. Duin, et al. Surface characterization of Ag/Titania adsorbents. *Applied Surface Science*, **256** (2010): 3647–3652. DOI: 10.1016/j.apsusc.2010.01.002.

[185] P. Norby, R. Dinnebier, and A. N. Fitch. Decomposition of Silver Carbonate; the Crystal Structure of Two High-Temperature Modifications of Ag2CO3. *Inorganic Chemistry*, **41** (14) (2002): 3628–3637. DOI: 10.1021/ic0111177.

[186] H. E. Swanson and E. Tatge. Standard X-ray diffraction powder patterns. Vol. I, Data for 54 inorganic substances. National Bureau of Standards circular, 539, v. 1. Washington, D.C.: National Bureau of Standards, 1953, 1–95.

[187] R. G. Pearson. Hard and soft acids and bases, HSAB, part 1: Fundamental principles. *Journal of Chemical Education*, **45** (9) (1968): 581–587. DOI: 10.1021/ed045p581.

[188] L. Chen, Y. Zhu, H. Zheng, et al. Aqueous-phase hydrodeoxygenation of carboxylic acids to alcohols or alkanes over supported Ru catalysts. *Journal of Molecular Catalysis A: Chemical*, **351** (2011): 217–227. DOI: 10.1016/j.molcata.2011.10.015.

[189] Y. Shiraishi, Y. Taki, T. Hirai, et al. A Novel Desulfurization Process for Fuel Oils Based on the Formation and Subsequent Precipitation of S-Alkylsulfonium Salts. 1. Light Oil Feedstocks. *Industrial & Engineering Chemistry Research*, **40** (4) (2001): 1213–1224. DOI: 10.1021/ie000547m.

[190] R. N. Fallah and S. Azizian. Removal of thiophenic compounds from liquid fuel by different modified activated carbon cloths. *Fuel Processing Technology*, **93** (1) (2012): 45–52. DOI: 10.1016/j.fuproc.2011.09.012.

[191] ASTM D975, 2008, ″Standard Specification for Diesel Fuel Oils″. ASTM International, West Conshohocken.

[192] D. Bathen and M. Breitbach. Adsorptionstechnik. 1st ed. Berlin Heidelberg: Springer-Verlag, 2001, 341. DOI: 10.1007/978-3-642-18235-8.

[193] A. Srivastav and V. C. Srivastava. Adsorptive desulfurization by activated alumina. *Journal of Hazardous Materials*, **170** (2-3) (2009): 1133–1140. DOI: 10.1016/j.jhazmat.2009.05.088.

[194] W. Plazinski, W. Rudzinski, and A. Plazinska. Theoretical models of sorption kinetics including a surface reaction mechanism: A review. *Advances in Colloid and Interface Science*, **152** (1-2) (2009): 2–13. DOI: 10.1016/j.cis.2009.07.009.

[195] S. Lagergren. Zur theorie der sogenannten adsorption gelöster stoffe. Kungliga Svenska Vetenskapsakademiens. *Handlingar*, **24** (4) (1898): 1–39.

[196] Y. S. Ho and G. McKay. Pseudo-second order model for sorption processes. *Process Biochemistry*, **34** (5) (1999): 451–465. DOI: 10.1016/S0032-9592(98)00112-5.

[197] W. Plazinski, J. Dziuba, and W. Rudzinski. Modeling of sorption kinetics: The pseudo-second order equation and the sorbate intraparticle diffusivity. *Adsorption*, **19** (5) (2013): 1055–1064. DOI: 10.1007/s10450-013-9529-0.

[198] W. Rudzinski and W. Plazinski. On the applicability of the pseudo-second order equation to represent the kinetics of adsorption at solid/solution interfaces: A theoretical analysis based on the statistical rate theory. *Adsorption*, **15** (2) (2009): 181–192. DOI: 10.1007/s10450-009-9167-8.

[199] Y. S. Ho and G. McKay. Sorption of dyes from aqueous solution by peat. *Chemical Engineering Journal*, **70** (1998): 115–124.

[200] G. F. Malash and M. I. El-khaiary. Piecewise linear regression : A statistical method for the analysis of experimental adsorption data by the intraparticle-diffusion models. *Chemical Engineering Journal*, **163** (3) (2010): 256–263. DOI: 10.1016/j.cej.2010.07.059.

[201] W. J. Weber and C. Morris. Kinetics of Adsorption on Carbon from Solution. *Journal of the Sanitary Engineering Division*, **89** (2) (1963): 31–60.

[202] D. Reichenberg. Properties of Ion-Exchange Resins in Relation to their Structure. III. Kinetics of Exchange. *Journal of the American Chemical Society*, **75** (1953): 589–597.

[203] I. Tsibranka and E. Hristova. Comparison of different kinetic models for adsorption of heavy metals onto activated carbon from apricot stones. *Bulgarian Chemical Communications*, **43** (3) (2011): 370–377.

[204] F.-C. Wu, R.-L. Tseng, and R.-S. Juang. Initial behavior of intraparticle diffusion model used in the description of adsorption kinetics. *Chemical Engineering Journal*, **153** (1-3) (2009): 1–8. DOI: 10.1016/j.cej.2009.04.042.

[205] R. Contreras, R. Cuevas-García, J. Ramírez, et al. Transformation of thiophene, benzothiophene and dibenzothiophene over Pt/HMFI, Pt/HMOR and Pt/HFAU: Effect of reactant molecular dimensions and zeolite pore diameter over catalyst activity. *Catalysis Today*, **130** (2-4) (2008): 320–326. DOI: 10.1016/j.cattod.2007.10.007.

[206] D. Papurello, A. Lanzini, S. Fiorilli, et al. Sulfur poisoning in Ni-anode solid oxide fuel cells (SOFCs): Deactivation in single cells and a stack. *Chemical Engineering Journal*, **283** (2016): 1224–1233. DOI: 10.1016/j.cej.2015.08.091.

[207] N. Márquez, M. T. Kreutzer, M. Makkee, et al. Infinite dilution binary diffusion coefficients of hydrotreating compounds in tetradecane in the temperature range from (310 to 475) K. *Journal of Chemical and Engineering Data*, **53** (2) (2008): 439–443. DOI: 10.1021/je700535q.

[208] J. Kärger, D. M. Ruthven, and D. N. Theodorou. Diffusion in Nanoporous Materials. Wiley-VCH: Weinheim, Germany, 2012. Chap. 1, Vol. 1, pp 3–24. DOI: 10.1002/9783527651276.

[209] V. Wichmann. "Konzepte und Betriebsstrategien für die Nutzung von Rapsölen in Verbrennungsmotoren für den Einsatz in Landmaschinen." Ph.D. Dissertation. University of Rostock, Germany, 2008.

[210] S. Dasgupta, P. Gupta, Aarti, et al. Adsorptive desulfurization of diesel by regenerable nickel based adsorbents. *Fuel*, **108** (2013): 184–189. DOI: 10.1016/j.fuel.2012.12.060.

[211] B. S. Liu, D. F. Xu, J. X. Chu, et al. Deep Desulfurization by the Adsorption Process of Fluidized Catalytic Cracking (FCC) Diesel over Mesoporous Al-MCM-41 Materials. *Energy and Fuels*, **21** (1) (2007): 250–255. DOI: 10.1021/ef060249n.

[212] A. Samokhvalov, E. C. Duin, S. Nair, et al. An in situ temperature-programmed XPS study of the surface chemical reactions of thiophene with Ag/titania. *Surface and Interface Analysis*, **42** (9) (2010): 1476–1482. DOI: 10.1002/sia.3314.

[213] I. Bezverkhyy, K. Bouguessa, C. Geantet, et al. Adsorption of tetrahydrothiophene on faujasite type zeolites : Breakthrough curves and FTIR spectroscopy study. *Applied Catalysis B: Environmental*, **62** (3-4) (2006): 299–305. DOI: 10.1016/j.apcatb.2005.08.010.

[214] J. A. Thote, R. V. Chatti, K. S. Iyer, et al. N-doped mesoporous alumina for adsorption of carbon dioxide. *Journal of Environmental Sciences*, **24** (11) (2012): 1979–1984. DOI: 10.1016/S1001-0742(11)61022-X.

[215] A. Samokhvalov, E. C. Duin, S. Nair, et al. Study of the Surface Chemical Reactions of Thiophene with Ag/Titania by the Complementary Temperature-Programmed Electron Spin Resonance, Temperature-Programmed Desorption, and X-ray Photoelectron Spectroscopy: Adsorption, Desorption, and Sorbent Regenera. *Journal of Physical Chemistry C*, **114** (9) (2010): 4075–4085. DOI: 10.1021/jp911458u.

[216] T. E. Caldwell, I. M. Abdelrehim, and D. P. Land. Thiophene decomposition on Pd(111) forms S and C₄ species: A laser-induced thermal desorption/Fourier transform mass spectrometry study. *Surface Science*, **367** (1) (1996): L26–L31. DOI: 10.1016/S0039-6028(96)00995-8.

[217] A. Galembeck and O. L. Alves. Thermal behavior of α-Ba(FeS2)2 and AgFeS2: quasi-unidimensional and 3D network compounds prepared from ion-exchange on the same precursor. *Journal of Materials Science*, **34** (13) (1999): 3275–3280. DOI: 10.1023/A:1004646326407.

[218] D. Živković, M. Sokić, Ž. Živković, et al. Thermal study and mechanism of Ag2S oxidation in air. *Journal of Thermal Analysis and Calorimetry*, **111** (2) (2013): 1173–1176. DOI: 10.1007/s10973-012-2300-z.

[219] S. Dasgupta, S. Divekar, A. Arya, et al. A vapor phase adsorptive desulfurization process for producing ultra low sulphur diesel using NiY zeolite as a regenerable adsorbent. *RSC Advances*, **5** (69) (2015): 56060–56066. DOI: 10.1039/C5RA05664K.

[220] M. Kurzawa and E. Tomaszewicz. Kinetics of reactions between some compounds from the three-component silver -oxygen -sulfur system. *Reaction Kinetics and Catalysis Letters*, **70** (1) (2000): 53–59. DOI: `10.1023/A:1010350329497`.

[221] S. W. Nam and G. R. Gavalas. Adsorption and oxidative adsorption of sulfur dioxide and γ-alumina. *Applied Catalysis*, **55** (22) (1989): 193–213. DOI: `10.1016/S0166-9834(00)82328-3`.

[222] O. Saur, M. Bensitel, A. B. M. Saad, et al. The Structure and Stability of Sulfated Alumina and Titania. *Journal of Catalysis*, **99** (1) (1986): 104–110. DOI: `10.1016/0021-9517(86)90203-4`.

[223] C. C. Chang. Infrared studies of SO2 on γ-alumina. *Journal of Catalysis*, **53** (3) (1978): 374–385. DOI: `10.1016/0021-9517(78)90109-4`.

[224] H. A. Papazian, P. J. Pizzolato, and R. Orrell. The Thermal Decomposition of Aluminum Sulfate and Hafnium Sulfate. *Thermochimica Acta*, **4** (2) (1971): 97–103. DOI: `10.1016/S0040-6031(72)80023-6`.

[225] S. Andersson, R. Pompe, and N.-G. Vannerberg. SOx adsorption/desorption processes on γ-alumina for SOx transfer catalyst. *Applied Catalysis*, **16** (1) (1985): 49–58. DOI: `10.1016/S0166-9834(00)84069-5`.

[226] J. M. H. Lo, T. Ziegler, and P. D. Clark. SO2 adsorption and transformations on γ-Al2O3 surfaces: A density functional theory study. *Journal of Physical Chemistry C*, **114** (23) (2010): 10444–10454. DOI: `10.1021/jp910895g`.

[227] J. Baltrusaitis, P. M. Jayaweera, and V. H. Grassian. Sulfur dioxide adsorption on TiO2 nanoparticles: Influence of particle size, coadsorbates, sample pretreatment, and light on surface speciation and surface coverage. *Journal of Physical Chemistry C*, **115** (2) (2011): 492–500. DOI: `10.1021/jp108759b`.

[228] T. Hamzehlouyan, C. S. Sampara, J. Li, et al. Kinetic study of adsorption and desorption of SO2 over γ-Al2O3 and Pt/γ-Al2O3. *Applied Catalysis B: Environmental*, **181** (2016): 587–598. DOI: `10.1016/j.apcatb.2015.08.003`.

[229] X. She, M. Flytzani-Stephanopoulos, C. Wang, et al. SO2-induced stability of Ag-alumina catalysts in the SCR of NO with methane. *Applied Catalysis B: Environmental*, **88** (1-2) (2009): 98–105. DOI: `10.1016/j.apcatb.2008.09.015`.

[230] E. Ruckenstein and S. H. Lee. The behavior of model Ag/Al2O3 catalysts in various chemical environments. *Journal of Catalysis*, **109** (1) (1988): 100–119. DOI: `10.1016/0021-9517(88)90188-1`.

[231] K. S. Blinn and H. Abernathy. Raman spectroscopic monitoring of carbon deposition on hydrocarbon-fed solid oxide fuel cell anodes. *Energy and Environmental Science*, **5** (7) (2012): 7913–7917. DOI: `10.1039/c2ee21499g`.

[232]   C. Schluckner, V. Subotić, V. Lawlor, et al. Carbon Deposition Simulation in Porous
        SOFC Anodes: A Detailed Numerical Analysis of Major Carbon Precursors. *Journal of
        Fuel Cell Science and Technology*, **12** (5) (2015): 051007. DOI: 10.1115/1.4031862.

[233]   Q.-K. Liu, Y. Xu, X.-C. Tan, et al. Pyrolysis of Asphaltenes in Subcritical and Supercritical
        Water : In fl uence of H - Donation from Hydrocarbon Surroundings. *Energy and Fuels*,
        31 (4) (2017): 3620–3628. DOI: 10.1021/acs.energyfuels.6b03135.

[234]   B. K. Debnath, B. B. Sahoo, U. K. Saha, et al. "Simulation of combustion and emission
        characteristics in a dual fuelled diesel engine." In: *Proceedings of the ASME 2010 Internal
        Combustion Engine Division Fall Technical Conference*. 2010. San Antonio: American Society
        of Mechanical Engineers, 2010, 767–776. DOI: 10.1115/ICEF2010-35095.

[235]   M. Shirani, A. Semnani, S. Habibollahi, et al. Synthesis and application of magnetic
        NaY zeolite composite immobilized with ionic liquid for adsorption desulfurization
        of fuel using response surface methodology. *Journal of Porous Materials*, **23** (3) (2016):
        701–712. DOI: 10.1007/s10934-016-0125-z.

[236]   S. A. Klein. EES - Engineering Equation Solver - User Manual. Vol. Academic Profes-
        sional V8.861. F-Chart Software, 2013.